Real-Time Load-Side Control of Electric Power Systems

Thesis by
Changhong Zhao

In Partial Fulfillment of the Requirements for the
Degree of
Doctor of Philosophy

CALIFORNIA INSTITUTE OF TECHNOLOGY
Pasadena, California

2016
Defended May 6, 2016

© 2016

Changhong Zhao
ORCID: 0000-0003-0539-8591

All rights reserved

ACKNOWLEDGEMENTS

I owe my deepest gratitude to Professor Steven Low, for his generous support and helpful guidance during my PhD studies. Steven is a great scholar. He always keeps learning, and is enthusiastic to tackle challenging research problems that make real impacts. He is also the best advisor I could ever imagine. He understands what the students do from big picture to technical details, and is ready to provide advice whenever the students need. His professionalism and personality have set up a role model for me. I feel fortune to have worked with him.

I am grateful to my colleagues around the world, including Scott Backhaus, Janusz Bialek, Lijun Chen, Misha Chertkov, Florian Dörfler, Na Li, Feng Liu, Enrique Mallada, Kiyoshi Nakayama, Ufuk Topcu, and Yingjun Zhang, for our fruitful discussions and collaborations. Some of them indeed worked as my mentors at different stages of my research. I also want to thank the members of my candidacy and thesis committees: Professors K. Mani Chandy, John Doyle, Victoria Kostina, Richard Murray, P. P. Vaidyanathan, and Adam Wierman. Their comments and suggestions have greatly helped improve my work. Among them, I would like to give special thanks to Adam for his help on scientific writing and presentation.

The EE and CMS Departments and RSRG at Caltech provide an open, creative, and friendly atmosphere that is ideal for a student and a researcher like myself. I have spent an enjoyable time with all my friends here: Subhonmesh Bose, Desmond Cai, Niangjun Chen, Krishnamurthy Dvijotham, Lingwen Gan, Minghong Lin, Zhenhua Liu, Qiuyu Peng, Xiaoqi Ren, and more. Moreover, the administrative staff, including Sydney Garstang, Lisa Knox, Maria Lopez, Christine Ortega, and Tanya Owen, have helped us a lot with their hard work.

Last but not least, I want to thank my parents, Ms. Cuisong Song and Mr. Junqing Zhao, for their endless love and support from China. It must be a hard time for them to have their only child in another continent that is thousands of miles away. I hope my efforts and achievements would make them proud.

ABSTRACT

Two trends are emerging from modern electric power systems: the growth of renewable (e.g., solar and wind) generation, and the integration of information technologies and advanced power electronics. The former introduces large, rapid, and random fluctuations in power supply, demand, frequency, and voltage, which become a major challenge for real-time operation of power systems. The latter creates a tremendous number of controllable intelligent endpoints such as smart buildings and appliances, electric vehicles, energy storage devices, and power electronic devices that can sense, compute, communicate, and actuate. Most of these endpoints are distributed on the *load side* of power systems, in contrast to traditional control resources such as centralized bulk generators. This thesis focuses on controlling power systems in real time, using these load-side resources. Specifically, it studies two problems.

Distributed load-side frequency control: We establish a mathematical framework to design distributed frequency control algorithms for flexible electric loads. In this framework, we formulate a category of optimization problems, called *optimal load control (OLC)*, to incorporate the goals of frequency control, such as balancing power supply and demand, restoring frequency to its nominal value, restoring inter-area power flows, etc., in a way that minimizes total disutility for the loads to participate in frequency control by deviating from their nominal power usage. By exploiting distributed algorithms to solve OLC and analyzing convergence of these algorithms, we design distributed load-side controllers and prove stability of closed-loop power systems governed by these controllers.

The general framework above is adapted and applied to different types of power systems described by different models, or to achieve different levels of control goals under different operation scenarios. We first consider a dynamically coherent power system which can be equivalently modeled with a single synchronous machine. Decentralized controllers are derived through a dual gradient algorithm for the OLC problem on this single-machine system, where the dual gradient, which is indeed the total mismatch between load and generation, is calculated at each load by an input estimator using local frequency measurements. Adding neighborhood communication between the loads can improve robustness of the controllers to the noise in local frequency measurements. Through analysis and simulations, we also investigate various practical issues that affect the performance of the proposed

control scheme, such as asynchronous measurements and actuations, robustness to model inaccuracies, and scalability of performance.

We then extend our framework to a multi-machine power network. We prove that the dynamics of these machines and the linearized power flows between them can be identified as part of a real-time primal-dual algorithm to solve the OLC problem. Then we implement the other part of the primal-dual algorithm as distributed controllers. With this method, we design completely decentralized primary frequency control where every controllable load only measures its local frequency without communicating with any other, and prove global asymptotic stability of the closed-loop system. The controller design and stability analysis are then extended to the scenarios with a more accurate nonlinear power flow model, generator dynamics and control, and secondary frequency control, et cetera. For the case with nonlinear power flows, the controllers designed from the OLC framework guarantee local stability. We also design a different version of secondary frequency control through local integral of frequency deviation, which ensures global convergence of the closed-loop system. The OLC problem can be solved by adding distributed averaging filters to the local integral controllers.

Two-timescale voltage control: The voltage of a power distribution system must be maintained closely around its nominal value in real time, even in the presence of highly volatile power supply or demand. For this purpose, we jointly control two types of reactive power sources: a capacitor operating at a slow timescale, and a power electronic device, such as a smart inverter or a D-STATCOM, operating at a fast timescale. Their control actions are solved from optimal power flow problems at two timescales. Specifically, the slow-timescale problem is a chance-constrained optimization, which minimizes power loss and regulates the voltage at the current time instant while limiting the probability of future voltage violations due to stochastic changes in power supply or demand. This control framework forms the basis of an optimal sizing problem, which determines the installation capacities of the control devices by minimizing the sum of power loss and capital cost. We develop computationally efficient heuristics to solve the optimal sizing problem and implement real-time control. Numerical experiments show that the proposed sizing and control schemes significantly improve the reliability of voltage control with a moderate increase in cost.

TABLE OF CONTENTS

Acknowledgements . . . iii
Abstract . . . iv
Table of Contents . . . vi
List of Illustrations . . . viii
List of Tables . . . xii
Chapter I: Introduction . . . 1
1.1 Distributed load-side frequency control . . . 3
1.2 Two-timescale voltage control . . . 8
1.3 Thesis outline . . . 10
Chapter II: Load-Side Frequency Control in Single-Machine Systems . . . 11
2.1 System model and problem formulation . . . 11
2.2 Estimating load-generation mismatch . . . 16
2.3 Decentralized load control: algorithm and convergence . . . 18
2.4 Asynchronous measurements and actuations . . . 23
2.5 Simulations . . . 25
2.6 Conclusion . . . 32
Appendices . . . 34
2.A Proof of Proposition 2.1 . . . 34
2.B Proof of Theorem 2.1 . . . 34
2.C Proof of Theorem 2.2 . . . 38
2.D Proof of Theorem 2.3 . . . 38
2.E Proof of Theorem 2.4 . . . 38
Chapter III: Load-Side Frequency Control in Multi-Machine Networks . . . 40
3.1 System model and problem formulation . . . 41
3.2 Load control and system dynamics as primal-dual algorithm . . . 47
3.3 Convergence analysis . . . 51
3.4 Generator and load-side primary control with nonlinear power flow . . . 58
3.5 Generator and load-side secondary control with nonlinear power flow 66
3.6 Decentralized frequency integral control . . . 72
3.7 Distributed averaging-based proportional integral control . . . 77
3.8 Simulations . . . 79
3.9 Conclusion . . . 89
Appendices . . . 92
3.A Frequently used notations . . . 92
3.B Frequency behavior of the test system . . . 92
3.C Proof of Lemma 3.1 . . . 93
3.D Proof of Lemma 3.2 . . . 94
3.E Proof of Lemma 3.3 . . . 94
3.F Proof of Lemma 3.4 . . . 95

3.G Proof of Lemma 3.5 96
Chapter IV: Two-Timescale Voltage Control 97
4.1 Distribution circuit and load models 97
4.2 Optimal voltage control and device sizing 100
4.3 Heuristic solution and implementation 104
4.4 Numerical results 111
4.5 Conclusion 116
Bibliography 117

LIST OF ILLUSTRATIONS

Number *Page*

1.1 A four-day real power consumption profile (sampled every five seconds) of the high performance computing load studied in this thesis. . 9

2.1 The single-machine power system model where Δg denotes a generation drop and $\Delta\omega$ denotes the frequency deviation. Load i obtains a measured value of the frequency deviation which may differ from $\Delta\omega$ by a stochastic noise ξ_i. Based on the measured frequency deviation, load i is reduced by Δd_i. 12

2.2 The home area network (HAN) supports the communication between appliances and smart meters. The neighborhood area network (NAN), which is used in our load control, aids the communication between utilities and smart meters. The wide area network (WAN) aids the long range communication between substations. This figure is a slightly modified version of a similar figure in [96]. 20

2.3 A single-machine power system model used in simulations. 25

2.4 An example communication graph of loads. 27

2.5 The frequency (N=100, K=5). The dash-dot line is the frequency without load control. The solid and dashed lines are those with load control where loads use different models. 28

2.6 The total load reduction (N=100, K=5). The dash-dot line is the generation drop. The solid and dashed lines are total load reductions by load control where loads use different models. 28

2.7 The total end-use disutility (N=100, K=5). The dash-dot line is the minimal disutility. The solid and dashed lines are trajectories of the disutility with load control where loads use different models. 29

2.8 The frequency when there is no communication in load control (N=100, K=0). The dash-dot line is the frequency without load control. The solid and dashed lines are respectively the frequencies without and with measurement noise in load control. 30

2.9 The total load reduction when there is no communication in load control (N=100, K=0). The dash-dot line is the generation drop. The solid and dashed lines are respectively the load reductions without and with measurement noise in load control. 30
2.10 The total disutility when there is no communication in load control (N=100, K=0). The dash-dot line is the minimal disutility. The solid and dashed lines are respectively the disutility without and with measurement noise in load control. 31
2.11 The total end-use disutility with different numbers K of neighbors in the load control (N=100). 31
2.12 The total end-use disutility with different numbers N of loads (K=5). 32
3.1 Schematic of a generator bus j, where $\Delta\omega_j$ is the frequency deviation; ΔP_j^m is the change in mechanical power minus aggregate uncontrollable load; $D_j\Delta\omega_j$ characterizes the effect of generator friction and frequency-sensitive loads; Δd_j is the change in aggregate controllable load; ΔP_{ij} is the deviation in branch power injected from another bus i to bus j; ΔP_{jk} is the deviation in branch power delivered from bus j to another bus k. 43
3.2 E is the set on which $\dot{U} = 0$, Z^* is the set of equilibrium points of (3.15), and Z^+ is a compact subset of Z^* to which all solutions $(\omega(t), P(t))$ approach as $t \to \infty$. Indeed every solution $(\omega(t), P(t))$ converges to a point $(\omega^*, P^*) \in Z^+$ that is dependent on the initial state. 55
3.3 Single line diagram of the IEEE 68-bus test system [105]. 80
3.4 The (a) frequency and (b) voltage at bus 66, under four cases: (i) no PSS, no OLC; (ii) with PSS, no OLC; (iii) no PSS, with OLC; (iv) with PSS and OLC, where the OLC is for primary frequency control. 81
3.5 The (a) new steady-state frequency, (b) lowest frequency, and (c) settling time of frequency at bus 66, against the total size of controllable loads. 82
3.6 The cost trajectory of OLC compared to its minimum. 83
3.7 Single line diagram of the IEEE 39-bus test system [58]. Dashed lines are communication links used in the simulations of DAPI control. 84
3.8 Frequencies of all the 10 generators under two cases of primary control: (1) only generators are controlled (dashed) and (2) both generators and loads are controlled (solid). The total control capacities are the same for both cases. 85

3.9 A four-machine network. This figure is from [58]. 86
3.10 Frequency of bus 12 under AGC and OLC. Control gains are tuned for best transient frequency within each case. All the four generators and two loads are controlled in both cases. 87
3.11 Frequency of bus 12 under cases (1) only generators are controlled and (2) both generators and loads are controlled. Both cases use OLC, and have the same aggregate control gain. 87
3.12 Frequencies of generators 2, 4, 6, 8, 10, under droop control, the completely decentralized integral control, and DAPI control. 89
3.13 Marginal costs $a_j p_j$ for generators 2, 4, 6, 8, 10 and controllable loads on buses 4, 15, 21, 24, 28, under the completely decentralized integral control in (a) and the DAPI control in (b). 90
3.14 Trajectories of the OLC objective value under the completely decentralized integral control and DAPI control. The blue dotted line is the minimum OLC objective value. 91
3.B.1 Frequencies at all the 68 buses shown in four groups, without OLC. . 93
4.1 Schematic of the simplified circuit with resistance r and reactance x supplying an HPC load at a voltage magnitude of v from a slack bus at a voltage magnitude of v_0. Variables P and Q are real and reactive power injections from the slack bus, and p and q are real and reactive power consumed by the HPC load. The current magnitude in the circuit is i. Three reactive power sources and a controller are installed near the load. Black lines are actual circuit lines and red lines represent signal flows. 98
4.2 Examples of probability density of p^+ conditioned on p and p^-. Subfigures (a) and (b) are for different p, and the legends label different p^-. 101
4.3 Time line of voltage control, which is broken into stages with significantly different average load power $p[t]$. The transition between stages $t-1$ and t occurs at time τ_t. Following this transition, a new optimal output $c_s^*[t]$ of the switchable capacitor is computed but not implemented until a time delay d after the transition. The D-STATCOM output $q_f^*(\tau)$ is computed and implemented at every time when $p(\tau)$ changes, which is especially important for voltage control during the interval from τ_t to $\tau_t + d$. 102

4.4 Sizes of control devices as functions of δ. The range of aggregate reactive power injection of the fixed capacitor and the D-STATCOM is plotted for (a) $c_s = 0$ and (b) $c_s = C_s^*$, respectively. 113
4.5 Real-time traces of (a) voltage magnitude and (b) power loss for different δ, and a benchmark case with only a fixed capacitor and no control. 115
4.6 Upper: the proportion of samples with voltage violations, which drops to zero when $\delta < 0.2$. Lower: cost of the system in one day, including cost of power loss and capital cost. 116

LIST OF TABLES

Number *Page*

2.1 Parameters used in the simulations of the single-machine system. . . 26

3.A.1 Frequently used notations in Chapter 3. 92

Chapter 1

INTRODUCTION

The evolution of electric power systems has never stopped since it started in the late 19th century. In the upcoming decades, this evolution will be driven by two major forces. The first is the growth of renewable generation, especially solar and wind generation. In 2000, renewable generation in US was about 350 billion kWh, or 9% of all the US electricity generation. This consists of mostly hydro power with negligible solar and wind generation. However, it is anticipated that, under the current energy policies, renewable generation will increase to about 900 billion kWh, or 18% of all the US electricity generation, by 2040. In particular, wind and solar generation will account for nearly 50% of the total renewable generation [1]. Some regional power systems have set more ambitious goals for their integration of renewable energy. For example, California targets 50% of renewable generation by 2030, with an emphasis on solar power [2]. Hawaii plans to generate 100% of its electricity from wind, solar, and geothermal power, by 2045 [3].

The second major force that drives the evolution of power systems is the integration of sensing, computation, and communication technologies, as well as advanced power electronics. These are some of the key factors that will lead to a "smart grid" in the future. Examples of the integration of sensing and communication technologies include the increase of total installation of phasor measurement units in US from 166 in 2009 to more than 1000 by 2015 [4], and the projected rise of global market for smart meters from $4 billion in 2011 to around $20 billion in 2018 [5]. As a result of this technology integration, a tremendous number of controllable intelligent endpoints, such as smart buildings and appliances, electric vehicles, and energy storage devices, are emerging rapidly. For example, the global shipments of smart appliances are predicted to grow from fewer than 1 million units in 2014 to more than 223 million units by 2020 [6]. The annual sales of plug-in electric vehicles in US are forecast to increase from 17,821 in 2011 to 360,000 in 2017 [7]. The annual installation of energy storage capacity in US is projected to increase from 62MW in 2014 to 861 MW in 2019 [8].

The confluence of these two forces above brings both a risk and an opportunity to future power systems. The risk is that the intermittent renewable (e.g., solar

and wind) generation introduces large, rapid, and random fluctuations in power supply, which will further cause fluctuations in frequency and voltage. In power systems, frequency and voltage must be controlled tightly around their nominal values, since severe frequency and voltage deviations can degrade power quality and load performance, damage the equipment, or cause blackouts. Traditional frequency and voltage control schemes mainly rely on a small number of large units, such as bulk generators for frequency control, and large transformers and capacitor banks for voltage control. To avoid excessive wear and tear, these units usually have limited speed of response and ramp rate, which make it difficult for them to follow fast changes in renewable generation. Also, the generators to be controlled must be partially loaded to reserve sufficient control capacity, which reduces their fuel efficiency and increases their emission [9]. The incurred costs will only increase with higher renewable portfolio, and may essentially neutralize the benefits of renewables.

Fortunately, we are also provided an opportunity to improve power system robustness, security, and efficiency. This opportunity lies in controlling the intelligent endpoints introduced above, which can sense, compute, communicate, and actuate, and therefore actively participate in power system control. Unlike the traditional control units which are mainly concentrated in a few locations, these endpoints are mostly distributed on the load side, and therefore can provide spatially more precise response to changes in demand, or disturbances from distributed renewable energy resources that are also located on the load side. These endpoints are ubiquitous and come in large numbers with each of them relatively small, so a system is more robust to the loss of one of them than the loss of a big unit. These endpoints are mostly driven by power electronics, and therefore can respond quickly to a disturbance, and can be continuously adjusted in real time. Moreover, controlling the electric loads is much cleaner than controlling the fossil-fuel generators [9].

This thesis addresses two key challenges for controlling these load-side endpoints in real time. The first challenge is that the large number and distributed nature of these endpoints may need us to design novel control schemes that are more scalable than the traditional schemes, especially centralized ones, on a small number of units. Specifically, we are interested in designing distributed control schemes which rely on local sensing, local computation, and neighborhood communication. The second challenge is to coordinate controls across multiple timescales, especially a traditional control scheme at a slow timescale and a load-side control scheme at

a fast timescale. We tackle the first challenge in *distributed load-side frequency control*, and the second in *two-timescale voltage control*.

1.1 Distributed load-side frequency control

The idea of ubiquitous continuous fast-acting distributed load participation in frequency control dates back to the late 1970s [10]. In the last decade or so, there have been several simulation studies and small-scale field trials demonstrating effectiveness of this idea. However, there is not much analytic study that relates the behavior of the loads and the equilibrium and dynamic behavior of power systems. Indeed this has been recognized, e.g., in [11], [12], [13], as a major unanswered question that must be resolved before ubiquitous continuous fast-acting distributed load participation in frequency control becomes widespread. Even though classical models for power system dynamics [14], [15], [16], [17] that focus on the generator control can be adapted to include load control, they do not consider the cost, or disutility, to the loads in participating in frequency control, an important aspect of such an approach [9], [10], [12], [18]. To overcome these hurdles, our work in this thesis allows the loads to choose their consumption pattern based on their need and the global power imbalance in the system, attaining an equilibrium that benefits both the utilities and their customers [10]. To the best of our knowledge, this is the first analytic study of large-scale distributed load-side frequency control.

Background and literature

Frequency control is traditionally implemented on the generation side and consists of three mechanisms that work at different timescales in concert [14], [15], [16], [17]. The primary frequency control operates at a timescale of up to low tens of seconds and uses a speed governor to adjust, around a setpoint, the mechanical power input to a generator based on the local frequency deviation. It is called the droop control and is completely decentralized. The primary control can rebalance power and stabilize the frequency but does not in itself restore the nominal frequency. The secondary frequency control, also called automatic generation control (AGC), operates at a timescale of up to a minute or so and adjusts the setpoints of speed governors in a control area in a centralized fashion to drive the frequency back to its nominal value and the inter-area power flows to their scheduled values. Economic dispatch, also called tertiary control, operates at a timescale of several minutes and up and schedules the output levels of generators that are online and the inter-area power flows. See [19], [20] for a hierarchical model of these three mechanisms and

its stability analysis.

The needs and technologies for ubiquitous continuous fast-acting distributed load participation in frequency control have started to mature in the last decade or so. The idea, however, dates back to the late 1970s. Schweppe *et al.* advocate its deployment to "assist or even replace turbine-governed systems and spinning reserve" [10]. Remarkably it was emphasized back then that such frequency adaptive loads will "allow the system to accept more readily a stochastically fluctuating energy source, such as wind or solar generation" [10]. This point is echoed recently in, e.g., [9], [11], [18], [21], [22], [23], [24], [25], [26], that argue for "grid-friendly" appliances, such as refrigerators, water or space heaters, ventilation systems, and air conditioners, as well as plug-in electric vehicles and energy storage devices to help manage energy imbalance. For further references, see [9]. Simulations in all these studies have consistently shown significant improvement in performance and reduction in the need for generator-side spinning reserves. The benefit of this approach can thus be substantial as the total capacity of grid-friendly appliances in the U.S. is estimated in [21] to be about 18% of the peak demand, comparable to the required operating reserve, currently at 13% of the peak demand. The feasibility of this approach is confirmed by experiments reported in [23] that measured the correlation between the frequency at a 230kV transmission substation and the frequencies at the 120V wall outlets at various places in a city in Montana. They show that local frequency measurements are adequate for loads to participate in primary frequency control as well as in the damping of electromechanical oscillations.

Indeed a small scale demonstration project has been conducted by the Pacific Northwest National Lab during early 2006 to March 2007 where 200 residential appliances participated in primary frequency control by automatically reducing their consumption (e.g, the heating element of a clothes dryer was turned off while the tumble continued) when the frequency of the household dropped below a threshold (59.95Hz) [12]. Field trials are also carried out in other countries around the globe, e.g., the U.K. Market Transformation Program [13]. Even though loads do not yet provide second-by-second or minute-by-minute *continuous* regulation service in any major electricity markets, the survey in [27] finds that they already provide 50% of the 2,400 MW contingency reserve in ERCOT (Electric Reliability Council of Texas) and 30% of dispatched reserve energy (in between continuous reserve and economic dispatch) in the U.K. market. Long Island Power Authority (LIPA) developed LIPA Edge that provides 24.9 MW of demand reduction and 75 MW of

spinning reserve by 23,400 loads for peak power management [28].

There are three other categories of work related to our analytic work on load-side frequency control. The first category is the design and analysis of generator-side frequency (and voltage) control, which focuses on stabilizing multi-machine power networks [29], [30], [31], [32], [33], [34], [35]. The second category includes studies, e.g., [36], [37], [38], on transient stability of power networks with frequency-dependent uncontrollable loads. The third category of studies integrate functions traditionally realized by slower-timescale economic dispatch with faster-timescale frequency control, as renewable generation introduces large and fast fluctuations in real power and frequency. Examples of these studies range from primary and/or secondary frequency control on the generator side [39], [40], [41], [42], [43], [44], or the load side [45], [46], to microgrids where controllable inverters interfacing distributed energy resources have similar dynamic behavior to generators [47], [48].

Summary of this work

We formulate a category of optimization problems, called *optimal load control (OLC)*, which informally takes the following general form:

$$\begin{aligned} \min_{d} \quad & c(d) \\ \text{subject to} \quad & \text{power rebalance} \\ & \text{physical constraints} \\ & \text{operational constraints} \end{aligned} \tag{1.1}$$

where d is the vector of load power consumption and c measures the disutility to loads for participating in control. The power rebalance constraint is necessary for stabilizing frequency after a disturbance in power supply or demand. The physical constraints, such as power flow equations, Kirchhoff's Laws, and Ohm's Law, describe the natural behavior of electricity. The operational constraints can be chosen to incorporate specific goals we want to achieve in (different levels of) frequency control. For example, these goals may include restoring frequency to its nominal value, restoring inter-area power flows to their scheduled values, respecting control capacity limits, and enforcing thermal limits on power lines. Then, from a distributed algorithm that solves OLC (and its dual problem), we develop distributed load-side controllers. Moreover, convergence of the distributed optimization algorithm ensures asymptotic stability of the closed-loop system under these controllers.

The general framework above is studied from two different aspects. The first is to deal with complexity of power system dynamics, and the second is to understand the impact of power network structures. We address them separately by considering the following two scenarios, described by different power system models.

Single-machine systems: In our papers [49], [50], [51], we consider a tightly coupled power system, e.g., a control area or balancing authority out of a huge interconnection, in which the electrical distances between geographically different parts are negligible [52]. Such a power system has coherent frequency everywhere even during transient, and therefore can be modeled as a single synchronous machine (generator) connected to a group of loads. To accurately capture the frequency dynamics of such a system under small disturbances, we use a high-order linear generator model which characterizes the details of various components, like governor, turbine, power system stabilizer, exciter, and automatic voltage regulator.

Decentralized load controllers are derived as a gradient algorithm to solve the dual of the OLC problem on this single machine system. It turns out that the gradient of the dual OLC problem is the mismatch between total load and generation across the system, and can be calculated at each load with an input estimator using local frequency measurements.

We further study some practical issues associated with the proposed control scheme. First, this scheme is robust to modeling inaccuracies in the sense that it performs well even when the controllers use a simplified and less accurate system model to estimate the dual gradient [49], [50], [51]. Second, to alleviate the degradation of control performance caused by stochastic noise in local frequency measurements, we add neighborhood communication between the loads. Simulations show that a moderate amount of such communication is enough to ensure good performance [51]. Third, we prove stability of the closed-loop system under asynchronous frequency measurements and control actions with bounded time delays [49]. Moreover, we show with simulations that the proposed scheme is scalable to a large number of loads, since its performance does not degrade as more loads participate [51].

Multi-machine networks: We apply our framework to a multi-machine power network, where different nodes may have different frequencies and are connected by lines transmitting power flows. In our papers [53], [54], we consider simple linearized swing dynamics for generator buses and linearized power flows. Our goal for OLC is primary frequency control, i.e., to rebalance power and stabilize frequency after a disturbance, without restoring the frequency to its nominal value.

We show that local frequency deviations emerge as a measure of the cost of power imbalance on the corresponding buses, and power flow deviations as a measure of frequency asynchronism across different buses. More strikingly the swing dynamics, power flow dynamics, and local frequency-based load control together serve as a distributed primal-dual algorithm to solve the dual of OLC. This primal-dual algorithm is globally asymptotically stable, steering the network to the unique global optimal of OLC.

These results have four important implications. First the local frequency deviation on each bus conveys exactly the right information about the global power imbalance for the loads themselves to make local decisions that turn out to be globally optimal. This allows a completely decentralized control without explicit communication to or among the loads. Second the global asymptotic stability of the primal-dual algorithm of OLC suggests that ubiquitous continuous decentralized load participation in primary frequency control is stable, addressing a question raised in several prior studies, e.g. [10], [11], [12], [13]. Third we present a "forward engineering" perspective where we start with the basic goal of load control and derive the frequency-based controller and power system dynamics as a distributed primal-dual algorithm to solve the dual of OLC. In this perspective the controller design mainly boils down to specifying an appropriate optimization problem (OLC). Fourth the opposite perspective of "reverse engineering" is useful as well where, given an appropriate controller design, the network dynamics will converge to a unique equilibrium that *inevitably* solves OLC with an objective function that depends on the controller design. For instance the linear controller in [11], [23] implies a quadratic disutility function and hence a quadratic objective in OLC.

In [55], we analyze stability of the controller above when it is applied to a more accurate nonlinear power flow model, generator control, and generator turbine and governor dynamics. A Lyapunov function for the nonlinear system is constructed to prove local asymptotic stability of the closed-loop system. In [56], we extend the approach and results in [55] to secondary frequency control, which not only stabilizes frequency, but also restores frequency to its nominal value and restores inter-area power flows to their scheduled values. The secondary frequency control not only needs local frequency measurements as in the primary control, but also requires real-time communication between neighboring buses connected by power lines. A modified version of secondary frequency control in our work [57] can also enforce thermal limits on power lines, such that the $N-1$ security criterion and chance

constraints associated with thermal limits may be relaxed in economic dispatch, resulting in significant savings. Performance improvement from our control schemes is shown by simulations of IEEE test cases on a realistic power network simulator Power System Toolbox [58].

It is worth remarking that the OLC framework above is not the only way to design distributed load-side frequency control. In [59], we design a different version of secondary frequency control based on completely decentralized integral of local frequency deviations. We prove global convergence of the closed-loop system under such control in a model with nonlinear power flows. Then, by adding distributed averaging filters which perform real-time communication between neighboring integrators, we obtain a distributed averaging-based proportional integral (DAPI) control which is locally asymptotically stable around an equilibrium that also solves the OLC problem.

1.2 Two-timescale voltage control

The effect of intermittent generation or load on the quality of voltage control in distribution systems has recently received significant attention [60]. Much of this focuses on the design of control algorithms for adjusting the reactive power injections along a distribution feeder to maintain voltage within acceptable bounds. The reactive power injections may be derived from spatially concentrated sources such as fixed and switchable capacitors [61], [62] and distributed static compensators (D-STATCOMs) [63], or distributed sources such as photovoltaic (PV) inverters [60], [64], [65], [66], [67], [68], [69], [70], [71] or inverters interfacing other distributed generation [72]. There are also various mechanisms to jointly control two or more kinds of devices, e.g., [73], [74], [75], [76] for switchable capacitors and tap-changing voltage regulators, [77] for switchable capacitors and inverters, and [78] for capacitors, reactors and static var compensators, et cetera. Meanwhile the problem of optimal placement and sizing of capacitors has been extensively studied using analytical methods [73], [74], [75], [79], [80], numerical programming [61], [62], [81], and probabilistic meta-heuristics like simulated annealing [82] and genetic algorithm [83], [84]; see [85] for more.

However, most of the work above considered voltage control either at a slow timescale (e.g., using switchable capacitors and tap-changing regulators) or at a fast timescale (e.g., using inverters), without combining the controls at two timescales for better performance. An exception is [77] where capacitors are controlled at a

slow timescale and inverters at a fast timescale. However the assumption in [77] that the load changes gradually over time and is well predicted does not hold for the case with highly intermittent generation or load. Moreover, absent in much of the work above are methods by which to size different reactive power sources that are jointly controlled. To the best of our knowledge, our work is the first to optimally control and size reactive power sources operating at different timescales, by incorporating statistical characterization of rapid and large changes in load.

While small distributed PV has stimulated much of the research in this area, large and highly intermittent load or generation can create similar, or perhaps more difficult, voltage problems. One such example is a large (several MW) PV generator. However, the motivating example for us is a high-performance computing (HPC) load at Los Alamos National Lab. Power consumption of a modern HPC load can easily swing by several MWs in a few seconds or less, as shown by Fig. 1.1.

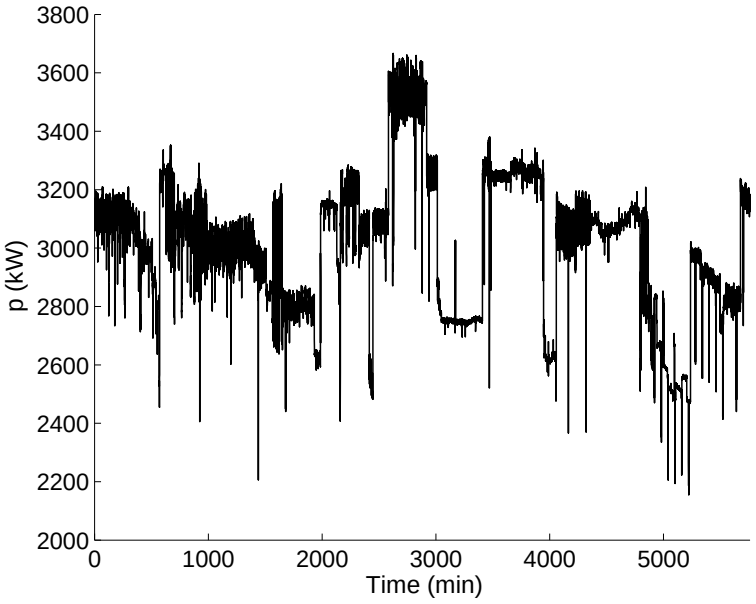

Figure 1.1: A four-day real power consumption profile (sampled every five seconds) of the high performance computing load studied in this thesis.

Fig. 1.1 shows a pattern that large transitions in the load are typically separated by minutes or hours, while relatively small fluctuations continuously occur during the period of time, called *stage*, between two consecutive large transitions. A voltage control scheme, which combines small, frequently controlled devices such as a D-STATCOM or a PV inverter, and large, infrequently controlled devices such as a switchable capacitor, is suitable for such a load pattern. Moreover, conditioned

on the current-stage average power, the probability distribution of the next-stage average power reveals information about the direction and size of voltage change that may occur in the next stage. We leverage this information to develop an improved voltage control scheme for distribution systems with large and rapid changes in load or generation. We then embed the proposed control into an optimal sizing problem for reactive power sources, which balances the capital cost of the devices with the expected cost due to power losses.

Specifically, the slow-timescale capacitor control is implemented by solving a chance-constrained optimal power flow (OPF) problem which minimizes power loss, regulates the current-stage voltage, and limits the probability of voltage violations in the next stage. At the fast timescale, we control a D-STATCOM without loss of generality, by solving an OPF problem with deterministic constraints. The control scheme above forms the basis of an optimal sizing problem, which determines the sizes of the two control devices above as well as a fixed capacitor to minimize the sum of the cost of expected power loss and the capital cost of all the devices. Exploiting structures of the chance-constrained OPF, we develop a computationally efficient heuristic based on simulated annealing to solve the sizing problem, and a heuristic for simpler real-time implementation of voltage control. Simulations on the realistic HPC load in Fig. 1.1 have shown that the proposed control and sizing schemes achieve a desired tradeoff between voltage safety and cost. In particular, voltage violations are significantly reduced with a moderate increase in cost.

1.3 Thesis outline

The rest of this thesis is organized as follows.

1. In Chapters 2 and 3 we design and analyze load-side distributed frequency control. Chapter 2 focuses on single-machine power systems [49], [50], [51], and Chapter 3 on multi-machine power networks. In Chapter 3, we work on the cases of load-side primary frequency control under a linearized power flow model [53], [54], and generator and load-side primary [55] and secondary [56] frequency controls under a nonlinear power network model. We also design a completely decentralized frequency integral control, as well as a distributed averaging-based proportional integral control [59].

2. In Chapter 4, we develop a voltage control scheme combining slow and fast reactive power sources, and develop efficient heuristics to optimally solve the sizes of these resources [86].

Chapter 2

LOAD-SIDE FREQUENCY CONTROL IN SINGLE-MACHINE SYSTEMS

We consider a dynamically coherent power system that can be equivalently modeled with a single synchronous machine connected to a group of loads. We propose a decentralized load-side frequency control scheme that stabilizes frequency after a sudden change in generation or load. The proposed scheme exploits flexibility of frequency responsive loads and neighborhood area communication to solve an optimal load control (OLC) problem that rebalances load and generation while minimizing end-use disutility of participating in load control. Local frequency measurements enable individual loads to estimate the mismatch between load and generation across the whole system. Neighborhood area communication alleviates performance degradation caused by frequency measurement noise. We also analyze convergence of the proposed scheme under asynchronous measurements and actuations with bounded time delays. Simulations show that the proposed scheme is robust to model inaccuracies, and its performance is scalable with the number of participating loads. Moreover, a moderate amount of neighborhood communication is enough to achieve significant performance improvement.

This chapter is organized as follows. Section 2.1 introduces the power system model and formulates the OLC problem. Section 2.2 introduces the approach of estimating total load-generation mismatch from local frequency measurements, a key part of our control algorithm. Section 2.3 presents the decentralized load-side frequency control algorithm and proves its convergence. Section 2.4 proves convergence of the decentralized load-side frequency control under asynchronous measurements and actuations. Section 2.5 shows simulation results. Finally, Section 2.6 concludes this chapter. The proofs of propositions, theorems, etc. are provided in the Appendices.

2.1 System model and problem formulation

We now introduce a dynamic power system model in which frequency responsive loads are controlled. We then formulate the OLC problem, which is to be solved by the load control scheme later.

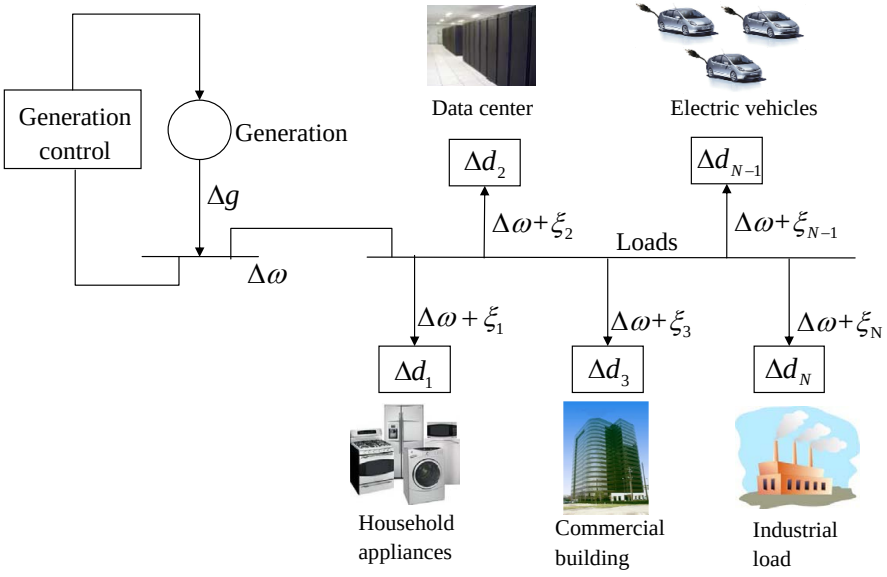

Figure 2.1: The single-machine power system model where Δg denotes a generation drop and $\Delta\omega$ denotes the frequency deviation. Load i obtains a measured value of the frequency deviation which may differ from $\Delta\omega$ by a stochastic noise ξ_i. Based on the measured frequency deviation, load i is reduced by Δd_i.

Power system model

We consider the power system model in Fig. 2.1. We assume that the electrical distances between geographically different parts of the system are negligible, and so are the differences in frequencies between them [52]. Therefore, the whole system has a universal frequency which can be equivalently regarded as the frequency of a single generator. A number of controllable loads are connected to the generator and consume the generated power. A controllable load may also be an aggregate of multiple, smaller controllable loads [9][24].

Let $V = \{1, 2, \ldots, N\}$ denote the set of loads. Suppose the system is working at an operating point where the total load and generation are balanced. Then suddenly a generation drop denoted by Δg occurs. To compensate for Δg, load i is reduced by Δd_i through load control to be designed. Let $\Delta\omega$ denote the universal frequency deviation from its nominal value. Load i measures the frequency deviation locally, and gets a measured value $\Delta\overline{\omega}_i$, which may differ from $\Delta\omega$ by a stochastic noise ξ_i.

We assume the loads measure the frequency deviation and make decisions simultaneously and synchronously at time instances $0, \Delta t, 2\Delta t, \ldots$, and we denote these time instances by $t = 0, 1, 2, \ldots$ for simplicity. This assumption will be relaxed by studying asynchronous measurements and actuations in Section 2.4. Let $\Delta d_i(t)$

stand for the reduction of load i at time t. Then, the total mismatch between load and generation at time t is

$$u(t) := -\sum_{i=1,\ldots,N} \Delta d_i(t) + \Delta g(t). \tag{2.1}$$

Without loss of generality, we let $\Delta d_i(t) > 0$ denote load reduction and $\Delta g(t) > 0$ generation drop, and therefore $u(t)$ is the load surplus. We consider a dynamic model of the power system, which takes u as the input and $\Delta\omega$ and $\Delta\overline{\omega}_i$ as the output. To simplify the analysis, we use a linearized model around the operating point [14], [16]. Let $x(t) \in \mathbb{R}^n$ denote the system state at time t. The elements in x depend on the specific power system model used in the algorithm. For example, they may include the valve position of the turbine, the mechanic power and the output voltage of the generator, and the frequency deviation $\Delta\omega$. We consider a stochastic disturbance to system state caused by environmental factors, e.g., change in temperature [87]. Such a disturbance is denoted by $\zeta \in \mathbb{R}^n$. Moreover, for every load i, the stochastic frequency measurement noise ξ_i is also considered. Then, the power system dynamic model is

$$\begin{aligned} x(t+1) &= Ax(t) + Bu(t) + \zeta(t), \\ \Delta\omega(t) &= Cx(t), \\ \Delta\overline{\omega}_i(t) &= \Delta\omega(t) + \xi_i(t). \end{aligned} \tag{2.2}$$

In this model, the frequency deviation $\Delta\omega$ is one element in the state x, and therefore the matrix $C \in \mathbb{R}^{1\times n}$ has one element 1 and other elements 0.

We assume, for all $t, s \geq 0$ and all $i, j \in V$, that the process disturbance ζ and the measurement noise ξ_i have zero mean, and are uncorrelated spatially and temporally and with each other, i.e., their covariances satisfy

$$\begin{aligned} \mathbb{E}\left[\zeta(t)\zeta(s)^T\right] &= Q\delta_{ts}, \\ \mathbb{E}\left[\xi_i(t)\xi_j(s)\right] &= W\delta_{ts}\delta_{ij}, \end{aligned} \tag{2.3}$$

where $Q \in \mathbb{R}^{n\times n}$ is positive semi-definite, $W \geq 0$, and δ_{ts} and δ_{ij} denote the Kronecker delta function. Here we assume that every load performs frequency measurement independently at every time step, so the measurement noise is independent across the loads and not correlated over time. Moreover, we assume the noises at different loads have the same variance.

Remark 2.1. There are power systems in which the electrical distances between different parts are not negligible. These systems cannot be accurately modeled by

a single generator. In Chapter 3, we model such a system as a network of multiple generators connected by transmission lines. In the multi-machine model, we mainly focus on the effects of network structure on load control; therefore, we will consider a simple swing dynamic model of generators, in contrast to the more general model in (2.2). We also ignore the process disturbance and the measurement noise for multi-machine networks. In the current chapter, however, we focus on capturing the underlying dynamics in more detail. □

Optimal load control

Without loss of generality, suppose the generation drops by a positive constant Δg at time 0. In response, load i will be reduced by $\Delta d_i(t)$ for $t \geq 0$. As $t \to \infty$, we want $\Delta d_i(t)$ to converge to some $\Delta d_i^* \in [0, \overline{d}_i]$, where $\overline{d}_i$ is the maximum reduction of load i allowed by appliance specification or user preference. Moreover, we desire Δd_i^* to be an optimal solution to the following optimization problem:

OLC (single machine):

$$\begin{aligned} \min_{\Delta d_i \in [0, \overline{d}_i]} \quad & \sum_{i=1}^{N} c_i(\Delta d_i) \\ \text{subject to} \quad & \Delta g - \sum_{i=1}^{N} \Delta d_i = 0, \end{aligned} \tag{2.4}$$

where $c_i(\Delta d_i)$ is the *disutility* due to interrupting the normal usage and compromising the end-use function of appliances [9][28]. By solving OLC (2.4), the total load and generation is rebalanced, which essentially stabilizes and restores the frequency to its nominal value, in a manner that minimizes the total end-use disutility.

For feasibility of OLC, we assume $\sum_{i=1}^{N} \overline{d}_i - \Delta g > 0$. This assumption holds if a large enough group of loads participate in frequency control. We make the following assumptions on the disutility functions c_i such that OLC is a convex problem.

Assumption 2.1. For all $i = 1, \ldots, N$, the function c_i is increasing, strictly convex, and twice continuously differentiable, on $[0, \overline{d}_i]$.

Assumption 2.2. For all $i = 1, \ldots, N$, there exists $\alpha_i > 0$, such that $c_i''(\Delta d_i) \geq 1/\alpha_i$ for all $\Delta d_i \in [0, \overline{d}_i]$. Let $\overline{\alpha} := \max_{i=1,\ldots,N} \alpha_i$.

Remark 2.2. The choice of disutility functions is based on physical characteristics of loads and user comfort levels. Example functions can be found for air conditioners in [88] and plug-in electric vehicles in [89]. See, e.g., [19], [90], [91], [92] for other disutility functions that satisfy Assumptions 2.1 and 2.2. □

Solving OLC using a traditional centralized scheme requires a control center and two-way communication between the loads and the center: load-to-center communication to collect information like disutility functions and capacities of load reduction, and center-to-load communication to send the control signals $\Delta d_i(t)$. This centralized scheme has the following limitations in implementation. First, it requires the center to maintain connections with all the loads and perform computation for the whole system-level problem. If a fault occurs to the center or the communication infrastructure, the whole system control function may fail. Second, due to privacy issues, the users may not want to reveal information about their power usage to the system operator in the control center.

As an alternative, we design a more robust, scalable, and privacy-preserving decentralized scheme where every load computes a small piece of the overall problem, and exchanges information with a small number of its neighbors. For the purpose of such a design, we consider solving the dual problem of OLC. Taking p as the dual variable, the dual problem of OLC is

$$\max_{p\in\mathbb{R}} \ \Psi(p) \quad := \quad \sum_{i=1}^{N} \Psi_i(p) + p\Delta g \tag{2.5}$$

where

$$\Psi_i(p) \quad := \quad \min_{\Delta d_i\in[0,\overline{d}_i]} c_i(\Delta d_i) - p\Delta d_i. \tag{2.6}$$

Under Assumption 2.1, given $p \in \mathbb{R}$, the problem

$$\min_{\Delta d_i\in[0,\overline{d}_i]} c_i(\Delta d_i) - p\Delta d_i \tag{2.7}$$

has a unique minimizer

$$\Delta d_i(p) = \min\left\{\max\{(c_i')^{-1}(p), 0\}, \overline{d}_i\right\}. \tag{2.8}$$

Note that the inverse function of c_i' exists over $[c_i'(0), c_i'(\overline{d}_i)]$ since c_i' is continuous and strictly increasing by Assumption 2.1. Since c_i is convex for all $i = 1, \ldots, N$ and OLC has affine constraints, Slater's condition implies that there is zero duality gap between OLC and its dual (2.5), and the optimal solution of (2.5), denoted by p^*, is attained [93, Sec. 5.5.3]. It follows that $\Delta d(p^*) := [\Delta d_1(p^*), \ldots, \Delta d_N(p^*)]^T$ is primal feasible and optimal [93, Sec. 5.5.2]. Moreover, it is easy to show that, for any given $\underline{p}$ and $\overline{p}$ such that $\underline{p} \le \min_i \ c_i'(0)$ and $\overline{p} \ge \max_i \ c_i'(\overline{d}_i)$, the problem

(2.5) has at least one optimal point $p^* \in [\underline{p}, \overline{p}]$. Hence, we can constrain p to $[\underline{p}, \overline{p}]$. Therefore, instead of solving OLC directly, we solve its modified dual problem

Dual OLC:

$$\max_{p\in[\underline{p},\overline{p}]} \Psi(p) \quad = \quad \sum_{i=1}^{N} \Psi_i(p) + p\Delta g. \tag{2.9}$$

Informally, the decentralized algorithm is as follows (see Section 2.3 for a formal treatment). Each load i updates its value of dual variable p at time t as

$$p_i(t) \quad = \quad \max\left\{\min\{p_i(t-1) + \gamma(t)u(t-1), \overline{p}\}, \underline{p}\right\}, \tag{2.10}$$

where $\gamma(t) > 0$ is some stepsize, and $u(t-1) = \Delta g - \sum_{i=1}^{N} \Delta d_i(t-1)$ is the mismatch between load and generation at time $(t-1)$. Then, load i calculates its load reduction at time t as $\Delta d_i(t) = \Delta d_i(p_i(t))$,[1] where $\Delta d_i(\cdot)$ is defined in (2.8). It can be observed from (2.5)–(2.6) that $u(t-1)$ is the gradient of the dual objective function Ψ in (2.9), if the dual variable $p = p_1(t-1) = \cdots = p_N(t-1)$. Therefore, this decentralized algorithm is essentially a gradient projection method [93] applied to Dual OLC. To implement this algorithm with frequency responsive loads, loads should be able to estimate u from local frequency measurements. Our estimation method is introduced in the next section.

2.2 Estimating load-generation mismatch

In Section 2.1, we informally introduced a decentralized algorithm to solve the optimal load control problem OLC. The algorithm requires every load to know $u = \Delta g - \sum_{i=1}^{N} \Delta d_i$, the total mismatch between load and generation. We now introduce a method for individual loads to estimate u from local measurements of frequency deviation. Since u is the input to the state-space model (2.2), we call this method *input estimation*.

In input estimation, load i uses frequency measurements $\Delta\overline{\omega}_i(1), \ldots, \Delta\overline{\omega}_i(t)$ to estimate $u(0), \ldots, u(t-1)$. In (2.2), we use $\hat{x}_i(t|s)$ and $\hat{u}_i(t|s)$ respectively to denote the estimates of $x(t)$ and $u(t)$ with frequency measurements up to time s. Starting from $\hat{x}_i(1|0)$, the input estimation is recursively [94]:

$$\begin{aligned} \hat{u}_i(t-1|t) &= M\left(\Delta\overline{\omega}_i(t) - C\hat{x}_i(t|t-1)\right), \\ \hat{x}_i(t|t) &= \hat{x}_i(t|t-1) + B\hat{u}_i(t-1|t), \\ \hat{x}_i(t+1|t) &= A\hat{x}_i(t|t), \end{aligned} \tag{2.11}$$

[1] We abuse notation by letting $\Delta d_i(\cdot)$ be either a function of time t or a function of the dual variable p_i, depending on the context.

where $M := (CB)^{-1}$. Note that $B \in \mathbb{R}^{n\times 1}$ and both $u(t)$ and CB are scalars. Therefore we only need the following assumption to ensure the existence of M.

Assumption 2.3. The matrices C and B satisfy $CB \neq 0$.

Assumption 2.3 holds for many practical power systems, including the one we will use in the case studies in Section 2.5.

The input estimation (2.11) gives an unbiased and minimum variance estimate of the state and the input. The covariance of $x_i(t|t)$, denoted by $\Sigma^i_{t|t} \in \mathbb{R}^{n\times n}$, is given recursively by

$$\Sigma^i_{t+1|t+1} = (I_n - BMC)(A\Sigma^i_{t|t}A^T + Q)(I_n - BMC)^T + BMWM^TB^T, \quad (2.12)$$

where Q and W are defined in (2.3). Denote the input estimate error by $e_i(t) := \hat{u}_i(t|t+1) - u(t)$. Define the σ-algebra $\mathcal{F}_{t-1} := \sigma\left(e_i(\tau - 1); i = 1, \ldots, N, 1 \leq \tau \leq t\right)$ which includes the historical information before time t for all the loads. The expectation and variance of $e_i(t)$ conditioned on $\mathcal{F}_{t-1}$ are [94]:

$$\mathbb{E}\left[e_i(t)|\mathcal{F}_{t-1}\right] = 0 \quad (2.13)$$

and

$$\mathbb{E}\left[(e_i(t))^2\,|\mathcal{F}_{t-1}\right] = \frac{CA\Sigma^i_{t|t}A^TC^T + W}{(CB)^2}. \quad (2.14)$$

The following proposition provides a condition under which $\mathbb{E}\left[(e_i(t))^2\,|\mathcal{F}_{t-1}\right]$ converges to a constant as $t \to \infty$.

Proposition 2.1. Denote the eigenvalues of $(I_n - B(CB)^{-1}C)A$ by λ_s, $s = 1, \ldots, n$. If $|\lambda_s| < 1$ for all $s = 1, \ldots, n$, then

$$\lim_{t\to\infty} \mathbb{E}\left[(e_i(t))^2\,|\mathcal{F}_{t-1}\right] = \sigma^2_\infty \quad (2.15)$$

where σ^2_∞ is a constant determined by A, B, C, Q, and W, and independent of i.

Proof. See Appendix 2.A. □

For any power system model in the form of (2.2), we can check a priori whether the condition in Proposition 2.1 is satisfied. However, the implications of this condition still need to be understood in future studies.

The following corollary, which is a straightforward consequence of Proposition 2.1, gives a bound on the variance of the input estimate error.

Corollary 2.1. If the condition for Proposition 2.1 holds, then $\mathbb{E}\left[(e_i(t))^2 \,|\mathcal{F}_{t-1}\right] \leq \overline{\sigma}^2$ for all $i = 1, \ldots, N$ and all $t \geq 0$, where $\overline{\sigma}^2$ is a constant which depends on A, B, C, Q, W, and the initial covariance $\Sigma^i_{0|0}$ for all $i = 1, \ldots, N$.

With the input estimation (2.11), every load can get a local estimate of u. The estimates of different loads i may not be the same, due to different realizations of measurement noise ξ_i for different i. By (2.10), the inconsistencies of estimates of u lead to inconsistencies of p_i between different loads i. However, in the decentralized algorithm informally given in Section 2.1, we desire p_i to converge to the optimal point of Dual OLC for all $i = 1, \ldots, N$. Therefore, the inconsistencies of p_i between the loads should be eliminated or mitigated. In Section 2.3 below, we will introduce a method to mitigate such inconsistencies. Then, we will formally propose the decentralized load control algorithm and prove its convergence.

2.3 Decentralized load control: algorithm and convergence

In this section, we introduce a method to mitigate the inconsistencies of p_i between different loads, and describe formally the decentralized, frequency-based algorithm that solves the optimal load control problem OLC. Then, we discuss the communication architecture that supports this algorithm. We also present convergence results of the proposed algorithm.

Decentralized load control algorithm

The decentralized algorithm was informally discussed in Section 2.1. The dual variable update in (2.10) requires estimating u locally. As shown in Section 2.2, there may be inconsistencies between local estimates of u, and hence between p_i, for different loads i.

We use neighborhood communication between the loads to mitigate such inconsistencies. The information flow of such communication can be regarded as an undirected graph, since the communication is in two ways. In this graph, denote the set of neighbors of load i at time t as $\mathcal{N}(i,t)$. Load i is assigned a weight $r_{ij}(t)$ for all $j \in \mathcal{N}(i,t)$, and a weight $r_{ii}(t)$ for itself. Note that if $j \in \mathcal{N}(i,t)$ then $i \in \mathcal{N}(j,t)$. We make $r_{ij}(t) = r_{ji}(t)$, and can always find the weights that satisfy

$$\sum_{j=i, j\in\mathcal{N}(i,t)} r_{ij}(t) = 1, \qquad \sum_{j=i, j\in\mathcal{N}(i,t)} r_{ji}(t) = 1. \tag{2.16}$$

Other conditions on the weights will be discussed later in this section. Through neighborhood communication, load i receives the values $p_j(t)$ of the dual variable

from all $j \in \mathcal{N}(i,t)$, and calculates their average value, denoted by $q_i(t)$, as

$$q_i(t) = \sum_{j=i, j\in\mathcal{N}(i,t)} r_{ij}(t) p_j(t). \tag{2.17}$$

This averaging procedure is typically used in consensus algorithms [95]. Consensus, in our problem, means that the loads seek agreement on the values of the dual variable p. In (2.17), q_i is an auxiliary variable which denotes a local average of the values of the dual variable across load i and its neighbors. As the algorithm iterates, this local averaging propagates to a global agreement on the values of the dual variable throughout the network. Combining such a consensus procedure with the estimation of u in Section 2.2, we have the following decentralized algorithm to solve OLC (2.4) and its dual (2.9).

Algorithm 2.1. *Decentralized load-side frequency control for single-machine systems*

At time $t = 0$, the following information is known to all loads $i = 1, \ldots, N$: the matrices A, B and C in system model (2.2), the lower bound $\underline{p}$ and upper bound $\overline{p}$ defined in Section 2.1, and a sequence of positive stepsizes $\{\gamma(t), t = 1, 2, \ldots\}$ which is the same for all the loads. Each load i starts from an arbitrary initial state estimate $\hat{x}_i(1|0)$ and an initial value of dual variable $q_i(0)$.

At time instants $t = 1, 2, \ldots$, every load i:

1. Measures the frequency deviation $\Delta\overline{\omega}_i(t)$, and calculates $\hat{u}_i(t-1|t)$ using the input estimation (2.11).

2. Updates the value of dual variable according to

$$p_i(t) = \max\left\{\min\{q_i(t-1) + \gamma(t)\hat{u}_i(t-1|t), \overline{p}\}, \underline{p}\right\} \tag{2.18}$$

   and transmits $p_i(t)$ to all of its neighbors $j \in \mathcal{N}(i,t)$.

3. Receives the $p_j(t)$ from all $j \in \mathcal{N}(i,t)$, and calculates $q_i(t)$ as (2.17).

4. Computes load reduction $\Delta d_i(t) = \Delta d_i(q_i(t))$ where $\Delta d_i(\cdot)$ is defined in (2.8).

Before proving the convergence of Algorithm 2.1, we first introduce the neighborhood communication supporting the information exchange in (2.17), and other conditions on $r_{ij}(t)$ besides (2.16), which are necessary for the convergence of Algorithm 2.1.

Neighborhood area communication

As an example, we take the smart grid communication architecture proposed by Trilliant, Inc. [96] shown in Fig. 2.2.

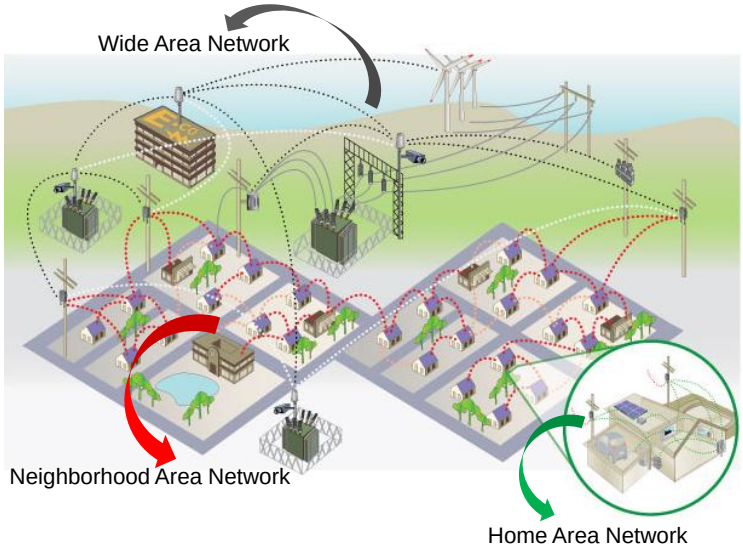

Figure 2.2: The home area network (HAN) supports the communication between appliances and smart meters. The neighborhood area network (NAN), which is used in our load control, aids the communication between utilities and smart meters. The wide area network (WAN) aids the long range communication between substations. This figure is a slightly modified version of a similar figure in [96].

The load control scheme given by Algorithm 2.1 does not rely on communication between all the loads and a control center. Instead, it uses communication between each load and its neighbors. This neighborhood communication uses mainly a neighborhood area network (NAN). In NAN, reliable, scalable, fast responding and cost-effective communication technologies such as 802.2.15.4/ZigBee are widely used to facilitate the implementation of the decentralized load control.

For the convergence proof of Algorithm 2.1, we make the following assumption on the weights $r_{ij}(t)$ in (2.17).

Assumption 2.4. There exists a scalar $0 < \eta < 1$ such that for all $i = 1, \ldots, N$ and all $t \geq 0$, we have $r_{ij}(t) \geq \eta$ if $j = i$ or $j \in \mathcal{N}(i,t)$, and $r_{ij}(t) = 0$ otherwise.

With Assumption 2.4, equation (2.17) simplifies to

$$q_i(t) \quad = \quad \sum_{j=1}^{N} r_{ij}(t) p_j(t). \tag{2.19}$$

Moreover, in order to make the information at load j affect load i infinitely often, we assume that within any fixed period of time, the set of communication links which have appeared form a connected, undirected graph. Define $E_t := \{(i,j)|r_{ij}(t) > 0\}$ to be the set of undirected links at time t. The connectivity requirement above is formally stated in the following assumption.

Assumption 2.5. There exists a integer $Q \geq 1$ such that the graph $(V, \bigcup_{\tau=1,\ldots,Q} E_{t+\tau-1})$ is connected for all t.

In reality, the NAN may have specific topologies, e.g., bus, ring, star, linear topology, or mixed topologies, as discussed in [97], [98]. All these topologies satisfy Assumption 2.5. However, the convergence analysis does not require any additional assumptions on the topology beyond Assumption 2.5. We will consider a realistic topology in case studies in Section 2.5.

Define $R(t)$ to be the matrix with (i,j)-th entry $r_{ij}(t)$, and define $\Phi(t,s) := R(t)R(t-1)\ldots R(s+1)$. The following result given by [95, Lemma 3.2] will be used in the convergence proof of Algorithm 2.1:

$$\left|[\Phi(t,s)]_{ij} - \frac{1}{N}\right| \leq \theta\beta^{t-s}, \tag{2.20}$$

where

$$\theta = \left(1 - \frac{\eta}{4N^2}\right)^{-2}, \qquad \beta = \left(1 - \frac{\eta}{4N^2}\right)^{\frac{1}{Q}}. \tag{2.21}$$

Convergence of Algorithm 2.1

Now we present results regarding the convergence of Algorithm 2.1. We first consider the case where the sequence $\{\gamma(t), t = 1,2,\ldots\}$ of stepsizes converges to some nonnegative constant. Theorem 2.1 gives a bound on the difference between the maximal expected value of the dual objective function Ψ and the optimal value of Dual OLC, denoted by Ψ^*.

Theorem 2.1. Suppose Assumptions 2.1–2.5 hold. If $\lim_{t\to\infty}\gamma(t) = \gamma \geq 0$ and $\sum_{t=1}^{\infty}\gamma(t) = \infty$, then, for all $i = 1,\ldots,N$,

$$\limsup_{t\to\infty}\mathbb{E}[\Psi(p_i(t))] \geq \Psi^* - \frac{\gamma(G^2+\overline{\sigma}^2)}{2} - \gamma G(\overline{\alpha}NL+G)\left(2+\frac{N\theta\beta}{1-\beta}\right), \tag{2.22}$$

where $G := \max\left\{\left|\sum_{i=1}^{N}\overline{d}_i - \Delta g\right|, |\Delta g|\right\}$, $\overline{\sigma}$ is the bound on input estimate error in Corollary 2.1, $\overline{\alpha}$ is defined in Assumption 2.2, N is the number of loads, and $L := \overline{p} - \underline{p}$.

Proof. See Appendix 2.B. □

Taking $\gamma = 0$ in (2.22), we have the following corollary, which is straightforward from Theorem 2.1.

Corollary 2.2. Suppose Assumptions 2.1–2.5 hold. If $\lim_{t\to\infty} \gamma(t) = 0$ and $\sum_{t=1}^{\infty} \gamma(t) = \infty$, then, for all $i = 1, \ldots, N$,

$$\limsup_{t\to\infty} \mathbb{E}\left[\Psi\left(p_i(t)\right)\right] \quad = \quad \Psi^*.$$

Define $\Delta d(t) = [\Delta d_1(t), \ldots, \Delta d_N(t)]^T$. With further restrictions on the stepsize $\gamma(t)$, the sequence $\{\Delta d(t),\ t = 1, 2, \ldots\}$ produced by Algorithm 2.1 converges almost surely to the optimal point of OLC, as stated in Theorem 2.2.

Theorem 2.2. Suppose Assumptions 2.1–2.5 hold, $\sum_{t=1}^{\infty} \gamma(t) = \infty$, and $\sum_{t=1}^{\infty} \gamma(t)^2 < \infty$. Then, for all $i = 1, \ldots, N$, the sequence $\{q_i(t)\}$ converges to the same optimal point of Dual OLC with probability 1 and in mean square. Moreover, the sequence $\{\Delta d(t)\}$ converges to the optimal point of OLC with probability 1.

Proof. See Appendix 2.C. □

In Algorithm 2.1, neighborhood communication is used to mitigate the effect of measurement noise. Now we consider a special case where the process disturbance ζ and the measurement noise ξ_i for all $i = 1, \ldots, N$ are zero. In this case, the following theorem shows that OLC can be solved by using a simplified version of Algorithm 2.1 which does not need neighborhood communication.

Theorem 2.3. Suppose Assumptions 2.1–2.3 hold, and the following conditions are satisfied:

1. $\zeta(t) = 0$ and $\xi_i(t) = 0$ for all $i = 1, \ldots, N$ and $t \geq 0$.
2. In Algorithm 2.1, for all $i = 1, \ldots, N$, $\hat{x}_i(1|0) = x(1)$, and $q_i(0)$ are the same.
3. For all $i = 1, \ldots, N$ and all $t \geq 0$, $r_{ii}(t) = 1$, and $\mathcal{N}(i, t) = \emptyset$.
4. Constant stepsize $\gamma(t) = \gamma$, where γ satisfies $0 < \gamma < 2/(\overline{\alpha}N)$, is used.

Then, for all $i = 1, \ldots, N$, any limit point (at least one exists) of the sequence $\{(\Delta d(t), q_i(t)),\ t = 1, 2, \ldots\}$ is primal-dual optimal for OLC and Dual OLC.

Proof. See Appendix 2.D. □

The algorithm and convergence proof above are based on an underlying assumption that all the loads simultaneously and synchronously measure their local frequency deviations and take control actions. In practice, this is obviously not the case. In the next section we will investigate convergence of the proposed scheme under asynchronous measurements and actuations with bounded time delays.

2.4 Asynchronous measurements and actuations

In this section, we ignore stochastic process disturbance and measurement noise, by assuming $\zeta(t) = 0$ and $\xi_i(t) = 0$ for all $i = 1, \ldots, N$ and $t \geq 0$.

In the asynchronous setting, the frequency deviation $\Delta\omega(t)$ at time t is accurately measured by load $i = 1, \ldots, N$ at some time within the interval $[t + r(i,t) - 1, t + r(i,t))$, where $r(i,t) \in \mathbb{N}$ is an arbitrary fixed number. In the time interval $[t-1, t)$, load i measures a set of frequency deviation signals, denoted by $\Omega_{i,t} = \{\Delta\hat{\omega}_{i,t}^1, ..., \Delta\hat{\omega}_{i,t}^{K_{i,t}}\}$, where $K_{i,t}$ is the number of measured frequency deviation samples ($\Omega_{i,t} = \emptyset$ and $K_{i,t} = 0$ means no frequency deviation signal is measured during $[t-1, t)$). Moreover, load i is able to change its power only at a subset of time instants, denoted by $T_i \subseteq \{0, 1, 2, \ldots\}$. For the asynchronous algorithm to converge, we make the following assumptions on $r(i,t)$ and T_i.

Assumption 2.6. For all $i = 1, \ldots, N$, $t \geq 0$, $l \in \{1, \ldots, K_{i,t}\}$ and $s \in \{1, \ldots, t\}$, if $\Delta\hat{\omega}_{i,t}^l$ is the measurement of $\Delta\omega_s$, then $\Delta\hat{\omega}_{i,t}^{l+1}$ is the measurement of $\Delta\omega_{s+1}$. Moreover, there exists $\bar{r} \in \mathbb{N}$ such that $r(i,t) \leq \bar{r}$ for all $i = 1, \ldots, N$ and $t \geq 0$.

Assumption 2.7. For all $i = 1, \ldots, N$, the difference between any two consecutive elements in T_i is bounded.

Assumption 2.6 says that the delayed frequency measurements arrive in order. In other words, the frequency deviation signal that occurs first is sensed first by the load. Moreover, the time delays in frequency measurement are bounded by $\bar{r}$. Assumption 2.7 says that the time between any consecutive change of any load is bounded.

With the settings above, we present the asynchronous algorithm as follows.

Algorithm 2.2. *Asynchronous decentralized load-side frequency control*

Suppose all loads $i = 1, \ldots, N$ know the matrices A, B and C in system model (2.2). Choose the same stepsize $\gamma > 0$ for all of them. At time $t = 0$, initialize each load i with $\hat{x}_0^i = x(0)$,[2] and $p_i(0) = 0$.

In the time interval $[t-1, t)$ for $t = 1, 2, \ldots,$ every load i:

1. At time $(t-1)$, sets $\hat{x}_{t-1}^i(0|0) = \hat{x}_{t-1}^i$, $p_{t-1}^i(0) = p_i(t-1)$.

2. Once load i measures a new frequency deviation signal $\Delta\hat{\omega}_{i,t}^k \in \Omega_{i,t}$ for $k = 1, \ldots, K_{i,t}$, it calculates $\hat{u}_{t-1}^i(k)$ by

$$\begin{aligned} \hat{x}_{t-1}^i(k|k-1) &= A\hat{x}_{t-1}^i(k-1|k-1), \\ \hat{u}_{t-1}^i(k) &= (CB)^{-1}(\Delta\hat{\omega}_{i,t}^k - C\hat{x}_{t-1}^i(k|k-1)), \\ \hat{x}_{t-1}^i(k|k) &= \hat{x}_{t-1}^i(k|k-1) + B\hat{u}_{t-1}^i(k), \end{aligned} \tag{2.23}$$

   and updates the value of p by

$$p_{t-1}^i(k) \;=\; p_{t-1}^i(k-1) + \gamma\hat{u}_{t-1}^i(k). \tag{2.24}$$

3. At time t, sets $\hat{x}_t^i = \hat{x}_{t-1}^i(K_{i,t}|K_{i,t})$ and $p_i(t) = p_{t-1}^i(K_{i,t})$.

4. If load i is able to change its power at time t, i.e., if $t \in T_i$, it determines this change as $\Delta d_i(t) = \Delta d_i(p_i(t))$ where $\Delta d_i(\cdot)$ is defined in (2.8); otherwise, $\Delta d_i(t) = \Delta d_i(t-1)$.

The following theorem states the convergence of Algorithm 2.2.

Theorem 2.4. Suppose Assumptions 2.1–2.3, 2.6, and 2.7 hold, and the stepsize γ satisfies

$$0 < \gamma < \frac{1}{\overline{\alpha}N/2 + 2\overline{r}}.$$

Then for all $i = 1, \ldots, N$, any limit point (at least one exists) of the sequence $\{(\Delta d(t), p_i(t)),\ t = 1, 2, \ldots\}$ is primal-dual optimal for OLC and Dual OLC.

Proof. See Appendix 2.E. □

[2] Assume the initial state of the system is known to all the loads.

2.5 Simulations

We take a relatively detailed example of the power system model introduced in (2.2) for simulation-based experiments. We use Algorithm 2.1 to control the loads when a sudden generation drop occurs, and observe frequency, load reduction and total end-use disutility to evaluate its performance. Additionally, we test the robustness of Algorithm 2.1 to model inaccuracies by letting the loads use a simplified, less accurate model to estimate the mismatch between total load and generation. We also discuss tradeoffs between the amount of communication and the performance of the proposed scheme, and the effect of the number of participating loads.

System settings

We consider an example of the single generator model (2.2), as shown in Fig. 2.3.

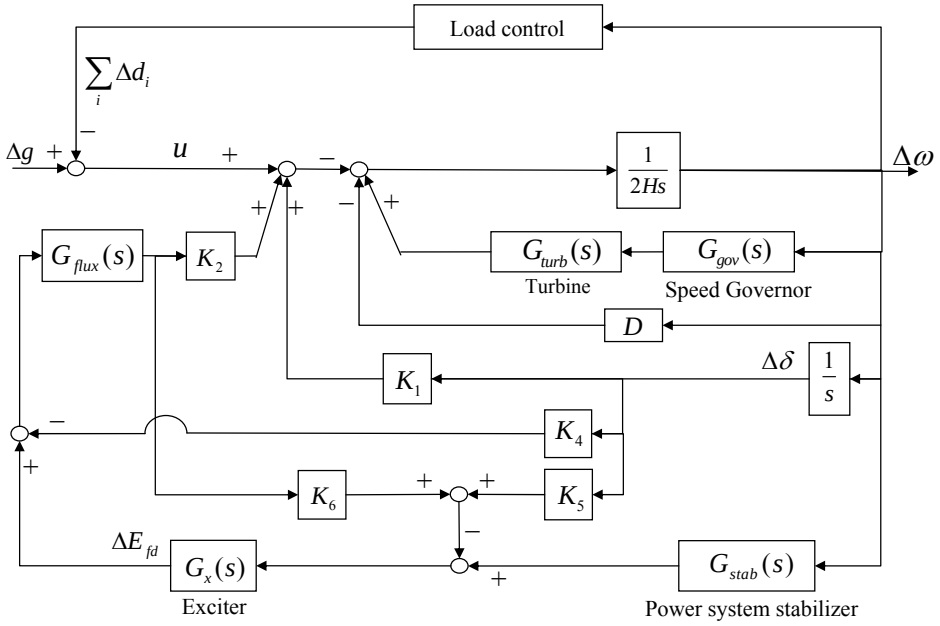

Figure 2.3: A single-machine power system model used in simulations.

This generator has a speed governor with the transfer function

$$G_{gov}(s) = -\frac{1}{R(1+sT_G)},$$

a turbine with the transfer function

$$G_{turb}(s) = \frac{(1+sF_{HP}T_{RH})}{(1+sT_{CH})(1+sT_{RH})},$$

and a power system stabilizer (PSS) with the transfer function

$$G_{stab}(s) = \frac{sK_w(1+sT_1)(1+sT_3)}{(1+sT_w)(1+sT_2)(1+sT_4)}.$$

The output voltage of the generator is regulated by an IEEE AC4A exciter [14], which has the transfer function

$$G_x(s) \quad = \quad \frac{K_A(1+sT_C)}{(1+sT_A)(1+sT_B)}.$$

Moreover, the flux decay transfer function of the generator is

$$G_{flux}(s) \quad = \quad \frac{K_3}{1+K_3\tau'_{d0}s}.$$

Table 2.1 gives the values of parameters used in the transfer functions above.

Param.	Value	Param.	Value (s)	Param.	Value (s)
K_A	200	H	5	T_1	0.2
K_1	1.0755	T_A	0.04	T_2	0.02
K_2	1.2578	T_B	12	T_3	0.4
K_3	0.3072	T_C	1	T_4	0.04
K_4	1.7124	τ'_{d0}	5.9	T_w	10
Param.	Value	Param.	Value (s)	Param.	Value (pu)
K_5	-0.0409	T_G	0.2	D	1
K_6	0.4971	T_{CH}	0.3	R	0.05
K_w	20	T_{RH}	7	F_{HP}	0.3

Table 2.1: Parameters used in the simulations of the single-machine system.

The continuous-time state-space form of the model above is

$$\begin{aligned} \dot{x} &= A_c x + B_c u, \\ \Delta\omega &= C_c x. \end{aligned}$$

Then, taking a sample time $\Delta t = 0.5$ s, we get the matrices A, B and C in (2.2) using the following equations:

$$\begin{aligned} A &= e^{A_c \Delta t}, \\ B &= A_c^{-1}(A - I_n)B_c, \\ C &= C_c. \end{aligned}$$

There are N controllable loads, which are placed and connected using a linear topology, the most commonly seen real-world topology for power distribution systems [98]. Each load i communicates directly with loads from $\max\{i-K, 1\}$ to $\min\{i+K, N\}$, as shown in Fig. 2.4.

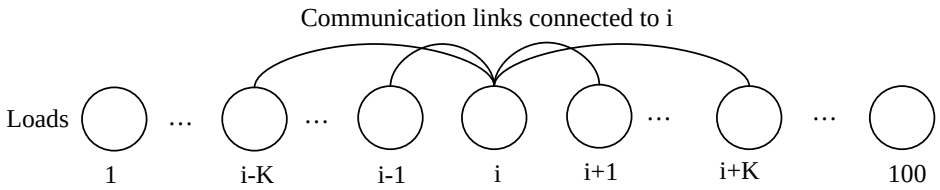

Figure 2.4: An example communication graph of loads.

Load i has a disutility function $c_i(\Delta d_i) = (\Delta d_i)^2/(2\alpha_i)$. In this section, we pick α_i subject to the uniform distribution on $[1, 3]$. The baseline power is $P_{base} = 200\,\text{MVA}$. For $i = 1, \ldots, N$, we have $\Delta d_i \in [0, \overline{d}_i]$. We choose $\overline{d}_i$ to be positive numbers such that $\sum_{i=1}^{N} \overline{d}_i = 0.30$ per unit (pu). Generation drop $\Delta g(t)$ makes two step changes resembling sudden generation loss events:

$$\Delta g(t) = \begin{cases} 0 & 0 \le t < 20 \text{ s} \\ 0.05 \text{ pu} & 20 \text{ s} \le t < 50 \text{ s} \\ 0.15 \text{ pu} & t \ge 50 \text{ s}. \end{cases}$$

The process disturbance ζ has covariance $Q = B(0.002\,\text{pu})^2 B^T$ for B obtained above. The measurement noise ξ_i for all $i = 1, \ldots, N$ has variance $W = (0.001 \text{ pu})^2$. In Algorithm 2.1, all the loads use a diminishing stepsize $\gamma(t) = \gamma(0)/(t^{0.8})$ for some arbitrarily selected $\gamma(0) > 0$, so that $\sum_{t=1}^{\infty} \gamma(t) = \infty$ and $\sum_{t=1}^{\infty} \gamma(t)^2 < \infty$. Therefore, all the conditions in Theorems 2.1 and 2.2 are satisfied.

Robustness to model inaccuracies

We compare the performance of the load control scheme Algorithm 2.1 between the two settings: "accurate modeling" and "simplified modeling." Under accurate modeling, loads use the accurate model given by matrices A, B and C for input estimation. Under simplified modeling, loads use a simplified, less accurate model, due to the practical consideration that the system operator or utility company may not reveal the exact system information to users because of privacy issues. There are multiple ways to simplify the system model. For example, in the model given by Fig. 2.3, we consider the swing dynamics only and ignore all the other parts, and, with the values of parameters given in Table 2.1, we have a simplified transfer function

$$\widetilde{G}(s) \;=\; -\frac{0.1555s + 0.0222}{s^2 + 0.9918s + 0.4666}$$

such that $\Delta\omega(s) = \widetilde{G}(s)u(s)$.

Figs. 2.5–2.7 respectively show the frequency, the total load reduction and the total end-use disutility with loads using different models. There are $N = 100$ loads, and every load communicates with $K = 5$ neighbors (except the loads at the two ends of the linear graph in Fig. 2.4).

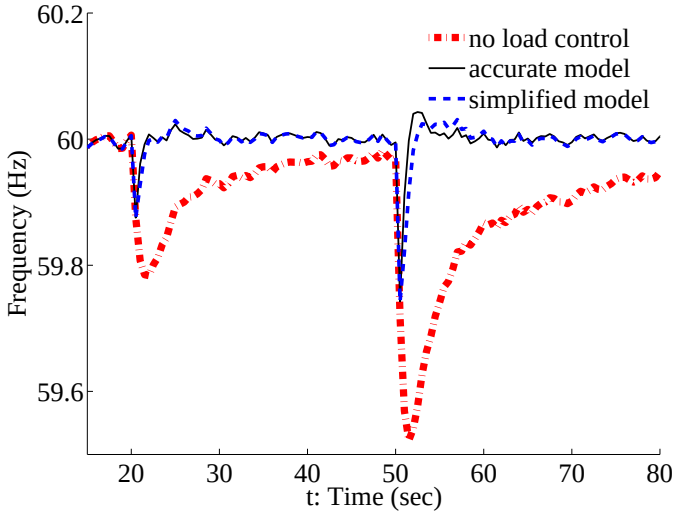

Figure 2.5: The frequency (N=100, K=5). The dash-dot line is the frequency without load control. The solid and dashed lines are those with load control where loads use different models.

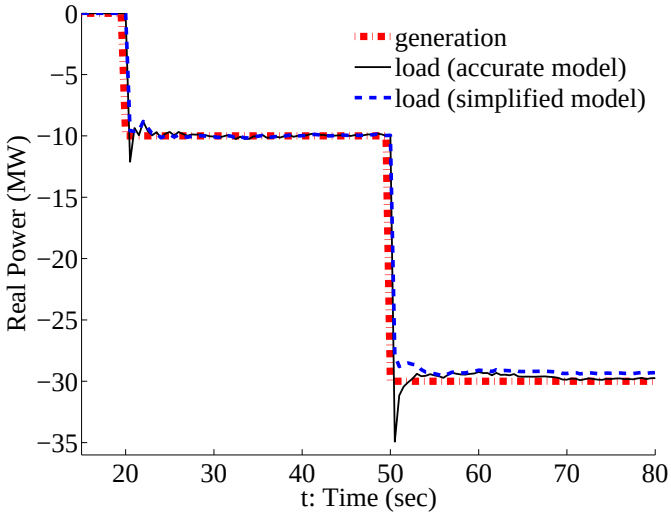

Figure 2.6: The total load reduction (N=100, K=5). The dash-dot line is the generation drop. The solid and dashed lines are total load reductions by load control where loads use different models.

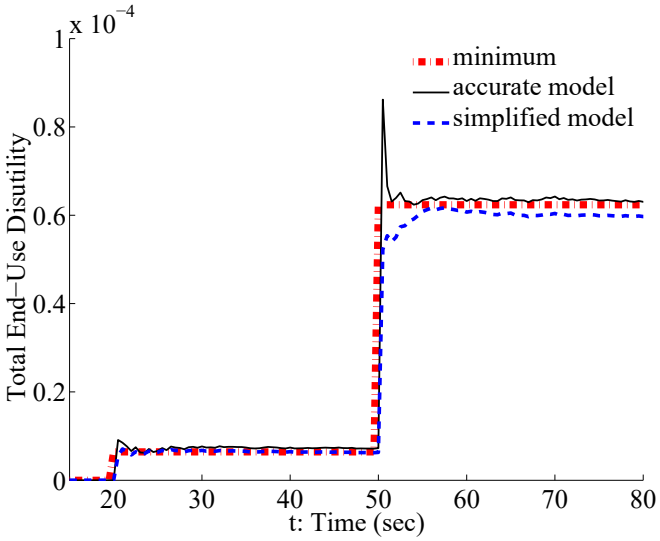

Figure 2.7: The total end-use disutility (N=100, K=5). The dash-dot line is the minimal disutility. The solid and dashed lines are trajectories of the disutility with load control where loads use different models.

In both scenarios of load control using different models, the frequency is recovered to 60 Hz faster than in the case without load control. The total load reduction follows the generation drop, and the total end-use disutility converges to the minimum, both within a short time. It takes 7 iterations (3.5 seconds) for the disutility to achieve and stay within ±5% of the new steady-state (minimum) value after the first generation drop, and 8 iterations (4 seconds) after the second. Moreover, all the results under the simplified model are close to those under the accurate model, which suggests the proposed scheme is robust to model inaccuracies considered here.

Tradeoffs between communication and performance

Theorem 2.3 states the convergence of Algorithm 2.1 without communication between loads, when there is no process disturbance or measurement noise in the system. Otherwise, communication is required to guarantee satisfactory performance of the proposed scheme. To demonstrate this, Figs. 2.8–2.10 respectively show the frequency, the total load reduction and the total end-use disutility when loads perform Algorithm 2.1 with $K = 0$, i.e., no communication between the loads. Constant stepsize $\gamma = 1.4/(\overline{\alpha}N)$ is used to satisfy the condition in Theorem 2.3.

Results show that without measurement noise, Algorithm 2.1 performs well without communication, as stated in Theorem 2.3. We relax the assumption in Theorem 2.3 by allowing non-zero process disturbance, and Algorithm 2.1 still works well

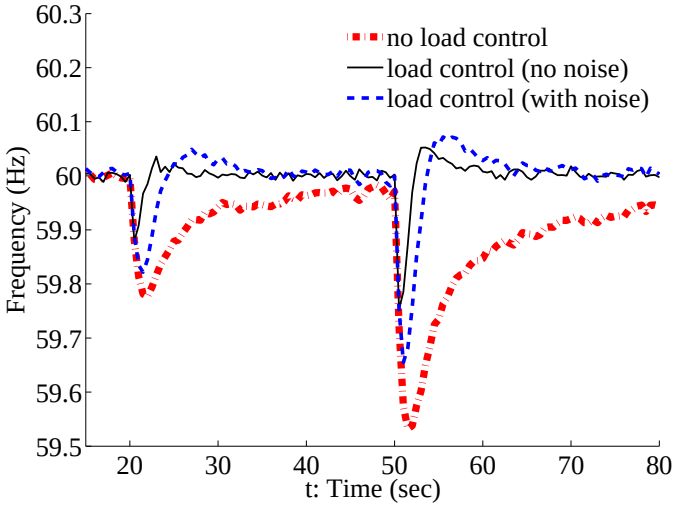

Figure 2.8: The frequency when there is no communication in load control (N=100, K=0). The dash-dot line is the frequency without load control. The solid and dashed lines are respectively the frequencies without and with measurement noise in load control.

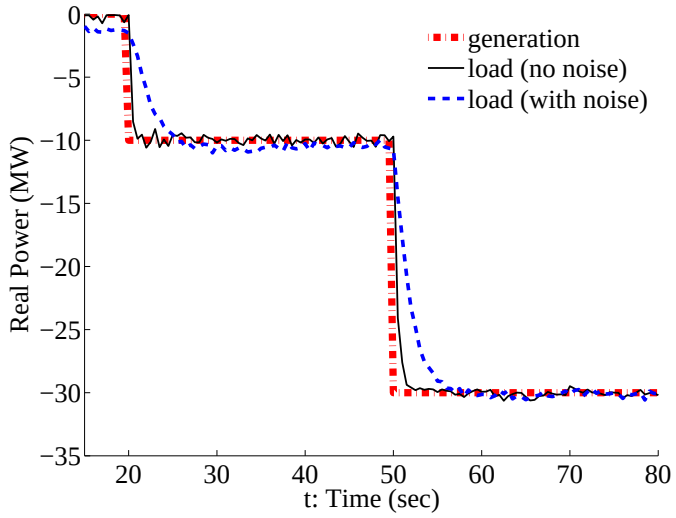

Figure 2.9: The total load reduction when there is no communication in load control (N=100, K=0). The dash-dot line is the generation drop. The solid and dashed lines are respectively the load reductions without and with measurement noise in load control.

without communication. However, when there is measurement noise, Algorithm 2.1 produces a lower nadir in frequency, a larger delay in load adjustment, and a disutility much higher than the minimum.

We further discuss tradeoffs between the amount of communication and the per-

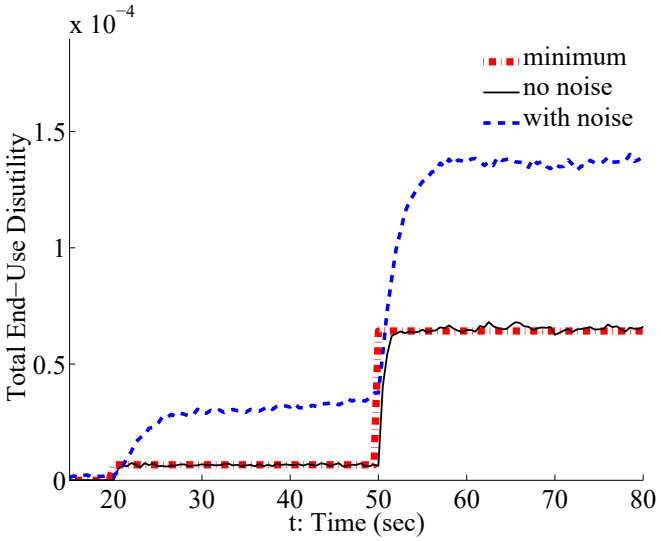

Figure 2.10: The total disutility when there is no communication in load control (N=100, K=0). The dash-dot line is the minimal disutility. The solid and dashed lines are respectively the disutility without and with measurement noise in load control.

formance of Algorithm 2.1. In the communication graph we use, as K grows, the connectivity gets stronger and more communication is used. We show the total end-use disutility with $K = 0, 1, 40$, in Fig. 2.11.

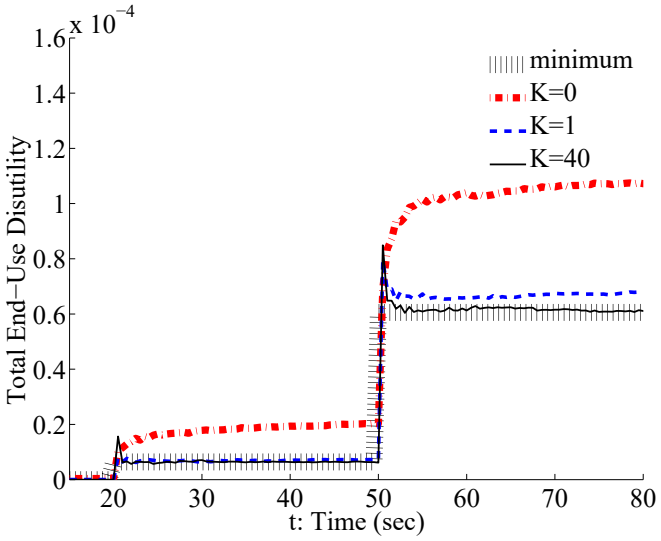

Figure 2.11: The total end-use disutility with different numbers K of neighbors in the load control (N=100).

We see from Fig. 2.11 and Fig. 2.7 (in which $K = 5$) that, with more communication, Algorithm 2.1 performs better by producing a total disutility closer to the minimum.

On the other hand, the results are significantly improved when K increases from 0 to 1, but not so distinguishable when increasing K from 5 to 40. It implies that the proposed scheme can effectively address frequency measurement noise, and receive most of its benefit, using a moderate amount of neighborhood communication.

Effects of the number of loads

We consider the effects of different numbers of loads that implement the decentralized load control Algorithm 2.1. Fig. 2.12 shows the total end-use disutility with $N = 10$, $N = 100$, and $N = 1000$. In all the three cases, every load communicates with the same number of neighbors $K = 5$. Moreover, the values of parameters in different cases are scaled so that they have the same minimal disutility.

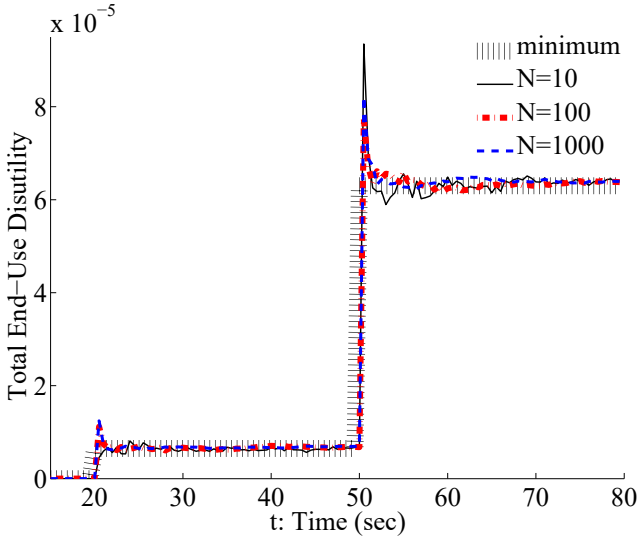

Figure 2.12: The total end-use disutility with different numbers N of loads (K=5).

We can see that the difference is negligible between different cases, which means the performance of the proposed scheme does not degrade as more and more loads participate. This result implies that the frequency-based, decentralized load control is suitable for large-scale deployment.

2.6 Conclusion

We proposed a decentralized optimal load control (OLC) scheme that rebalances power, stabilizes frequency, and restores frequency to 60 Hz, in a manner that minimizes total disutility, after a change in generation or load in a single-machine power system. In the proposed scheme, loads estimate the total load-generation mismatch from local frequency measurements. Neighborhood communication between loads

is added to mitigate the performance degradation caused by frequency measurement noise. Convergence of the proposed algorithm was proved, under synchronous and asynchronous measurements and actuations. Simulation-based experiments showed effectiveness of the proposed scheme, even when the loads use a simplified, less accurate system model to estimate the total load-generation mismatch. We also showed with simulations that the performance of the proposed scheme can be significantly improved with a small amount of communication, and is scalable to a large number of loads.

APPENDICES

2.A Proof of Proposition 2.1

Recall that $M = (CB)^{-1}$. The matrix $(I_n - BMC)Q(I_n - BMC)^T + BMWM^TB^T$ is positive semi-definite, since both Q and W are positive semi-definite. Then, if $|\lambda_s| < 1$ for all $s = 1, \ldots, n$, the equation

$$\begin{aligned}\Sigma =&(I_n - BMC)A\Sigma A^T(I_n - BMC)^T \\ &+ (I_n - BMC)Q(I_n - BMC)^T + BMWM^TB^T\end{aligned}$$

has a unique, positive semi-definite solution Σ^* [99]. Additionally, $\lim_{t\to\infty} \Sigma^i_{t|t}$ exists and is Σ^*. By (2.14), we have

$$\lim_{t\to\infty} \mathbb{E}\left[(e_i(t))^2 \,|\mathcal{F}_{t-1}\right] \;=\; \frac{CA\Sigma^*A^TC^T + W}{(CB)^2},$$

where the right-hand-side is independent of i and can be determined by A, B, C, Q, and W.

2.B Proof of Theorem 2.1

We first show two lemmas as a preparation for proving Theorem 2.1. Define $y(t) := \frac{1}{N}\sum_{i=1}^N p_i(t)$.

Lemma 2.1. Suppose Assumptions 2.4 and 2.5 hold. Then for all $i = 1, \ldots, N$ and $t \geq 0$,

$$\begin{aligned}|y(t) - p_i(t)| \leq&\theta\beta^t \sum_{j=1}^N |p_j(0)| + \theta \sum_{\tau=1}^{t-1} \gamma(\tau)\beta^{t-\tau} \sum_{j=1}^N (G + |e^j_{\tau-1}|) \\ &+ \frac{\gamma(t)}{N} \sum_{j=1}^N (G + |e^j_t|) + \gamma(t)(G + |e^i_t|),\end{aligned} \tag{2.25}$$

where $G = \max\{|\sum_{i=1}^N \overline{d}_i + \Delta g|, |\Delta g|\}$, and θ, β are defined in (2.21).

Proof. By the fact that $\Delta d_i \in [0, \overline{d}_i]$ for $i = 1, \ldots, N$, we have

$$\left|\sum_{i=1}^N \Psi'_i(q_i(t-1)) - \Delta g\right| \;=\; \left|-\sum_{i=1}^N \Delta d_i(q_i(t-1)) - \Delta g\right| \leq G.$$

Following [95, Lemma 4.1], we get Lemma 2.1. □

Lemma 2.2. Suppose Assumptions 2.1–2.5 hold. Then for all $t \geq 0$ and any $x \in [\underline{p}, \overline{p}]$, we have

$$\begin{aligned}\sum_{i=1}^{N} \left(q_i(t+1) - x\right)^2 \leq \quad & \sum_{i=1}^{N} \left(q_i(t) - x\right)^2 + 2\gamma(t+1) \sum_{i=1}^{N} e_t^i \left(q_i(t) - x\right) \\ & + 2\gamma(t+1)N \left(\Psi(y(t)) - \Psi(x)\right) \\ & + 2\gamma(t+1)N\overline{\alpha}L \sum_{i=1}^{N} |y(t) - p_i(t)| \\ & + \gamma^2(t+1) \sum_{i=1}^{N} (G + |e_t^i|)^2,\end{aligned} \tag{2.26}$$

where $L = \overline{p} - \underline{p}$.

Proof. By (2.19) and the convexity of squared norm, we have

$$\begin{aligned}\sum_{i=1}^{N} \left(q_i(t+1) - x\right)^2 \leq \quad & \sum_{i=1}^{N} \sum_{j=1}^{N} r_{ij}(t+1) \left(p_j(t+1) - x\right)^2 \\ & = \sum_{j=1}^{N} \left(p_j(t+1) - x\right)^2.\end{aligned} \tag{2.27}$$

Moreover, by (2.18) and the projection property, we have

$$\begin{aligned}\left(p_i(t+1) - x\right)^2 \leq & \left(q_i(t) + \gamma(t+1)(\sum_{j=1}^{N} \Psi_j'(q_j(t)) - \Delta g + e_t^i) - x\right)^2 \\ = \quad & \left(q_i(t) - x\right)^2 + 2\gamma(t+1)e_t^i \left(q_i(t) - x\right) \\ & + 2\gamma(t+1)\left(\sum_{j=1}^{N} \Psi_j'(q_j(t)) - \Delta g\right)\left(q_i(t) - x\right) \\ & + \gamma^2(t+1)\left(\sum_{j=1}^{N} \Psi_j'(q_j(t)) - \Delta g + e_t^i\right)^2.\end{aligned} \tag{2.28}$$

By mean value theorem [100], we have

$$\begin{aligned}& \left(\sum_{j=1}^{N} \Psi_j'(q_j(t)) - \Delta g\right) \sum_{i=1}^{N} (q_i(t) - x) \\ = \quad & N\left(\Psi'(y(t)) + \sum_{j=1}^{N} \Psi_j''(z_j(t))(q_j(t) - y(t))\right)(y(t) - x),\end{aligned} \tag{2.29}$$

where $z_i(t)$ is some value between $q_i(t)$ and $y(t)$.[3] To obtain (2.29), we use the fact $y(t) = \frac{1}{N}\sum_{i=1}^{N} q_i(t)$. By (2.27)–(2.29), we have

$$\begin{aligned}\sum_{i=1}^{N}\left(q_i(t+1)-x\right)^2 \le & \sum_{i=1}^{N}\left(q_i(t)-x\right)^2 \\ & + 2\gamma(t+1)N\left(\Psi'(y(t)) + \sum_{j=1}^{N}\Psi_j''(z_j(t))(q_j(t)-y(t))\right) \\ & \times\left(y(t)-x\right) + 2\gamma(t+1)\sum_{i=1}^{N} e_t^i\left(q_i(t)-x\right) \\ & + \gamma^2(t+1)\sum_{i=1}^{N}\left(\sum_{j=1}^{N}\Psi_j'(q_j(t)) - \Delta g + e_t^i\right)^2.\end{aligned} \tag{2.30}$$

By concavity of Ψ, we have

$$\Psi'(y(t))(y(t)-x) \quad \le \quad \Psi(y(t)) - \Psi(x). \tag{2.31}$$

We also have

$$\begin{aligned}& \left(\sum_{j=1}^{N}\Psi_j''(z_j(t))(q_j(t)-y(t))\right)(y(t)-x) \\ \le \quad & \overline{\alpha}L\sum_{j=1}^{N}|y(t)-q_j(t)| \le \overline{\alpha}L\sum_{j=1}^{N}|y(t)-p_j(t)|,\end{aligned} \tag{2.32}$$

where the first inequality is due to $\Psi_j''(z_j(t)) \le \alpha_i \le \overline{\alpha}$ (by Assumption 2.2) and the fact that $|y(t)-x| \le L$. The second inequality is due to convexity of the absolute value function. Moreover, since G is the bound on $|u(t)|$ for all t, we have

$$\begin{aligned}\left(\sum_{j=1}^{N}\Psi_j'(q_j(t)) - \Delta g + e_t^i\right)^2 &= (-u(t)+e_t^i)^2 \\ &\le (G+|e_t^i|)^2.\end{aligned} \tag{2.33}$$

Incorporating (2.31)–(2.33) into (2.30), we get Lemma 2.2. □

With Lemmas 2.1 and 2.2, we can complete the proof of Theorem 2.1. In (2.26), we take x as p^*, which is an optimal point of Dual OLC. We then add up (2.26) over

[3] At the point where Ψ_i' is not differentiable, Ψ_i'' should be replaced by the subgradient of Ψ_i', without influencing the proof.

$t = 0, \ldots, T-1$, which leads to

$$\begin{aligned}\sum_{i=1}^{N} \mathbb{E}[(q_i(T) - p^*)^2] \leq \quad & \sum_{i=1}^{N} \mathbb{E}[(q_i(0) - x)^2] \\ & + 2N \sum_{t=0}^{T-1} \gamma(t+1) \left(\mathbb{E}[\Psi(y(t))] - \Psi^*\right) \\ & + 2N\overline{\alpha}L \sum_{t=0}^{T-1} \gamma(t+1) \sum_{i=1}^{N} \mathbb{E}(|y(t) - p_i(t)|) \\ & + N(G^2 + \overline{\sigma}^2) \sum_{t=0}^{T-1} \gamma^2(t+1).\end{aligned}$$

It follows that

$$\begin{aligned}& 2N \sum_{t=0}^{T-1} \gamma(t+1) \left\{ \mathbb{E}[\Psi(y(t))] - \Psi^* + \overline{\alpha}L \sum_{i=1}^{N} \mathbb{E}(|y(t) - p_i(t)|) + \frac{\gamma(t+1)(G^2 + \overline{\sigma}^2)}{2} \right\} \\ & \quad \geq - \sum_{i=1}^{N} \mathbb{E}[(q_i(0) - x)^2].\end{aligned}$$

Then, with $\lim_{t\to\infty} \gamma(t) = \gamma$ and $\sum_t \gamma(t) = \infty$, we have

$$\limsup_{t\to\infty} \mathbb{E}[\Psi(y(t))] \geq \Psi^* - \overline{\alpha}L \sum_{i=1}^{N} \limsup_{t\to\infty} \mathbb{E}(|y(t) - p_i(t)|) - \frac{\gamma(G^2 + \overline{\sigma}^2)}{2}. \quad (2.34)$$

On the other hand, we have

$$\begin{aligned}\mathbb{E}[\Psi(p_i(t)) - \Psi(y(t))] &\geq -\mathbb{E}[\Psi'(z_i(t))(p_i(t) - y(t))] \\ &\geq -G\, \mathbb{E}(|y(t) - p_i(t)|),\end{aligned} \quad (2.35)$$

where $z_i(t)$ is some value between between $p_i(t)$ and $y(t)$. Moreover, taking the expectation on both sides of (2.25) and considering $\mathbb{E}(|e_i(t)|) = 0$ from (2.13), we have

$$\mathbb{E}(|y(t) - p_i(t)|) \quad \leq \quad \theta\beta^t \sum_{j=1}^{N} |p_j(0)| + \theta NG \sum_{\tau=1}^{t-1} \gamma(\tau)\beta^{t-\tau} + 2\gamma(t)G. \quad (2.36)$$

By [95, Lemma 3.1(a)], we have $\lim\limits_{t\to\infty} \sum\limits_{\tau=1}^{t-1} \gamma(\tau)\beta^{t-\tau} = \frac{\beta\gamma}{1-\beta}$. Therefore,

$$\lim_{t\to\infty} \mathbb{E}(|y(t) - p_i(t)|) \quad \leq \quad \gamma G \left(2 + \frac{N\theta\beta}{1-\beta}\right). \quad (2.37)$$

Incorporating (2.35)(2.37) into (2.34), we have (2.22), i.e., Theorem 2.1 is proved.

2.C Proof of Theorem 2.2

With Assumptions 2.1–2.5, Equation (2.13), and Corollary 2.1, all the conditions for [95, Theorem 6.2] are satisfied. Hence for all $i = 1, \ldots, N$ the sequence $\{q_i(t), t = 1, 2, \ldots\}$ converges to the same optimal point of Dual OLC with probability 1 and in mean square. Define $\Delta d(q(t)) = [\Delta d_1(q_1(t)), \ldots, \Delta d_N(q_N(t))]^T$. By the result in Section 2.1, $\{\Delta d(q(t)), t = 1, 2, \ldots\}$ converges to the optimal point of the primal problem OLC with probability 1. Since $\Delta d(t) = \Delta d\,(q(t))$, Theorem 2.2 holds.

2.D Proof of Theorem 2.3

It is easy to show that, for all $i = 1, \ldots, N$ and $t \geq 0$, if $\zeta(t) = 0$, $\xi_i(t) = 0$, and $\hat{x}_i(1|0) = x(1)$, then $\hat{u}_i(t-1|t) = u(t-1)$. Moreover, since $r_{ii}(t) = 1$, and $\mathcal{N}(i,t) = \emptyset$, by (2.17), $q_i(t) = p_i(t)$ for all $i = 1, \ldots, N$ and all $t \geq 0$. Then, since $q_i(0)$ are the same for all i, equation (2.18) implies that there is a sequence $\{q(t),\ t = 1, 2, \ldots\}$ such that $q_i(t) = q(t)$ for all $i = 1, \ldots, N$ and $t \geq 0$.

To complete the proof of Theorem 2.3, we give two lemmas regarding the properties of Ψ. We skip their proofs since Lemma 2.3 follows directly from Assumption 2.1, and the proof of Lemma 2.4 uses the same technique as [101, Lemma 2-3].

Lemma 2.3. Suppose Assumption 2.1 holds. Then Ψ is concave, continuously differentiable and bounded on $\left[\underline{p},\ \overline{p}\right]$.

Lemma 2.4. Suppose Assumptions 2.1–2.2 hold. Then for any $p, q \in \left[\underline{p},\ \overline{p}\right]$

$$|\Psi'(q) - \Psi'(p)| \quad \leq \quad \overline{\alpha} N |q - p|.$$

Given Lemma 2.3, Lemma 2.4, and $0 < \gamma < 2/(\overline{\alpha}N)$, by [102, Proposition 3.4], any limit point of the sequence $\{q(t),\ t = 1, 2, \ldots\}$ (if one exists) is an optimal point of Dual OLC. Moreover, since $q(t) \in \left[\underline{p},\ \overline{p}\right]$ lies in a compact set for all t, there exists at least one limit point of $\{q(t),\ t = 1, 2, \ldots\}$ denoted by q^*. By (2.8), $\Delta d_i(\cdot)$ is continuous on $\left[\underline{p},\ \overline{p}\right]$, and thus $\Delta d(q^*)$ is a limit point of $\{\Delta d(t),\ t = 1, 2, \ldots\}$. By strong duality between OLC and Dual OLC, $\Delta d(q^*)$ is primal optimal.

2.E Proof of Theorem 2.4

To prove Theorem 2.4 (convergence of Algorithm 2.2), we first show that Algorithm 2.2 is a special case of the asynchronous flow control algorithm [101, Algorithm A2].

In Algorithm 2.2, load $i = 1, \ldots, N$ generates a sequence

$$U_{i,t} := \hat{u}_0^i(1), \ldots, \hat{u}_0^i(K_{i,1}), \ldots, \hat{u}_{t-1}^i(1), \ldots, \hat{u}_{t-1}^i(K_{i,t})$$

and a sequence

$$P_{i,t} := p_0^i(1), \ldots, p_0^i(K_{i,1}), \ldots, p_{t-1}^i(1), \ldots, p_{t-1}^i(K_{i,t}).$$

We formulate another sequence $\{p(t), t \geq 0\}$ starting from $p(0) = 0$ such that

$$p(t) \quad = \quad p(t-1) + \gamma u(t-1). \tag{2.38}$$

Define $\tau(i,t) := \max\{\tau = 0, 1, \ldots | \tau + r(i,\tau) = t\}$ where $r(i,\tau)$ is load i's measurement delay for $\Delta\omega(\tau)$. It is easy to prove that when all the process disturbance and measurement noise are ignored, i.e., $\zeta(t) = 0$ and $\xi_i(t) = 0$ for all $i = 1, \ldots, N$ and $t \geq 0$, the input estimator (2.11) generates precise estimate $\hat{u}_i(t-1|t) = u(t-1)$. Then the following lemma is straightforward from (2.24)(2.38).

Lemma 2.5. The sequence $U_{i,t}$ is exactly $u(0), \ldots, u(\tau(i,t)-1)$, and the sequence $P_{i,t}$ is exactly $p(1), \ldots, p(\tau(i,t))$.

Recall that in Algorithm 2.2, $p_i(t) = p_{t-1}^i(K_{i,t})$. Now we can consider $p(t)$, $u(t)$, $p_i(t)$ and $\Delta d_i(t)$ respectively as the link price $p_l(t)$, the estimate of gradient $\lambda_l(t)$, the estimate of link price $\hat{p}^s(t)$ and the transmission rate $x_s(t)$ in the asynchronous flow control algorithm [101, Algorithm A2]. We can see that Algorithm 2.2 is a special case of the asynchronous flow control algorithm. By the proof of [101, Theorem 2], if Assumptions 2.1–2.3, 2.6, and 2.7 hold and the stepsize γ satisfies $0 < \gamma < 1/((\overline{\alpha}N/2) + 2\overline{r})$, any limit point (at least one exists) of the sequence $\{(\Delta d(t), p(t)),\ t = 1, 2, \ldots\}$ (and hence the sequence $\{(\Delta d(t), p_i(t)),\ t = 1, 2, \ldots\}$ for all $i = 1, \ldots, N$) is primal-dual optimal for OLC and Dual OLC.

Chapter 3

LOAD-SIDE FREQUENCY CONTROL IN MULTI-MACHINE NETWORKS

Not all power systems are tightly electrically coupled, and therefore have coherent frequency and can be modeled as single-machine systems as in Chapter 2. In the current chapter, we study load-side frequency control in a multi-machine power network, where different nodes may have different frequencies. Under a linearized power network model, we develop decentralized load-side primary frequency control by exploiting power network dynamics as part of a primal-dual algorithm that solves an optimal load control (OLC) problem. Such a control scheme rebalances power and stabilizes frequency after a change in generation or load, in a manner that minimizes total disutility for load control. We then extend controller design and stability analysis to the case with a nonlinear power flow model and generator dynamics and control. We also design and analyze stability of distributed secondary frequency control which, using local frequency and power flow measurements and communication between neighboring nodes, can restore frequency and inter-area power flows to their nominal values. Moreover, we design a completely decentralized frequency integral control that restores frequency to its nominal value and ensures global convergence of the system, and a distributed averaging-based PI control that makes the system locally asymptotically stable at an OLC solution.

This chapter is organized as follows. Section 3.1 introduces the power network model and formulates the OLC problem. Section 3.2 presents the decentralized load-side primary frequency control algorithm, whose convergence is proved in Section 3.3 under a linearized power flow model. Sections 3.4 and 3.5 design and analyze generator and load-side distributed control under a nonlinear power flow model, where Section 3.4 is for primary frequency control, and Section 3.5 is for secondary. Section 3.6 introduces the completely decentralized frequency integral control, which, in Section 3.7, is modified to a distributed control to solve OLC by adding averaging filters. Section 3.8 shows simulation results which demonstrate effectiveness of the proposed control schemes. Section 3.9 concludes this chapter. The Appendices provide a table of frequently used notations, a simulation result to validate our model, and proofs of some lemmas in this chapter.

3.1 System model and problem formulation

Let $\mathbb{R}$ denote the set of real numbers and $\mathbb{N}$ denote the set of non-zero natural numbers. For a finite set $\mathcal{N} \subset \mathbb{N}$, let $|\mathcal{N}|$ denote its cardinality. For a set of scalar numbers $\{\omega_j \in \mathbb{R} \mid j \in \mathcal{N}\}$, we use $\omega_{\mathcal{N}}$ to denote the column vector of ω_j for $j \in \mathcal{N}$; we usually drop the subscript $\mathcal{N}$ when $\mathcal{N}$ is clear from the context, e.g., $\omega := \omega_{\mathcal{N}}$ if $\mathcal{N}$ is the set of *all* the buses in a network. For two vectors $a \in \mathbb{R}^{|\mathcal{G}|}$ and $b \in \mathbb{R}^{|\mathcal{L}|}$, $(a, b) \in \mathbb{R}^{|\mathcal{G}|+|\mathcal{L}|}$ is a column vector. For two vectors $a, b \in \mathbb{R}^{|\mathcal{N}|}$, $a \geq b$ ($a \leq b$) means $a_j \geq b_j$ ($a_j \leq b_j$) for all $j \in \mathcal{N}$.

For a matrix A, we use A^T to denote its transpose, and A_i to denote its i-th row. We use $A_{\mathcal{G}}$ to denote the submatrix of A composed only of the rows A_i for $i \in \mathcal{G}$. The diagonal matrix of a sequence $\{a_j,\ j \in \mathcal{N}\}$ is represented by $\mathrm{diag}(a_{\mathcal{N}}) = \mathrm{diag}(a_j,\ j \in \mathcal{N})$, or $a_{\mathcal{N}}$ for short when its meaning is clear. We use $1(0)$ to denote the vector/matrix of all ones (zeros), whose dimension is understood from the context. For a square matrix A, the expression $A \succ 0$ ($A \prec 0$) means it is positive (negative) definite, $A \succeq 0$ ($A \preceq 0$) means it is positive (negative) semi-definite.

For $a, b \in \mathbb{R}$, $a \leq b$, let $[\cdot]_a^b$ denote $\max\{\min\{\cdot,\ b\},\ a\}$. For a signal $\omega(t)$ of time, let $\dot{\omega}$ denote its time derivative $\frac{d\omega}{dt}$.

Power network model

We consider a power transmission network described by a graph $(\mathcal{N}, \mathcal{E})$ where $\mathcal{N} = \{1, \ldots, |\mathcal{N}|\}$ is the set of buses and $\mathcal{E} \subseteq \mathcal{N} \times \mathcal{N}$ is the set of transmission lines connecting the buses. We make the following assumptions:[1]

- The lines $(i, j) \in \mathcal{E}$ are lossless and characterized by their reactances x_{ij}.
- The voltage magnitudes $|V_j|$ of buses $j \in \mathcal{N}$ are constants.
- Reactive power injections at the buses and reactive power flows on the lines are ignored.

We assume that $(\mathcal{N}, \mathcal{E})$ is directed, with an arbitrary orientation, so that if $(i, j) \in \mathcal{E}$ then $(j, i) \notin \mathcal{E}$. We use (i, j) and $i \to j$ interchangeably to denote a link in $\mathcal{E}$, and use "$i : i \to j$" and "$k : j \to k$" respectively to denote the set of buses i that are predecessors of bus j and the set of buses k that are successors of bus j. We also assume without loss of generality that $(\mathcal{N}, \mathcal{E})$ is connected.

[1] These assumptions are similar to the standard DC approximation except that we do not assume the nominal phase angle difference is small across each link.

The network has two types of buses: generator buses and load buses. A generator bus not only has loads, but also an AC generator that converts mechanical power into electric power through a rotating prime mover. A load bus has only loads but no generator. We assume that the system is three-phase balanced. For a bus $j \in \mathcal{N}$, its phase a voltage at time t is $\sqrt{2}|V_j|\cos(\omega^0 t + \theta_j^0 + \Delta\theta_j(t))$ where ω^0 is the nominal frequency, θ_j^0 is the nominal voltage phase angle, and $\Delta\theta_j(t)$ is the time-varying phase angle deviation. The frequency at bus j is defined as $\omega_j := \omega^0 + \Delta\dot{\theta}_j$, and we call $\Delta\omega_j := \Delta\dot{\theta}_j$ the frequency deviation at bus j. We assume that the frequency deviations $\Delta\omega_j$ are small for all the buses $j \in \mathcal{N}$ and the differences $\Delta\theta_i - \Delta\theta_j$ between phase angle deviations are small across all the links $(i, j) \in \mathcal{E}$. We adopt a standard dynamic model, e.g., in [16, Section 11.4].

Generator buses. We assume coherency between the internal and terminal (bus) voltage phase angles of a generator; see our technical report [103, Sec. VII-C] for a detailed justification. Then the dynamic on a generator bus j is modeled by the swing equation

$$M_j\Delta\dot{\omega}_j + D'_j\Delta\omega_j \quad = \quad P_j^{m\prime} - P^0_{\text{loss},j} - P_j^e,$$

where $M_j > 0$ is the inertia constant of the generator. The term $D'_j\Delta\omega_j$ with $D'_j > 0$ represents the (first-order approximation of) deviation in generator power loss due to friction [16] from its nominal value $P^0_{\text{loss},j} := \left(D'_j\omega^0\right)/2$. Here $P_j^{m\prime}$ is the mechanical power injection to the generator, and P_j^e is the electric power export of the generator, which equals the sum of loads at bus j and the net power flow from bus j to the rest of the network.

In general, load power may depend on both the bus voltage magnitude (which is assumed fixed) and frequency. We distinguish between three types of loads, *frequency-sensitive*, *frequency-insensitive but controllable*, and *uncontrollable loads*. We assume the power consumptions of frequency-sensitive (e.g., motor-type) loads increase linearly with frequency deviation and model the aggregate power consumption of these loads by $\hat{d}_j^0 + D''_j\Delta\omega_j$ with $D''_j > 0$, where $\hat{d}_j^0$ is its nominal value. We assume frequency-insensitive loads can be actively controlled and our goal is to design and analyze these control laws. Let d_j denote the aggregate power of the controllable (but frequency-insensitive) loads at bus j. Finally let P_j^l denote the aggregate power consumption of uncontrollable (constant power) loads at bus j that are neither of the above two types of loads; we assume P_j^l may change over time but is pre-specified. Then the electric power P_j^e is the sum of frequency-sensitive loads,

controllable loads, uncontrollable loads, and the net power injection from bus j to other buses:

$$P_j^e \;:=\; \hat{d}_j^0 + D_j''\Delta\omega_j + d_j + P_j^l + \sum_{k:j\to k} P_{jk} - \sum_{i:i\to j} P_{ij},$$

where P_{jk} is the branch power flow from bus j to bus k.

Hence the dynamics on a generator bus j is

$$M_j\Delta\dot{\omega}_j \;=\; -\left(D_j\Delta\omega_j + d_j - P_j^m + P_j^{\text{out}} - P_j^{\text{in}}\right),$$

where $D_j := D_j' + D_j''$, $P_j^m := P_j^{m\prime} - P_{\text{loss},j}^0 - \hat{d}_j^0 - P_j^l$, and $P_j^{\text{out}} := \sum_{k:j\to k} P_{jk}$ and $P_j^{\text{in}} := \sum_{i:i\to j} P_{ij}$ are respectively the total branch power flows out of and into bus j. Note that P_j^l is integrated with $P_j^{m\prime}$ into a single term P_j^m, so that any change in power injection, whether on the generation side or the load side, is considered a change in P_j^m. Let $d_j^0, P_j^{m,0}, P_{ij}^0$ denote the nominal (operating) point at which $d_j^0 - P_j^{m,0} + P_j^{\text{out},0} - P_j^{\text{in},0} = 0$. Let $d_j(t) = d_j^0 + \Delta d_j(t), P_j^m(t) = P_j^{m,0} + \Delta P_j^m(t), P_{ij}(t) = P_{ij}^0 + \Delta P_{ij}(t)$. Then the deviations satisfy

$$M_j\Delta\dot{\omega}_j \;=\; -\left(D_j\Delta\omega_j + \Delta d_j - \Delta P_j^m + \Delta P_j^{\text{out}} - \Delta P_j^{\text{in}}\right). \tag{3.1}$$

Fig. 3.1 is a schematic of the generator bus model (3.1).

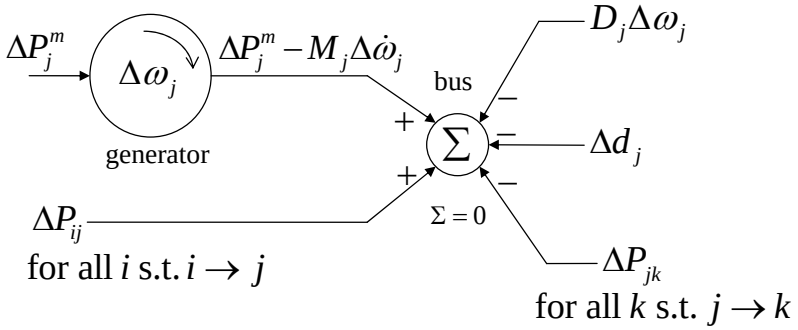

Figure 3.1: Schematic of a generator bus j, where $\Delta\omega_j$ is the frequency deviation; ΔP_j^m is the change in mechanical power minus aggregate uncontrollable load; $D_j\Delta\omega_j$ characterizes the effect of generator friction and frequency-sensitive loads; Δd_j is the change in aggregate controllable load; ΔP_{ij} is the deviation in branch power injected from another bus i to bus j; ΔP_{jk} is the deviation in branch power delivered from bus j to another bus k.

Load buses. A load bus that has no generator is modeled by the following algebraic equation that represents power balance at bus j:[2]

$$0 \;=\; D_j\Delta\omega_j + \Delta d_j - \Delta P_j^m + \Delta P_j^{\text{out}} - \Delta P_j^{\text{in}} \tag{3.2}$$

[2]There may be load buses with large inertia that can be modeled by swing dynamics (3.1) as proposed in [104]. We will treat them as generator buses mathematically.

where ΔP_j^m represents the change in the aggregate uncontrollable load.

Branch flows. The deviations ΔP_{ij} from the nominal branch flows follow the (linearized) dynamics

$$\Delta \dot{P}_{ij} \quad = \quad B_{ij} \left(\Delta \omega_i - \Delta \omega_j \right), \tag{3.3}$$

where

$$B_{ij} \quad := \quad 3 \frac{|V_i||V_j|}{x_{ij}} \cos \left(\theta_i^0 - \theta_j^0 \right) \tag{3.4}$$

is a constant determined by the nominal bus voltages and the line reactance. The same model is studied in the literature [15], [16] based on quasi-steady-state assumptions. In [103, Section VII-A] we derive this model by solving the differential equation that characterizes the dynamics of three-phase instantaneous power flow on reactive lines, without explicitly using quasi-steady-state assumptions. Note that (3.3) omits the specification of the initial deviations in branch flows $\Delta P(0)$. In practice $\Delta P(0)$ cannot be an arbitrary vector, but must satisfy

$$\Delta P_{ij}(0) \quad = \quad B_{ij} \left(\Delta \theta_i(0) - \Delta \theta_j(0) \right) \tag{3.5}$$

for some vector $\Delta\theta(0)$ of phase angles. In Remark 3.6 we discuss the implication of this omission on the convergence analysis.

Dynamic network model. We denote the set of generator buses by $\mathcal{G}$, the set of load buses by $\mathcal{L}$, and use $|\mathcal{G}|$ and $|\mathcal{L}|$ to denote the number of generator buses and load buses respectively. Without loss of generality label the generator buses so that $\mathcal{G} = \{1, ..., |\mathcal{G}|\}$ and the load buses so that $\mathcal{L} = \{|\mathcal{G}| + 1, ..., |\mathcal{N}|\}$. In summary the dynamic model of the transmission network is specified by (3.1)–(3.3). To simplify notation we drop the Δ from the variables denoting deviations and write (3.1)–(3.3) as:

$$\dot{\omega}_j \quad = \quad -\frac{1}{M_j}(D_j \omega_j + d_j - P_j^m + P_j^{\text{out}} - P_j^{\text{in}}) \qquad \text{for all } j \in \mathcal{G}, \tag{3.6a}$$

$$0 \quad = \quad D_j \omega_j + d_j - P_j^m + P_j^{\text{out}} - P_j^{\text{in}} \qquad \text{for all } j \in \mathcal{L}, \tag{3.6b}$$

$$\dot{P}_{ij} \quad = \quad B_{ij} \left(\omega_i - \omega_j \right) \qquad \text{for all } (i,j) \in \mathcal{E}, \tag{3.6c}$$

where B_{ij} are given by (3.4). Hence for the rest of this thesis all variables represent *deviations* from their nominal values. We will refer to the term $D_j \omega_j$ as the deviation in the (aggregate) frequency-sensitive load even though it also includes the deviation

in generator power loss due to friction. We will refer to P_j^m as a disturbance whether it is in generation or load.

An *equilibrium point* of the dynamic system (3.6) is a state (ω, P) where $\dot{\omega}_j = 0$ for $j \in \mathcal{G}$ and $\dot{P}_{ij} = 0$ for $(i, j) \in \mathcal{E}$, i.e., where all power deviations and frequency deviations are constant over time.

Remark 3.1. The model (3.6) captures the power system behavior at the timescale of seconds. In this thesis we only consider a step change in generation or load (constant P^m), which implies that the model does not include the actions of the governor and turbine that change the mechanical power injection in response to frequency deviation to rebalance power. Nor does it include any secondary frequency control mechanism such as automatic generation control that operates at a slower timescale to restore the nominal frequency. This model therefore explores the feasibility of fast timescale load control as a supplement to the turbine-governor mechanism to resynchronize frequency and rebalance power. □

We use a much more realistic simulation model developed in [58], [105] to validate our simple analytic model. The detailed simulations can be found in [103, Section VII]. We summarize the key conclusions from those simulations as follows.

1. In a power network with long transmission lines, the internal and terminal voltage phase angles of a generator swing coherently, i.e., the rotating speed of the generator is almost the same as the frequency at the generator bus even during transient.

2. Different buses, particularly those in different coherent groups [105] and far apart in electrical distance [52], may have different local frequencies for a duration similar to the time for them to converge to a new equilibrium, as opposed to resynchronizing almost instantaneously to a common system frequency. This particular simulation result justifies a key feature of our analytic model and is included in Appendix 3.B.

3. The simulation model and our analytic model exhibit similar transient behaviors and steady state values for bus frequencies and branch power flows.

Optimal load control

Suppose a constant disturbance $P^m = (P_j^m, j \in \mathcal{N})$ is injected to the set $\mathcal{N}$ of buses. How should we adjust the controllable loads d_j in (3.6) to rebalance power in a way

that minimizes the aggregate disutility of these loads? In general we can design state feedback controllers of the form $d_j(t) := d_j(\omega(t), P(t))$, prove the feedback system is globally asymptotically stable, and evaluate the aggregate disutility to the loads at the equilibrium point. Here we take an alternative approach by directly formalizing our control goals as an optimal load control (OLC) problem and derive the feedback controller as a *distributed* algorithm to solve OLC.

Remark 3.2. In this thesis, OLC refers to a class of optimization problems which take the general form (1.1). Depending on the types of frequency control (primary, secondary, etc.) and system model (single or multiple machines), we choose a specific OLC problem to solve. For example, we use OLC (2.4) in Chapter 2 to restore frequency to its nominal value in a single-machine system, OLC (3.7) below for load-side primary frequency control in a multi-machine network, and OLC (3.49) in Section 3.5 for generator and load-side secondary frequency control. □

The objective function of OLC consists of two costs. First suppose the (aggregate) controllable load at bus j incurs a cost (disutility) $\tilde{c}_j(d_j)$ when it is changed by d_j. Second the frequency deviation ω_j causes the (aggregate) frequency-sensitive load at bus j to change by $\hat{d}_j := D_j\omega_j$. For reasons that will become clear later, we assume that this results in a cost to the frequency-sensitive load that is proportional to the squared frequency deviation weighted by its relative damping constant:

$$\frac{\kappa D_j}{\sum_{i\in\mathcal{N}} D_i}\omega_j^2 \;=:\; \frac{\kappa}{D_j\left(\sum_{i\in\mathcal{N}} D_i\right)}\hat{d}_j^2$$

where $\kappa > 0$ is a constant. Hence the total cost is

$$\sum_{j\in\mathcal{N}}\left(\tilde{c}_j(d_j) + \frac{\kappa}{D_j\left(\sum_{i\in\mathcal{N}} D_i\right)}\hat{d}_j^2\right).$$

To simplify notation, we scale the total cost by $\frac{1}{2\kappa}\sum_{i\in\mathcal{N}} D_i$ without loss of generality and define $c_j(d_j) := \tilde{c}_j(d_j)\cdot\frac{1}{2\kappa}\sum_{i\in\mathcal{N}} D_i$. Then OLC minimizes the total cost over d and $\hat{d}$ while balancing generation and load across the network:

OLC (network, load-side primary control):

$$\min_{\underline{d}\le d\le\overline{d},\ \hat{d}} \quad \sum_{j\in\mathcal{N}}\left(c_j(d_j) + \frac{1}{2D_j}\hat{d}_j^2\right) \tag{3.7a}$$

$$\text{subject to} \quad \sum_{j\in\mathcal{N}}\left(d_j + \hat{d}_j\right) = \sum_{j\in\mathcal{N}} P_j^m \tag{3.7b}$$

where $-\infty < \underline{d}_j \le \overline{d}_j < \infty$.

Remark 3.3. Note that (3.7b) does not require the balance of generation and load at each individual bus, but only balance across the entire network. This constraint is less restrictive and offers more opportunity to minimize costs. Additional constraints can be imposed if it is desirable that certain buses, e.g., in the same control area, rebalance their own supply and demand, for economic or regulatory reasons. □

We make the following assumption regarding OLC (3.7).

Assumption 3.1. OLC (3.7) is feasible. The cost functions c_j are strictly convex and twice continuously differentiable on $\left[\underline{d}_j, \overline{d}_j\right]$.

See Remark 2.2 for examples of practical load control cost functions that satisfy Assumption 3.1.

3.2 Load control and system dynamics as primal-dual algorithm

We present the main results of this chapter, and prove them in Section 3.3.

Main results

The objective function of the dual problem of OLC is

$$\sum_{j\in\mathcal{N}} \Phi_j(\nu) \quad := \quad \sum_{j\in\mathcal{N}} \min_{\underline{d}_j \le d_j \le \overline{d}_j, \hat{d}_j} \left(c_j(d_j) - \nu d_j + \frac{1}{2D_j}\hat{d}_j^2 - \nu \hat{d}_j + \nu P_j^m \right)$$

where the minimization can be solved explicitly as

$$\Phi_j(\nu) \quad := \quad c_j(d_j(\nu)) - \nu d_j(\nu) - \frac{1}{2} D_j \nu^2 + \nu P_j^m \tag{3.8}$$

with

$$d_j(\nu) \quad := \quad \left[c_j'^{-1}(\nu)\right]_{\underline{d}_j}^{\overline{d}_j}. \tag{3.9}$$

This objective function has a scalar variable ν and is not separable across buses $j \in \mathcal{N}$. Its direct solution hence requires coordination across buses. We propose the following *distributed* version of the dual problem over the vector $\nu := \left(\nu_j, j \in \mathcal{N}\right)$, where each bus j optimizes over its own variable ν_j, which are constrained to be equal at optimality:

DOLC:

$$\max_{\nu} \qquad \Phi(\nu) := \sum_{j\in\mathcal{N}} \Phi_j(\nu_j) \tag{3.10a}$$

$$\text{subject to} \qquad \nu_i = \nu_j \qquad \text{for all } (i,j) \in \mathcal{E}. \tag{3.10b}$$

The following two results are proved in Appendices 3.C and 3.D. Instead of solving OLC directly, they suggest solving DOLC and recovering the unique optimal point $(d^*, \hat{d}^*)$ of OLC from the unique dual optimal ν^*.

Lemma 3.1. The objective function Φ of DOLC is strictly concave over $\mathbb{R}^{|\mathcal{N}|}$.

Lemma 3.2.
1. DOLC has a unique optimal point ν^* with $\nu_i^* = \nu_j^* = \nu^*$ for all $i, j \in \mathcal{N}$.[3]
2. OLC has a unique optimal point $(d^*, \hat{d}^*)$ where $d_j^* = d_j(\nu^*)$ and $\hat{d}_j^* = D_j \nu^*$ for all $j \in \mathcal{N}$.

To derive a distributed solution for DOLC, consider its Lagrangian

$$L(\nu, \pi) \;:=\; \sum_{j \in \mathcal{N}} \Phi_j(\nu_j) - \sum_{(i,j) \in \mathcal{E}} \pi_{ij}(\nu_i - \nu_j), \tag{3.11}$$

where $\nu \in \mathbb{R}^{|\mathcal{N}|}$ is the (vector) variable for DOLC and $\pi \in \mathbb{R}^{|\mathcal{E}|}$ is the associated dual variable for the dual of DOLC. Hence π_{ij}, for all $(i, j) \in \mathcal{E}$, measure the cost of not synchronizing the variables ν_i and ν_j across buses i and j. Using (3.8)–(3.11) a partial primal-dual algorithm for DOLC takes the form

$$\dot{\nu}_j \;=\; \gamma_j \frac{\partial L}{\partial \nu_j}(\nu, \pi) = -\gamma_j \left(d_j(\nu_j) + D_j \nu_j - P_j^m + \pi_j^{\text{out}} - \pi_j^{\text{in}} \right) \tag{3.12a}$$
$$\text{for } j \in \mathcal{G},$$
$$0 \;=\; \frac{\partial L}{\partial \nu_j}(\nu, \pi) = -\left(d_j(\nu_j) + D_j \nu_j - P_j^m + \pi_j^{\text{out}} - \pi_j^{\text{in}} \right) \text{ for } j \in \mathcal{L}, \tag{3.12b}$$
$$\dot{\pi}_{ij} \;=\; -\xi_{ij} \frac{\partial L}{\partial \pi_{ij}}(\nu, \pi) \;=\; \xi_{ij}(\nu_i - \nu_j) \qquad \text{for } (i, j) \in \mathcal{E}, \tag{3.12c}$$

where $\gamma_j > 0$, $\xi_{ij} > 0$ are stepsizes and $\pi_j^{\text{out}} := \sum_{k: j \to k} \pi_{jk}$, $\pi_j^{\text{in}} := \sum_{i: i \to j} \pi_{ij}$. We interpret (3.12) as an algorithm iterating on the primal variables ν and dual variables π over time $t \geq 0$. Set the stepsizes to be:

$$\gamma_j = M_j^{-1}, \qquad \xi_{ij} = B_{ij}.$$

Then (3.12) becomes identical to (3.6a)–(3.6c) if we identify ν with ω and π with P, and use $d_j(\omega_j)$ defined by (3.9) for d_j in (3.6a)–(3.6b). *This means that the frequency deviations ω and the branch flows P are respectively the primal and dual variables of DOLC, and the network dynamics, together with frequency-based load control, execute a primal-dual algorithm for solving DOLC.*

[3] For simplicity, we abuse the notation and use ν^* to denote both the vector $\left(\nu_j^*, j \in \mathcal{N}\right)$ and the common value of its components. Its meaning should be clear from the context.

Remark 3.4. Note the consistency of units between the following pairs of quantities: 1) γ_j and M_j^{-1}, 2) ξ_{ij} and B_{ij}, 3) ν and ω, 4) π and P. Indeed, since the unit of D_j is [watt · s] from (3.6a), the cost (3.7a) is in $\left[\text{watt} \cdot \text{s}^{-1}\right]$. From (3.8) and (3.11), ν and π are respectively in $\left[\text{s}^{-1}\right]$ (or equivalently $\left[\text{rad} \cdot \text{s}^{-1}\right]$) and [watt]. From (3.12a), γ_j is in $\left[\text{watt}^{-1} \cdot \text{s}^{-2}\right]$ which is the same as the unit of M_j^{-1} from (3.6a). From (3.12c), ξ_{ij} is in [watt] which is the same as the unit of B_{ij} from (3.6c). □

For convenience, we collect here the system dynamics and load control equations:

$$\dot{\omega}_j = -\frac{1}{M_j}\left(d_j + \hat{d}_j - P_j^m + P_j^{\text{out}} - P_j^{\text{in}}\right) \quad \text{for all } j \in \mathcal{G} \tag{3.13a}$$

$$0 = d_j + \hat{d}_j - P_j^m + P_j^{\text{out}} - P_j^{\text{in}} \quad \text{for all } j \in \mathcal{L} \tag{3.13b}$$

$$\dot{P}_{ij} = B_{ij}\left(\omega_i - \omega_j\right) \quad \text{for all } (i,j) \in \mathcal{E} \tag{3.13c}$$

$$\dot{\hat{d}}_j = D_j \omega_j \quad \text{for all } j \in \mathcal{N} \tag{3.13d}$$

$$d_j = \left[c_j'^{-1}(\omega_j)\right]_{\underline{d}_j}^{\overline{d}_j} \quad \text{for all } j \in \mathcal{N}. \tag{3.13e}$$

The dynamics (3.13a)–(3.13d) are automatically carried out by the power system while the active control (3.13e) needs to be implemented at each controllable load. Let $(d(t), \hat{d}(t), \omega(t), P(t))$ denote a trajectory of (deviations of) controllable loads, frequency-sensitive loads, frequencies and branch flows generated by the dynamics (3.13) of the load-controlled system.

Theorem 3.1. Starting from any feasible[4] initial point $(d(0), \hat{d}(0), \omega(0), P(0))$, every trajectory $(d(t), \hat{d}(t), \omega(t), P(t), t \geq 0)$ generated by (3.13) converges to a limit $(d^*, \hat{d}^*, \omega^*, P^*)$ as $t \to \infty$ such that

1. $(d^*, \hat{d}^*)$ is the unique vector of optimal load control for OLC;
2. ω^* is the unique vector of optimal frequency deviations for DOLC;
3. P^* is a vector of optimal branch flows for the dual of DOLC.

We will prove Theorem 3.1 and other results in Section 3.3.

Implications

Our main results have several important implications:

[4] A point is feasible for (3.13) if it satisfies the algebraic equations (3.13b), (3.13d), and (3.13e).

1. *Ubiquitous continuous load-side primary frequency control.* Like the generator-side droop control, frequency-adaptive loads can rebalance power and resynchronize frequencies after a disturbance. Theorem 3.1 implies that a multi-machine network under such control is globally asymptotically stable. The load-side control is often faster because of the larger time constants associated with valves and prime movers on the generator side. Furthermore OLC explicitly optimizes the aggregate disutility using the cost functions of heterogeneous loads.

2. *Complete decentralization.* The local frequency deviations $\omega_j(t)$ at each bus convey exactly the right information about global power imbalance for the loads to make local decisions that turn out to be globally optimal. This allows a completely decentralized solution without explicit communication among the buses.

3. *Equilibrium frequency.* The frequency deviations $\omega_j(t)$ at all the buses are synchronized to ω^* at optimality even though they can be different during transient. However ω^* at optimality is in general nonzero, implying that the new common frequency may be different from the common frequency before the disturbance. Mechanisms such as isochronous generators [15] or automatic generation control are needed to drive the new system frequency to its nominal value, usually through integral action on the frequency deviations. We develop distributed control schemes to restore frequency to its nominal value, in Sections 3.5, 3.6, and 3.7.

4. *Frequency and branch flows.* In the context of optimal load control, the frequency deviations $\omega_j(t)$ emerge as the Lagrange multipliers of OLC that measure the cost of power imbalance, whereas the branch flow deviations $P_{ij}(t)$ emerge as the Lagrange multipliers of DOLC that measure the cost of frequency asynchronism.

5. *Uniqueness of solution.* Lemma 3.2 implies that the optimal frequency deviation ω^* is unique and hence the optimal load control $(d^*, \hat{d}^*)$ is unique. As shown below, the vector P^* of optimal branch flows is unique if and only if the network is a tree. Nonetheless Theorem 3.1 says that, even for a mesh network, any trajectory of branch flows indeed converges to a limit point. See Remark 3.6 for further discussion.

3.3 Convergence analysis

This section is devoted to the proof of Theorem 3.1 and other properties as given by Theorems 3.2 and 3.3 below. Before going into the details we first sketch out the key steps in establishing Theorem 3.1, the convergence of the trajectories generated by (3.13).

1. Theorem 3.2: The set of optimal points (ω^*, P^*) of DOLC and its dual and the set of equilibrium points of (3.13) are nonempty and the same. Denote both of them by Z^*.

2. Theorem 3.3: If $(\mathcal{N}, \mathcal{E})$ is a tree network, Z^* is a singleton with a unique equilibrium point (ω^*, P^*), otherwise (if $(\mathcal{N}, \mathcal{E})$ is a mesh network), Z^* has an uncountably infinite number (a subspace) of equilibria with the same ω^* but different P^*.

3. Theorem 3.1: We use a Lyapunov argument to prove that every trajectory $(\omega(t), P(t))$ generated by (3.13) approaches a nonempty, compact subset Z^+ of Z^* as $t \to \infty$. Hence, if $(\mathcal{N}, \mathcal{E})$ is a tree network, then Theorem 3.3 implies that any trajectory $(\omega(t), P(t))$ converges to the unique optimal point (ω^*, P^*). If $(\mathcal{N}, \mathcal{E})$ is a mesh network, we show with a more careful argument that $(\omega(t), P(t))$ still converges to a point in Z^+, as opposed to oscillating around Z^+. Theorem 1 then follows from Lemma 3.2.

We now elaborate on these ideas.

Given ω, the optimal loads $(d, \hat{d})$ are uniquely determined by (3.13d)–(3.13e). Hence we focus on the variables (ω, P). Decompose $\omega^T := \begin{bmatrix} \omega_{\mathcal{G}}^T & \omega_{\mathcal{L}}^T \end{bmatrix}$ into frequency deviations at generator buses and load buses. Let C be the $|\mathcal{N}| \times |\mathcal{E}|$ incidence matrix with $C_{je} = 1$ if $e = (j, k) \in \mathcal{E}$ for some bus $k \in \mathcal{N}$, $C_{je} = -1$ if $e = (i, j) \in \mathcal{E}$ for some bus $i \in \mathcal{N}$, and $C_{je} = 0$ otherwise. We decompose C into an $|\mathcal{G}| \times |\mathcal{E}|$ submatrix $C_{\mathcal{G}}$ corresponding to generator buses and an $|\mathcal{L}| \times |\mathcal{E}|$ submatrix $C_{\mathcal{L}}$ corresponding to load buses, i.e., $C = \left[\begin{smallmatrix} C_{\mathcal{G}} \\ C_{\mathcal{L}} \end{smallmatrix} \right]$. Let

$$\Phi_{\mathcal{G}}(\omega_{\mathcal{G}}) := \sum_{j \in \mathcal{G}} \Phi_j(\omega_j) \quad \text{and} \quad L_{\mathcal{G}}(\omega_{\mathcal{G}}, P) := \Phi_{\mathcal{G}}(\omega_{\mathcal{G}}) - \omega_{\mathcal{G}}^T C_{\mathcal{G}} P,$$
$$\Phi_{\mathcal{L}}(\omega_{\mathcal{L}}) := \sum_{j \in \mathcal{L}} \Phi_j(\omega_j) \quad \text{and} \quad L_{\mathcal{L}}(\omega_{\mathcal{L}}, P) := \Phi_{\mathcal{L}}(\omega_{\mathcal{L}}) - \omega_{\mathcal{L}}^T C_{\mathcal{L}} P.$$

Identifying v with ω and π with P, we can rewrite the Lagrangian for DOLC defined in (3.11), in terms of $\omega_{\mathcal{G}}$ and $\omega_{\mathcal{L}}$, as

$$L(\omega, P) \;=\; \Phi(\omega) - \omega^T C P \;=\; L_{\mathcal{G}}(\omega_{\mathcal{G}}, P) + L_{\mathcal{L}}(\omega_{\mathcal{L}}, P). \tag{3.14}$$

Then (3.13) (equivalently, (3.12)) can be rewritten in the vector form as

$$\dot{\omega_{\mathcal{G}}} \;=\; \Gamma_{\mathcal{G}} \left[\frac{\partial L_{\mathcal{G}}}{\partial \omega_{\mathcal{G}}}(\omega_{\mathcal{G}}, P)\right]^T \;=\; \Gamma_{\mathcal{G}} \left(\left[\frac{\partial \Phi_{\mathcal{G}}}{\partial \omega_{\mathcal{G}}}(\omega_{\mathcal{G}})\right]^T - C_{\mathcal{G}} P\right), \tag{3.15a}$$

$$0 \;=\; \frac{\partial L_{\mathcal{L}}}{\partial \omega_{\mathcal{L}}}(\omega_{\mathcal{L}}, P) \;=\; \left[\frac{\partial \Phi_{\mathcal{L}}}{\partial \omega_{\mathcal{L}}}(\omega_{\mathcal{L}})\right]^T - C_{\mathcal{L}} P, \tag{3.15b}$$

$$\dot{P} \;=\; -\Xi \left[\frac{\partial L}{\partial P}(\omega, P)\right]^T \;=\; \Xi\, C^T \omega, \tag{3.15c}$$

where $\Gamma_{\mathcal{G}} := \mathrm{diag}(\gamma_j,\ j \in \mathcal{G})$ and $\Xi := \mathrm{diag}(\xi_{ij},\ (i,j) \in \mathcal{E})$. The differential algebraic equations (3.15) describe the dynamics of the power network.

A pair (ω^*, P^*) is called a *saddle point* of L if

$$L(\omega, P^*) \;\le\; L(\omega^*, P^*) \;\le\; L(\omega^*, P) \qquad \text{for all } (\omega, P). \tag{3.16}$$

By [93, Section 5.4.2], (ω^*, P^*) is primal-dual optimal for DOLC and its dual if and only if it is a saddle point of $L(\omega, P)$. The following theorem establishes the equivalence between the primal-dual optimal points and the equilibrium points of (3.15).

Theorem 3.2. A point (ω^*, P^*) is primal-dual optimal for DOLC and its dual if and only if it is an equilibrium point of (3.15). Moreover, at least one primal-dual optimal point (ω^*, P^*) exists and ω^* is unique among all points (ω^*, P^*) that are primal-dual optimal.

Proof. Recall that we identified v with ω and π with P. In DOLC, the objective function Φ is (strictly) concave over $\mathbb{R}^{|\mathcal{N}|}$ (by Lemma 3.1), its constraints are linear, and a finite optimal ω^* is attained (by Lemma 3.2). These facts imply that there is no duality gap between DOLC and its dual, and there exists a dual optimal point P^* [93, Section 5.2.3]. Moreover, (ω^*, P^*) is optimal for DOLC and its dual if and only if the following Karush-Kuhn-Tucker (KKT) conditions [93, Section 5.5.3] are satisfied:

$$\text{Stationarity:} \qquad \frac{\partial \Phi}{\partial \omega}(\omega^*) \;=\; (CP^*)^T, \tag{3.17}$$

$$\text{Primal feasibility:} \qquad \omega_i^* \;=\; \omega_j^* \quad \text{for all } (i,j) \in \mathcal{E}. \tag{3.18}$$

On the other hand $(\omega^*, P^*) = (\omega^*_{\mathcal{G}}, \omega^*_{\mathcal{L}}, P^*)$ is an equilibrium point of (3.15) if and only if

$$\begin{aligned}\left[\frac{\partial \Phi_{\mathcal{G}}}{\partial \omega_{\mathcal{G}}}\left(\omega^*_{\mathcal{T}}\right)\right]^T &= C_{\mathcal{G}} P^*,\\ \left[\frac{\partial \Phi_{\mathcal{L}}}{\partial \omega_{\mathcal{L}}}\left(\omega^*_{\mathcal{L}}\right)\right]^T &= C_{\mathcal{L}} P^*,\\ \Xi C^T \omega^* &= 0,\end{aligned}$$

which are identical to (3.17)–(3.18). Hence (ω^*, P^*) is primal-dual optimal if and only if it is an equilibrium of (3.15). The uniqueness of ω^* follows from Lemma 3.2. □

From Lemma 3.2, we denote the unique optimal point of DOLC by $\omega^* 1_{\mathcal{N}} = \left[\begin{smallmatrix}\omega^* 1_{\mathcal{G}} \\ \omega^* 1_{\mathcal{L}}\end{smallmatrix}\right]$, where $1_{\mathcal{N}} \in \mathbb{R}^{|\mathcal{N}|}$, $1_{\mathcal{G}} \in \mathbb{R}^{|\mathcal{G}|}$ and $1_{\mathcal{L}} \in \mathbb{R}^{|\mathcal{L}|}$ have all their elements equal to 1. From (3.17)–(3.18), define the nonempty set of equilibrium points of (3.15) (or equivalently, primal-dual optimal points of DOLC and its dual) as

$$Z^* := \left\{(\omega, P) \mid \omega = \omega^* 1_{\mathcal{N}},\ CP = \left[\frac{\partial \Phi}{\partial \omega}\left(\omega^* 1_{\mathcal{N}}\right)\right]^T\right\}. \tag{3.19}$$

Let $(\omega^* 1_{\mathcal{N}}, P^*) = (\omega^* 1_{\mathcal{G}}, \omega^* 1_{\mathcal{L}}, P^*) \in Z^*$ be *any* equilibrium point of (3.15). We consider a candidate Lyapunov function

$$U(\omega, P) = \frac{1}{2}\left(\omega_{\mathcal{G}} - \omega^* 1_{\mathcal{G}}\right)^T \Gamma_{\mathcal{G}}^{-1}\left(\omega_{\mathcal{G}} - \omega^* 1_{\mathcal{G}}\right) + \frac{1}{2}\left(P - P^*\right)^T \Xi^{-1}\left(P - P^*\right). \tag{3.20}$$

Obviously $U(\omega, P) \geq 0$ for all (ω, P) with equality if and only if $\omega_{\mathcal{G}} = \omega^* 1_{\mathcal{G}}$ and $P = P^*$. We will show below that $\dot{U}(\omega, P) \leq 0$ for all (ω, P), where $\dot{U}$ denotes the derivative of U over time along the trajectory $(\omega(t), P(t))$.

Even though U depends explicitly only on $\omega_{\mathcal{G}}$ and P, $\dot{U}$ depends on $\omega_{\mathcal{L}}$ as well through (3.15c). However, it will prove convenient to express $\dot{U}$ as a function of only $\omega_{\mathcal{G}}$ and P. To this end, write (3.15b) as $F(\omega_{\mathcal{L}}, P) = 0$. Then $\frac{\partial F}{\partial \omega_{\mathcal{L}}}(\omega_{\mathcal{L}}, P) = \frac{\partial^2 \Phi_{\mathcal{L}}}{\partial \omega_{\mathcal{L}}^2}(\omega_{\mathcal{L}})$ is nonsingular for all $(\omega_{\mathcal{L}}, P)$ from the proof of Lemma 3.1 in Appendix 3.C. By the inverse function theorem [106], $\omega_{\mathcal{L}}$ can be written as a continuously differentiable function of P, denoted by $\omega_{\mathcal{L}}(P)$, with

$$\frac{\partial \omega_{\mathcal{L}}}{\partial P}(P) = \left(\frac{\partial^2 \Phi_{\mathcal{L}}}{\partial \omega_{\mathcal{L}}^2}\left(\omega_{\mathcal{L}}(P)\right)\right)^{-1} C_{\mathcal{L}}. \tag{3.21}$$

Then we can rewrite the Lagrangian $L(\omega, P)$ as a function of $(\omega_{\mathcal{G}}, P)$ as

$$L(\omega, P) \;=\; L_{\mathcal{G}}(\omega_{\mathcal{G}}, P) + L_{\mathcal{L}}\left(\omega_{\mathcal{L}}(P), P\right) \;=:\; \tilde{L}\left(\omega_{\mathcal{G}}, P\right). \tag{3.22}$$

We have the following lemma, proved in Appendix 3.E, regarding the properties of $\tilde{L}$.

Lemma 3.3. $\tilde{L}$ is strictly concave in $\omega_{\mathcal{G}}$ and convex in P.

Rewrite (3.15) as

$$\dot{\omega}_{\mathcal{G}} \;=\; \Gamma_{\mathcal{G}}\left[\frac{\partial \tilde{L}}{\partial \omega_{\mathcal{G}}}\left(\omega_{\mathcal{G}}, P\right)\right]^{T}, \tag{3.23a}$$

$$\dot{P} \;=\; -\Xi\left[\frac{\partial \tilde{L}}{\partial P}\left(\omega_{\mathcal{G}}, P\right)\right]^{T}. \tag{3.23b}$$

Then the derivative of U along any trajectory $(\omega(t), P(t))$ generated by (3.15) is

$$\begin{aligned}
\dot{U}(\omega, P) \;&=\; \left(\omega_{\mathcal{G}} - \omega^{*}1_{\mathcal{G}}\right)^{T}\Gamma_{\mathcal{G}}^{-1}\,\dot{\omega}_{\mathcal{G}} + \left(P - P^{*}\right)^{T}\Xi^{-1}\dot{P} \\
&=\; \frac{\partial \tilde{L}}{\partial \omega_{\mathcal{G}}}(\omega_{\mathcal{G}}, P)\left(\omega_{\mathcal{G}} - \omega^{*}1_{\mathcal{G}}\right) - \frac{\partial \tilde{L}}{\partial P}(\omega_{\mathcal{G}}, P)\left(P - P^{*}\right) && (3.24) \\
&\leq\; \tilde{L}\left(\omega_{\mathcal{G}}, P\right) - \tilde{L}\left(\omega^{*}1_{\mathcal{G}}, P\right) + \tilde{L}(\omega_{\mathcal{G}}, P^{*}) - \tilde{L}\left(\omega_{\mathcal{G}}, P\right) && (3.25) \\
&=\; L\left(\omega_{\mathcal{G}}, \omega^{*}1_{\mathcal{L}}, P^{*}\right) - \tilde{L}\left(\omega^{*}1_{\mathcal{G}}, P\right) && (3.26) \\
&\leq\; L\left(\omega^{*}1_{\mathcal{N}}, P\right) - \tilde{L}\left(\omega^{*}1_{\mathcal{G}}, P\right) && (3.27) \\
&=\; L_{\mathcal{G}}\left(\omega^{*}1_{\mathcal{G}}, P\right) + L_{\mathcal{L}}\left(\omega^{*}1_{\mathcal{L}}, P\right) - \left[L_{\mathcal{G}}\left(\omega^{*}1_{\mathcal{G}}, P\right) + L_{\mathcal{L}}\left(\omega_{\mathcal{L}}(P), P\right)\right] \\
&\leq\; 0. && (3.28)
\end{aligned}$$

Here (3.24) follows from (3.23). The inequality in (3.25) results from Lemma 3.3. The equality in (3.26) holds since $\omega_{\mathcal{L}}(P^{*}) = \omega^{*}1_{\mathcal{L}}$ by (3.17). The inequality in (3.27) is due to $L\left(\omega_{\mathcal{G}}, \omega^{*}1_{\mathcal{L}}, P^{*}\right) \leq L\left(\omega^{*}1_{\mathcal{N}}, P^{*}\right) \leq L\left(\omega^{*}1_{\mathcal{N}}, P\right)$ by the saddle point condition (3.16). The inequality in (3.28) follows since $\omega_{\mathcal{L}}(P)$ is the maximizer of $L_{\mathcal{L}}(\cdot, P)$ given P, by the concavity of $L_{\mathcal{L}}$ in $\omega_{\mathcal{L}}$ and the definition of $\omega_{\mathcal{L}}(P)$.

The next lemma, proved in Appendix 3.F, characterizes the set in which the value of U does not change over time.

Lemma 3.4. $\dot{U}(\omega, P) = 0$ if and only if either of the following two conditions holds:

1.

$$\omega_{\mathcal{G}} \;=\; \omega^{*}1_{\mathcal{G}} \quad \text{and} \quad C_{\mathcal{L}}P \;=\; \left[\frac{\partial \Phi_{\mathcal{L}}}{\partial \omega_{\mathcal{L}}}\left(\omega^{*}1_{\mathcal{L}}\right)\right]^{T}, \tag{3.29}$$

2.

$$\omega_{\mathcal{G}} = \omega^* 1_{\mathcal{G}} \quad \text{and} \quad \omega_{\mathcal{L}}(P) = \omega^* 1_{\mathcal{L}}. \tag{3.30}$$

Lemma 3.4 motivates the definition of the set

$$\begin{aligned} E &:= \{(\omega, P) \mid \dot{U}(\omega, P) = 0\} \\ &= \left\{(\omega, P) \mid \omega = \omega^* 1_{\mathcal{N}},\ C_{\mathcal{L}} P = \left[\frac{\partial \Phi_{\mathcal{L}}}{\partial \omega_{\mathcal{L}}}(\omega^* 1_{\mathcal{L}})\right]^T\right\}, \end{aligned} \tag{3.31}$$

in which $\dot{U} = 0$ along any trajectory $(\omega(t), P(t))$. The definition of Z^* in (3.19) implies that $Z^* \subseteq E$, as shown in Fig. 3.2. As shown in the figure, E may contain

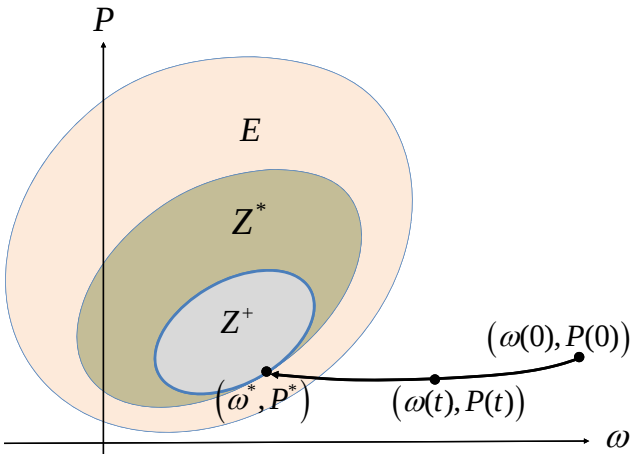

Figure 3.2: E is the set on which $\dot{U} = 0$, Z^* is the set of equilibrium points of (3.15), and Z^+ is a compact subset of Z^* to which all solutions $(\omega(t), P(t))$ approach as $t \to \infty$. Indeed every solution $(\omega(t), P(t))$ converges to a point $(\omega^*, P^*) \in Z^+$ that is dependent on the initial state.

points that are not in Z^*. Nonetheless every accumulation point (limit point of any convergent subsequence) of a solution $(\omega(t), P(t))$ of (3.15) is in Z^*, as the next lemma shows.

Lemma 3.5. Starting from any feasible initial point $(\omega(0), P(0))$, every trajectory $(\omega(t), P(t))$ of (3.15) approaches a nonempty, compact subset (denoted Z^+) of Z^* as $t \to \infty$.

The proof of Lemma 3.5 is given in Appendix 3.G. The sets $Z^+ \subseteq Z^* \subseteq E$ are illustrated in Fig. 3.2. Lemma 3.5 only guarantees that $(\omega(t), P(t))$ approaches Z^+ as $t \to \infty$, but does not guarantee that it converges to any point in Z^*. We now show that $(\omega(t), P(t))$ indeed converges to an equilibrium point in Z^+. Indeed the

convergence is immediate in the special case when Z^* is a singleton, but needs a more careful argument when Z^* has multiple points. The next theorem reveals the relation between the number of points in Z^* and the network topology.

Theorem 3.3. 1. If $(\mathcal{N}, \mathcal{E})$ is a tree then Z^* is a singleton.

2. If $(\mathcal{N}, \mathcal{E})$ is a mesh (i.e., contains a cycle if regarded as an undirected graph) then Z^* has an uncountably infinite number of points with the same ω^* but different P^*.

Proof. From (3.19), the projection of Z^* on the space of ω is always a singleton $\omega^* 1_{\mathcal{N}}$, and hence we only look at the projection of Z^* on the space of P, which is

$$Z_P^* \;:=\; \{P \mid CP = h^*\}$$

where $h^* := \left[\frac{\partial \Phi}{\partial \omega}(\omega^* 1_{\mathcal{N}})\right]^T$. By Theorem 3.2, Z_P^* is nonempty, i.e., there is $P^* \in Z_P^*$ such that $CP^* = h^*$ and hence $1_{\mathcal{N}}^T h^* = 1_{\mathcal{N}}^T CP^* = 0$. Therefore we have

$$Z_P^* \;:=\; \left\{P \mid \tilde{C}P = \tilde{h}^*\right\}, \tag{3.32}$$

where $\tilde{C}$ is the $(|\mathcal{N}|-1)\times|\mathcal{E}|$ reduced incidence matrix obtained from C by removing any one of its rows, and $\tilde{h}^*$ is obtained from h^* by removing the corresponding row. Note that $\tilde{C}$ has a full row rank of $|\mathcal{N}|-1$ [107]. If $(\mathcal{N}, \mathcal{E})$ is a tree, then $|\mathcal{E}| = |\mathcal{N}|-1$. Hence $\tilde{C}$ is square and invertible, so Z_P^* is a singleton. If $(\mathcal{N}, \mathcal{E})$ is a (connected) mesh, then $|\mathcal{E}| > |\mathcal{N}| - 1$, so $\tilde{C}$ has a nontrivial null space and there are uncountably many points in Z_P^*. □

With all the results above we can now finish the proof of Theorem 3.1.

Proof of Theorem 3.1. For the case in which $(\mathcal{N}, \mathcal{E})$ is a tree, Lemma 3.5 and Theorem 3.3(1) guarantees that every trajectory$(\omega(t), P(t))$ converges to the unique primal-dual optimal point (ω^*, P^*) of DOLC and its dual, which, by Lemma 3.2, immediately implies Theorem 3.1.

For the case in which $(\mathcal{N}, \mathcal{E})$ is a mesh, since $\dot{U}(\omega, P) \le 0$ for all (ω, P), any solution $(\omega(t), P(t))$ for $t \ge 0$ stays in the compact set $\{(\omega, P) | U(\omega, P) \le U(\omega(0), P(0))\}$. Hence there exists a convergent subsequence $\{(\omega(t_k), P(t_k)),\ k \in \mathbb{N}\}$, where $0 \le t_1 < t_2 < \ldots$ and $t_k \to \infty$ as $k \to \infty$, such that $\lim_{k\to\infty} \omega(t_k) = \omega^\infty$ and $\lim_{k\to\infty} P(t_k) = P^\infty$ for some $(\omega^\infty, P^\infty)$. Lemma 3.5 implies that $(\omega^\infty, P^\infty) \in Z^+ \subseteq Z^*$, and hence $\omega^\infty = \omega^* 1_{\mathcal{N}}$ by (3.19). Recall that the Lyapunov function U

in (3.20) can be defined in terms of any equilibrium point $(\omega^* 1_{\mathcal{N}}, P^*) \in Z^*$. In particular, select $(\omega^* 1_{\mathcal{N}}, P^*) = (\omega^* 1_{\mathcal{N}}, P^\infty)$, i.e.,

$$U(\omega, P) := \frac{1}{2} (\omega_{\mathcal{G}} - \omega^* 1_{\mathcal{G}})^T \Gamma_{\mathcal{G}}^{-1} (\omega_{\mathcal{G}} - \omega^* 1_{\mathcal{G}}) + \frac{1}{2} (P - P^\infty)^T \Xi^{-1} (P - P^\infty) .$$

Since $U \geq 0$ and $\dot{U} \leq 0$ along all trajectories $(\omega(t), P(t))$, $U(\omega(t), P(t))$ must converge as $t \to \infty$. Moreover it converges to 0 due to the continuity of U in both ω and P:

$$\lim_{t\to\infty} U(\omega(t), P(t)) = \lim_{k\to\infty} U(\omega(t_k), P(t_k)) = U(\omega^\infty, P^\infty) = 0.$$

Due to the form of U, the equation above implies that the trajectory $(\omega(t), P(t))$ converges to $(\omega^\infty, P^\infty) \in Z^+ \subseteq Z^*$, a primal-dual optimal point for DOLC and its dual. Theorem 3.1 then follows from Lemma 3.2. □

Remark 3.5. The standard technique of using a Lyapunov function that is quadratic in both the primal and the dual variables was first proposed by Arrow *et al.* [108], and has been revisited recently, e.g., in [109], [110]. We apply a variant of this technique to our problem with the following features. First, because of the algebraic equation (3.15b) in the system, our Lyapunov function is not a function of all the primal variables, but only the part $\omega_{\mathcal{G}}$ corresponding to generator buses. Second, in the case of a mesh network when there is a subspace of equilibrium points, we show that the system trajectory still converges to one of the equilibrium points instead of oscillating around the equilibrium set. □

Remark 3.6. Theorems 3.1–3.3 are based on our analytic model (3.13) which omits an important constraint on the initial condition on the branch flows $P(0)$. As mentioned earlier, in practice, the initial branch flows must satisfy (3.5) for some $\theta(0)$ (with Δ dropped). With this requirement the branch flow model (3.3)–(3.5) implies $P(t) \in \mathrm{Col}(BC^T)$ for all t, where Col denotes the column space, B is the diagonal matrix with entries B_{ij}, and C is the incidence matrix. Indeed $P(t) \in \mathrm{Col}(B\tilde{C}^T)$ since $C^T 1_{\mathcal{N}} = 0$ and $\tilde{C}^T$ with one column from C^T removed has a full column rank. A simple derivation from (3.32) shows that $Z_P^* \cap \mathrm{Col}(B\tilde{C}^T) = \left\{ B\tilde{C}^T \left(\tilde{C}B\tilde{C}^T\right)^{-1} \tilde{h}^* \right\}$ is a singleton, where $\tilde{C}B\tilde{C}^T$ is invertible [107]. Then by Lemma 3.5, $P(t) \to B\tilde{C}^T \left(\tilde{C}B\tilde{C}^T\right)^{-1} \tilde{h}^*$ as $t \to \infty$. In other words, though for a mesh network the dynamics (3.13) have a subspace of equilibrium points, all the practical trajectories, whose initial points $(\omega(0), P(0))$ satisfy (3.5) for some arbitrary $\theta(0)$, converge to a *unique* equilibrium point. □

3.4 Generator and load-side primary control with nonlinear power flow

The linearized model (3.6) is a reasonably accurate approximation of power network behavior when the disturbance is sufficiently small. To deal with large disturbances from, e.g., increased penetration of renewable generation, in this section we consider a more realistic nonlinear power flow model. Moreover, in previous sections we only consider load control and ignore generator control. In practice, both generators and loads can participate in frequency control, and their interactions remain to be studied. In this section, we include generator dynamics in our model, and extend the decentralized *primary* frequency control developed in Section 3.2 to the generator side as well. In Section 3.5, we will develop and analyze a distributed *secondary* frequency control under nonlinear power flows and generator dynamics and control.

Power network model

We modify the power network model (3.6) by using nonlinear power flows, and also include the generator speed governor and turbine models from [16], [19], [20], [31], [32], [33]. The modified power network model is

$$
\begin{aligned}
M_j\dot{\omega}_j &= r_j + P_j^m - d_j - D_j\omega_j - P_j^{\text{out}} + P_j^{\text{in}} && \text{for all } j \in \mathcal{G}, && \text{(3.33a)}\\
0 &= r_j - d_j - D_j\omega_j - P_j^{\text{out}} + P_j^{\text{in}} && \text{for all } j \in \mathcal{L}, && \text{(3.33b)}\\
P_{ij} &= B_{ij}\sin\left(\theta_i - \theta_j\right) && \text{for all } (i,j) \in \mathcal{E}, && \text{(3.33c)}\\
\dot{\theta}_j &= \omega_j && \text{for all } j \in \mathcal{N}, && \text{(3.33d)}\\
T_{g,j}\dot{a}_j &= -a_j + p_j && \text{for all } j \in \mathcal{G}, && \text{(3.33e)}\\
T_{b,j}\dot{P}_j^m &= -P_j^m + a_j && \text{for all } j \in \mathcal{G}. && \text{(3.33f)}
\end{aligned}
$$

In equations (3.33a)–(3.33b), variables r_j represent uncontrollable generations or loads which, at time 0, make a step change on an arbitrary subset of buses, as the disturbance to the system. Note that r_j replaces the uncontrollable P_j^m in (3.6), since P_j^m in (3.33) is a variable driven by generator control. Equations (3.33c) are the nonlinear power flows, and (3.33d) are the relation between voltage phase angle (with respect to the rotating framework of nominal frequency) θ_i and frequency deviation ω_i from its nominal value. Equations (3.33e) and (3.33f) are, respectively, the dynamics of speed governors and turbines, where a_j is the valve position of the turbine, p_j is the control command to the generator, and P_j^m is the mechanical power injection to the generator. The time constants $T_{g,j}$ and $T_{b,j}$ characterize respectively the time-delay in governor actuations and the approximated fluid dynamics in turbines. Traditionally, there is a frequency feedback term $-\frac{1}{R_j}\omega_j$ on the right-hand-side of (3.33e), known as the droop control. Here we ignore this

term to allow for a general form of feedback control p_j on generators. In Sections 3.4–3.7, since we are considering a nonlinear model, all the variables in (3.33) represent their full quantities, instead of deviations from their nominal values as in Sections 3.1–3.3.[5] An exception is ω_i, which is still the frequency *deviation* from its nominal value.

The state variables of the dynamical system (3.33) are $x := (\theta, \omega, P, P^m_{\mathcal{G}}, a_{\mathcal{G}})$, the disturbance is r. The controls include generator control $p_{\mathcal{G}}$ on all the generator buses $\mathcal{G}$ and load control d on both generator buses $\mathcal{G}$ and load buses $\mathcal{L}$. We make the following two definitions related to our frequency control goals.

Definition 3.1. A *frequency-synchronized point* of the dynamical system (3.33) is a solution $(x^*, p^*_{\mathcal{G}}, d^*)$ of (3.33), where $\omega^*_i = \omega^*_j$ for all $i, j \in \mathcal{N}$, and $\dot{\omega}^*_j = \dot{a}^*_j = \dot{P}^{m,*}_j = 0$ for all $j \in \mathcal{G}$.

Definition 3.2. An *equilibrium point* of the dynamical system (3.33) is a solution $(x^*, p^*_{\mathcal{G}}, d^*)$ of (3.33), where $\dot{\theta}^*_j = 0$ for all $j \in \mathcal{N}$, and $\dot{\omega}^*_j = \dot{a}^*_j = \dot{P}^{m,*}_j = 0$ for all $j \in \mathcal{G}$.

Remark 3.7. As is clear from (3.33) and Definitions 3.1 and 3.2, ω^*, P^*, $P^{m,*}_{\mathcal{G}}$, $a^*_{\mathcal{G}}$, $p^*_{\mathcal{G}}$, d^* are all constant at both a frequency-synchronized point and an equilibrium point. The difference between them is that an equilibrium point not only requires ω^*_j to be the same across all $j \in \mathcal{N}$, but also requires them to be all zero such that θ^*_j for all $j \in \mathcal{N}$ are constant.[6] We focus on driving the dynamical system (3.33) to a frequency synchronized point through primary frequency control in the current section, and an equilibrium point through secondary frequency control in Section 3.5. □

Primary frequency control problem and decentralized algorithm

As in Section 3.1, given step changes r_j in generation or load on an arbitrary subset of buses at time 0, the goal of primary frequency control is to drive the system (3.33) to a frequency-synchronized point that is optimal for:

[5] In (3.33d), the constants are $B_{ij} = 3\frac{|V_i||V_j|}{x_{ij}}$ if full quantities of P and θ are considered, different from the values of B in (3.4) when deviations are considered.

[6] However, in Sections 3.1–3.3, we called a point where ω^*_j for all $j \in \mathcal{N}$ are the same but not zero as an equilibrium point, since phase angle θ is ignored in the dynamical system (3.6).

OLC (network, generator and load-side primary control):

$$\min_{\substack{\underline{p}_{\mathcal{G}} \le p_{\mathcal{G}} \le \overline{p}_{\mathcal{G}} \\ \underline{d} \le d \le \overline{d},\ \hat{d}}} \quad \sum_{j\in\mathcal{G}} c_j^p(p_j) + \sum_{j\in\mathcal{N}} c_j^d(d_j) + \sum_{j\in\mathcal{N}} \frac{1}{2D_j}\hat{d}_j^2 \tag{3.34a}$$

$$\text{subject to} \quad \sum_{j\in\mathcal{N}} d_j + \sum_{j\in\mathcal{N}} \hat{d}_j \;=\; \sum_{j\in\mathcal{N}} r_j + \sum_{j\in\mathcal{G}} p_j, \tag{3.34b}$$

where $-\infty < \underline{p}_j \le \overline{p}_j < \infty$ for $j \in \mathcal{G}$ and $-\infty < \underline{d}_j \le \overline{d}_j < \infty$ for $j \in \mathcal{N}$ specify generator and load control capacities, respectively, and c_j^p for $j \in \mathcal{G}$ and c_j^d for $j \in \mathcal{N}$ are cost functions for generator and load control, respectively. The motivation of (3.34) is the same as (3.7), except that (3.34) includes generator control $p_{\mathcal{G}}$. Note that at any frequency-synchronized point, the generator control $p_{\mathcal{G}}$, the valve positions $a_{\mathcal{G}}$, and the actual mechanical power input $P_{\mathcal{G}}^m$ to the generators are the same.

We make the following assumptions regarding OLC (3.34).

Assumption 3.2. OLC (3.34) is feasible. The cost functions c_j^p for $j \in \mathcal{G}$ and c_j^d for $j \in \mathcal{N}$ are strictly convex and twice continuously differentiable on $\left[\underline{p}_j,\ \overline{p}_j\right]$ and $\left[\underline{d}_j,\ \overline{d}_j\right]$, respectively.

Remark 3.8. Assumption 3.2 extends Assumption 3.1 to include generator control. The cost functions for various generator control schemes in, e.g., [19], [39], [40], [41], [43], [48] all satisfy Assumption 3.2. □

Based on Assumption 3.2 we have Lemma 3.6 below, which can be proved in a similar way that Lemma 3.2 is proved in Appendix 3.D. We define functions

$$p_j(\omega_j) := \left[\left(c_j^p\right)'^{-1}(-\omega_j)\right]_{\underline{p}_j}^{\overline{p}_j} \qquad \text{for all } j \in \mathcal{G}, \tag{3.35a}$$

$$d_j(\omega_j) := \left[\left(c_j^d\right)'^{-1}(\omega_j)\right]_{\underline{d}_j}^{\overline{d}_j} \qquad \text{for all } j \in \mathcal{N}, \tag{3.35b}$$

which are indeed the primary frequency control law we will discuss later.

Lemma 3.6. Suppose Assumption 3.2 holds. There exist a unique optimal $(p_{\mathcal{G}}^*, d^*, \hat{d}^*)$ for OLC (3.34) and a unique optimal ω^* for its dual, with zero duality gap. Moreover, we have $p_j^* = p_j(\omega^*)$ for all $j \in \mathcal{G}$, and $d_j^* = d_j(\omega^*)$ and $\hat{d}_j^* = D_j\omega^*$ for all $j \in \mathcal{N}$, where functions $p_j(\cdot)$ and $d_j(\cdot)$ are defined in (3.35).

Lemma 3.6, however, guarantees neither existence nor uniqueness of phase angles θ^* and power flows P^* that, together with $(\omega^*, P_{\mathcal{G}}^{m,*} = a_{\mathcal{G}}^* = p_{\mathcal{G}}^*, d^*)$, form a frequency-synchronized point of (3.33). In particular, power engineers are interested in θ^*

inside the *principal region*, i.e., $|\theta_i^* - \theta_j^*| < \frac{\pi}{2}$ for all $(i,j) \in \mathcal{E}$, for stability of the power network [111]. Therefore we make the following assumption.

Assumption 3.3. For any optimal $(p_{\mathcal{G}}^*, d^*, \hat{d}^* = D\omega^*)$ of OLC (3.34), there exist $\theta^* \in \mathbb{R}^{|\mathcal{N}|}$ where $\left|\theta_i^* - \theta_j^*\right| < \frac{\pi}{2}$ for all $(i,j) \in \mathcal{E}$, and $P^* \in \mathbb{R}^{|\mathcal{E}|}$, such that

$$
\begin{aligned}
0 &= r_j + p_j^* - d_j^* - D_j\omega_j^* - P_j^{\text{out},*} + P_j^{\text{in},*} && \text{for all } j \in \mathcal{G}, && \text{(3.36a)}\\
0 &= r_j - d_j^* - D_j\omega_j^* - P_j^{\text{out},*} + P_j^{\text{in},*} && \text{for all } j \in \mathcal{L}, && \text{(3.36b)}\\
P_{ij}^* &= B_{ij}\sin\left(\theta_i^* - \theta_j^*\right) && \text{for all } (i,j) \in \mathcal{E}. && \text{(3.36c)}
\end{aligned}
$$

A lot of work, e.g., [111], studies conditions for feasibility of power flow equations (3.36), which are beyond the scope of this thesis. Using a common practice in these previous studies, we treat θ^1 and θ^2 as the same point if $\left(\theta_j^1 - \theta_j^2\right) \mod 2\pi$ are the same across all $j \in \mathcal{N}$.[7] With this definition of the uniqueness of θ, it is shown in [111] that, given $(p_{\mathcal{G}}^*, d^*, \hat{d}^* = D\omega^*)$, the power flow solution (θ^*, P^*) of (3.36) is unique in the principal region. Then the following lemma follows from Lemma 3.6.

Lemma 3.7. Suppose Assumptions 3.2 and 3.3 hold. Then there is a *unique* $(\theta^*, \omega^*, P^*, p_{\mathcal{G}}^*, d^*)$ that satisfies all of the following:

- $(\theta^*, \omega^*, P^*, p_{\mathcal{G}}^*, d^*)$ is a solution of (3.36);
- $\left|\theta_i^* - \theta_j^*\right| < \frac{\pi}{2}$ for all $(i,j) \in \mathcal{E}$; and
- $(p_{\mathcal{G}}^*, d^*, \hat{d}^* = D\omega^*)$ and ω^* are optimal for OLC (3.34) and its dual.

We design the generator and load-side primary frequency control as (3.35), which extends the load control in Section 3.2 to generator control as well. The following theorem states our main result regarding the frequency-synchronized point of the closed-loop system (3.33)(3.35). We skip its proof since it is straightforward from Lemma 3.7 and Definition 3.1.

Theorem 3.4. Suppose Assumptions 3.2 and 3.3 hold. Then the closed-loop system (3.33)(3.35) has a unique frequency synchronized point $(\theta^*, \omega^*, P^*, P_{\mathcal{G}}^{m,*} = a_{\mathcal{G}}^* = p_{\mathcal{G}}^*, d^*)$ which satisfies both of the following:

- $\left|\theta_i^* - \theta_j^*\right| < \frac{\pi}{2}$ for all $(i,j) \in \mathcal{E}$; and
- $(p_{\mathcal{G}}^*, d^*, \hat{d}^* = D\omega^*)$ and ω^* are the unique optimal for OLC (3.34) and its dual.

[7] This treatment can be formally defined using an equivalent class of θ; see [112] for details.

Stability analysis

Now we study stability of the closed-loop system (3.33)(3.35) at the frequency-synchronized point in Theorem 3.4, denoted $(x^*, p^*_{\mathcal{G}}, d^*)$ in the rest of this section. Our approach for stability analysis is compositional [113], in that we find Lyapunov function candidates separately for the power network and the generators, and add them up to construct a Lyapunov function for the entire system.

We make the following assumption for our main result Theorem 3.5 regarding stability of (3.33)(3.35).

Assumption 3.4. The following is satisfied in a neighborhood of $(x^*, p^*_{\mathcal{G}}, d^*)$:
For all $j \in \mathcal{G}$, there are positive constants $\underline{\beta}_j$ and L_j such that the load control cost functions satisfy $\left(c_j^d\right)''(d_j) \leq \frac{1}{\underline{\beta}_j}$ and the generator control cost functions satisfy $\left(c_j^p\right)''(p_j) \geq \frac{1}{L_j}$. Moreover, $L_j < D_j + \underline{\beta}_j$ if $\underline{d}_j < d_j^* < \overline{d}_j$, and $L_j < D_j$ if $d_j^* = \underline{d}_j$ or $d_j^* = \overline{d}_j$.

In Assumption 3.4, the condition on L_j is less stringent when load control d_j^* in equilibrium stays strictly within its capacity limit, than when d_j^* reaches its limit.

Theorem 3.5. Suppose Assumptions 3.2, 3.3, and 3.4 hold. Then the closed-loop system (3.33)(3.35) has a unique frequency-synchronized point $(x^*, p^*_{\mathcal{G}}, d^*)$ characterized in Theorem 3.4, which is locally asymptotically stable.

Proof. We use the following energy function [36] as part of the Lyapunov function candidate for the closed-loop system (3.33)(3.35):

$$U_0 \;=\; \frac{1}{2}\sum_{j\in\mathcal{G}} M_j(\omega_j - \omega^*)^2 + \sum_{(i,j)\in\mathcal{E}} \int_{\theta_{ij}^*}^{\theta_{ij}} B_{ij}(\sin u - \sin\theta_{ij}^*)du, \qquad (3.37)$$

where $\theta_{ij} := \theta_i - \theta_j$. For θ_{ij} in a neighborhood of θ_{ij}^*, the integral in (3.37) is nonnegative, and zero if and only if $\theta_{ij} = \theta_{ij}^*$, since $|\theta_{ij}^*| < \pi/2$ for all $(i,j) \in \mathcal{E}$.

Let $(\tilde{x}, \tilde{p}_{\mathcal{G}}, \tilde{d}) := (x, p_{\mathcal{G}}, d) - (x^*, p^*_{\mathcal{G}}, d^*)$. For all $j \in \mathcal{G}$, let $\underline{\beta}'_j = \underline{\beta}_j$ if $\underline{d}_j < d_j^* < \overline{d}_j$, and $\underline{\beta}'_j = 0$ if $d_j^* = \underline{d}_j$ or $d_j^* = \overline{d}_j$. The time derivative of U_0 (3.37) along any

trajectory of the system (3.33)(3.35) is

$$\begin{aligned}
\dot{U}_0 &= \sum_{j\in\mathcal{G}} M_j\tilde{\omega}_j\dot{\omega}_j + \sum_{(i,j)\in\mathcal{E}} B_{ij}(\sin\theta_{ij} - \sin\theta^*_{ij})(\omega_i - \omega_j) \\
&= \sum_{j\in\mathcal{G}} \tilde{\omega}_j(r_j + P^m_j - d_j - D_j\omega_j - P^{\text{out},*}_j + P^{\text{in},*}_j) \\
&\quad + \sum_{j\in\mathcal{L}} \tilde{\omega}_j(r_j - d_j - D_j\omega_j - P^{\text{out},*}_j + P^{\text{in},*}_j) \qquad (3.38) \\
&= -\sum_{j\in\mathcal{N}} D_j\tilde{\omega}^2_j + \sum_{j\in\mathcal{G}} \tilde{\omega}_j\tilde{P}^m_j - \sum_{j\in\mathcal{N}} \tilde{\omega}_j\tilde{d}_j \qquad (3.39) \\
&\le -\sum_{j\in\mathcal{L}} D_j\tilde{\omega}^2_j + \sum_{j\in\mathcal{G}} \left(\tilde{\omega}_j\tilde{P}^m_j - (D_j + \underline{\beta}'_j)\tilde{\omega}^2_j\right), \qquad (3.40)
\end{aligned}$$

where we have (3.38) from (3.33a)–(3.33c), (3.39) from (3.36a)–(3.36b), and (3.40) from

$$\begin{aligned}
-(\omega_j - \omega^*)(d_j(\omega_j) - d_j(\omega^*)) &\le -\underline{\beta}'_j(\omega_j - \omega^*)^2 \qquad \text{for all } j \in \mathcal{G}, \\
-(\omega_j - \omega^*)(d_j(\omega_j) - d_j(\omega^*)) &\le 0 \qquad \text{for all } j \in \mathcal{L}
\end{aligned}$$

due to Assumption 3.4 for $j \in \mathcal{G}$ and the fact that $d_j(\cdot)$ in (3.35b) is monotonically increasing for $j \in \mathcal{N}$.

The other parts of the Lyapunov function candidate are constructed from turbine-governor dynamics of generators $j \in \mathcal{G}$. We rewrite (3.33e)–(3.33f) as

$$\dot{\tilde{y}}_j = A_j\tilde{y}_j + B_j\tilde{p}_j \qquad j \in \mathcal{G} \qquad (3.41)$$

where $\tilde{y}_j := \left[\tilde{a}_j, \tilde{P}^m_j\right]^T$, and $\tilde{p}_j := p_j(\omega_j) - p_j(\omega^*)$, and

$$A_j := \begin{bmatrix} -\frac{1}{T_{g,j}} & 0 \\ \frac{1}{T_{b,j}} & -\frac{1}{T_{b,j}} \end{bmatrix} \qquad B_j := \begin{bmatrix} \frac{1}{T_{g,j}} \\ 0 \end{bmatrix}.$$

A Lyapunov function candidate for the linear subsystem (3.41) takes the form

$$U_j = \frac{1}{2}\tilde{y}^T_j Q_j \tilde{y}_j \qquad j \in \mathcal{G}$$

where $Q_j \in \mathbb{R}^{2\times 2}$ is positive definite. The time derivative of U_j along the trajectory of (3.33)(3.35) is

$$\dot{U}_j = \frac{1}{2}\tilde{y}^T_j(Q_jA_j + A^T_jQ_j)\tilde{y}_j + \tilde{y}^T_jQ_jB_j\tilde{p}_j \qquad j \in \mathcal{G}. \qquad (3.42)$$

For all $j \in \mathcal{G}$ we claim (and will soon prove) that there exist $Q_j \succ 0$ and constant α_j, β_j, γ_j, and η_j that satisfy

$$\alpha_j > 0, \quad \gamma_j > 0, \tag{3.43a}$$

$$\beta_j < D_j + \underline{\beta}'_j, \tag{3.43b}$$

$$4\alpha_j(D_j + \underline{\beta}'_j - \beta_j) > 1 \tag{3.43c}$$

and

$$\dot{U}_j \leq -\alpha_j \left(\tilde{P}^m_j\right)^2 + \beta_j \tilde{\omega}_j^2 - \gamma_j \left(\tilde{a}_j + \eta_j \tilde{P}^m_j\right)^2. \tag{3.44}$$

Then, by (3.38)–(3.40), the time derivative of $U := U_0 + \sum_{j\in\mathcal{G}} U_j$ satisfies

$$\begin{aligned}\dot{U} \leq & -\sum_{j\in\mathcal{L}} D_j \tilde{\omega}_j^2 - \sum_{j\in\mathcal{G}} \gamma_j \left(\tilde{a}_j + \eta_j \tilde{P}^m_j\right)^2 \\ & + \sum_{j\in\mathcal{G}} \left(-(D_j + \underline{\beta}'_j - \beta_j)\tilde{\omega}_j^2 + \tilde{\omega}_j \tilde{P}^m_j - \alpha_j \left(\tilde{P}^m_j\right)^2\right),\end{aligned}$$

where, by (3.43), the third summation is non-positive, and zero only if $\tilde{\omega}_j = \tilde{P}^m_j = 0$ for all $j \in \mathcal{G}$. It is straightforward that $U \geq 0$ and $\dot{U} \leq 0$ in a neighborhood of $(x^*, p^*_{\mathcal{G}}, d^*)$, with both zero only at $(x^*, p^*_{\mathcal{G}}, d^*)$, which implies local asymptotic stability of $(x^*, p^*_{\mathcal{G}}, d^*)$. In the rest of this proof, it is sufficient to find $Q_j \succ 0$ and constant α_j, β_j, γ_j, and η_j which satisfy (3.43)–(3.44) for all $j \in \mathcal{G}$.

We choose Q_j to be diagonal with positive entries $Q_{j,11}$ and $Q_{j,22}$. To ensure $Q_j A_j + A_j^T Q_j \prec 0$, we require

$$\frac{Q_{j,22}}{T_{g,j}} > \frac{Q_{j,22}}{4T_{b,j}}.$$

A calculation from (3.42) gives

$$\begin{aligned}\dot{U}_j &= -\frac{Q_{j,22}}{T_{g,j}}\tilde{a}_j^2 - \frac{Q_{j,22}}{T_{b,j}}\left(\tilde{P}^m_j\right)^2 + \frac{Q_{j,22}}{T_{b,j}}\tilde{a}_j\tilde{P}^m_j + \frac{Q_{j,22}}{T_{g,j}}\tilde{a}_j\tilde{p}_j \\ &= -\left(\frac{Q_{j,22}}{T_{b,j}} - \frac{Q_{j,22}^2}{4\gamma_j T_{b,j}^2}\right)\left(\tilde{P}^m_j\right)^2 + \frac{Q_{j,22}^2}{4T_{g,j}(Q_{j,22} - \gamma_j T_{g,j})}\left(\tilde{p}_j\right)^2 \\ &\quad -\gamma_j\left(\tilde{a}_j - \frac{Q_{j,22}}{2\gamma_j T_{b,j}}\tilde{P}^m_j\right)^2 - \left(\frac{Q_{j,22}}{T_{g,j}} - \gamma_j\right)\left(\tilde{a}_j - \frac{Q_{j,22}\cdot\tilde{p}_j}{2(Q_{j,22} - \gamma_j T_{g,j})}\right)^2\end{aligned} \tag{3.45}$$

for arbitrary $\gamma_j \in \left(\frac{Q_{j,22}}{4T_{b,j}}, \frac{Q_{j,22}}{T_{g,j}}\right)$. By Assumption 3.4 and the function $p_j(\cdot)$ in (3.35a), we have $\left(\tilde{p}_j\right)^2 \leq L_j^2 \tilde{\omega}_j^2$ in a neighborhood of ω^*. Take

$$\alpha_j = \frac{Q_{j,22}}{T_{b,j}} - \frac{Q_{j,22}^2}{4\gamma_j T_{b,j}^2}, \qquad \beta_j = \frac{Q_{j,22}^2 L_j^2}{4T_{g,j}(Q_{j,22} - \gamma_j T_{g,j})}, \qquad \eta_j = -\frac{Q_{j,22}}{2\gamma_j T_{b,j}}.$$

Note that α_j and γ_j satisfy (3.43a). By (3.45) we have (3.44). We still need to show (3.43b)–(3.43c). To this end, we make the following transformation

$$\xi_j = \frac{Q_{j,22}}{4T_{b,j}}, \qquad \sigma_j = \frac{\xi_j}{\gamma_j}, \qquad z_j = \frac{T_{g,j}\gamma_j}{Q_{j,22}}, \tag{3.46}$$

so that

$$\xi_j > 0, \qquad 0 < \sigma_j < 1, \qquad 0 < z_j < 1. \tag{3.47}$$

Hence (3.43b)–(3.43c) become

$$D_j + \underline{\beta}'_j - \frac{L_j^2 \xi_j}{4\sigma_j z_j (1 - z_j)} \;>\; 0 \tag{3.48a}$$

$$16\xi_j(1 - \sigma_j)\left(D_j + \underline{\beta}'_j - \frac{L_j^2 \xi_j}{4\sigma_j z_j (1 - z_j)}\right) \;>\; 1. \tag{3.48b}$$

Subject to (3.47)(3.48a), the maximum of the left-hand-side of (3.48b) is

$$\left(D_j + \underline{\beta}'_j\right)^2 / L_j^2,$$

attained at $z_j = 1/2$, $\xi_j = \sigma_j \left(D_j + \underline{\beta}'_j\right) / \left(2L_j^2\right)$, and $\sigma_j = \frac{1}{2}$. By Assumption 3.4 we have $\left(D_j + \underline{\beta}'_j\right)^2 / L_j^2 > 1$, i.e., there exists a (ξ_j, σ_j, z_j) that satisfies (3.47)–(3.48). Through inverse transformation of (3.46), we can find positive definite, diagonal matrices Q_j and constant α_j, β_j, γ_j, and η_j that satisfy (3.43)–(3.44), and hence finish the proof. □

Remark 3.9. The local asymptotic stability in Theorem 3.5 means that any trajectory of (3.33) and (3.35) starting within a region of attraction around the frequency-synchronized point $(x^*, p^*_{\mathcal{G}}, d^*)$ will converge to $(x^*, p^*_{\mathcal{G}}, d^*)$. This region of attraction can be estimated using the methods in, e.g., [114], [115], [116] and taking into consideration the region where Assumption 3.4 holds. □

We prove local asymptotic stability in Theorem 3.5 using a Lyapunov function for the nonlinear dynamics, instead of the common approach based on linearization [117]. Theorem 3.5 provides a sufficient condition, which may not be necessary, for stability, since our proof assumes the particular (diagonal) structure of Q_j and constructs the particular bound (3.44) of $\dot{U}_j$. In future work we would like to understand how conservative the sufficient stability condition in Theorem 3.5 is, and derive less conservative conditions.

3.5 Generator and load-side secondary control with nonlinear power flow

As in Section 3.4, we use the power network model (3.33) which includes nonlinear power flow and generator dynamics and control. In this section, we develop and analyze distributed *secondary* frequency control to restore frequency to its nominal value and inter-area power flows to their scheduled values.

Secondary frequency control problem

Given step changes r_j in generation or load on an arbitrary subset of buses at time 0, the goal of secondary frequency control is to drive the system (3.33) to an equilibrium point (defined by Definition 3.2) that is optimal for:

OLC (network, generator and load-side secondary control):

$$\min_{\substack{\underline{p}_{\mathcal{G}} \le p_{\mathcal{G}} \le \overline{p}_{\mathcal{G}} \\ \underline{d} \le d \le \overline{d},\ P}} \quad \sum_{j\in\mathcal{G}} c_j^p(p_j) + \sum_{j\in\mathcal{N}} c_j^d(d_j) \tag{3.49a}$$

$$\text{subject to} \quad r_j + p_j = d_j + P_j^{\text{out}} - P_j^{\text{in}} \quad \text{for all } j \in \mathcal{G}, \tag{3.49b}$$

$$r_j = d_j + P_j^{\text{out}} - P_j^{\text{in}} \quad \text{for all } j \in \mathcal{L}, \tag{3.49c}$$

$$\sum_{j\in\mathcal{N}} E_{kj}\left(P_j^{\text{out}} - P_j^{\text{in}}\right) = \hat{P}_k \quad \text{for all } k \in \mathcal{K}. \tag{3.49d}$$

Now we explain (3.49) by comparing it with the primary OLC problem (3.34).

The first difference is that the variables $\hat{d}_j$ for $j \in \mathcal{N}$ do not appear in (3.49). Indeed, at any equilibrium point of (3.33), we have $\hat{d}_j^* = D_j\omega^* = 0$ which means frequencies at all the buses are restored to their common nominal value.

The second difference is that the branch power flows P_{ij} for all $(i,j) \in \mathcal{E}$ are explicitly included in (3.49) as optimization variables. Moreover, the per-bus power balance constraints (3.49a)–(3.49b), where branch power flows play an important role, are considered instead of the network-wide power balance (3.34b). Including branch flows is a prerequisite for introducing the third difference below.

The third difference lies in the additional constraint (3.49d), which is called the *inter-area flow* constraint. In practice, the power network $(\mathcal{N},\mathcal{E})$ is often partitioned into several control areas, i.e., subgraphs. Let $\mathcal{K}$ be the set of control areas, and define matrix $E \in \{0,1\}^{|\mathcal{K}|\times|\mathcal{N}|}$ such that $E_{k,j} = 1$ if bus j lies in area k, and $E_{k,j} = 0$ otherwise. Then (3.49d) says that the net power flows out of areas $k \in \mathcal{K}$ must be equal to their pre-scheduled (at a slower time scale in, e.g., the tertiary control) values $\hat{P}_k$.

Remark 3.10. In our work [57], which is not included in this thesis, we develop a modified version of the secondary frequency control in this section to enforce thermal limits, i.e., maximum branch power flows allowed. The control scheme in [57] extends those in [45], [46] to include generator dynamics, while all of these studies are based on the linearized power flow model (3.3)–(3.5). Under the nonlinear power flow model (3.33c), we can enforce thermal limits on a subset of lines where each line forms a cutset of the graph. We do this by generalizing the constraint (3.49d) in the following way. For any given subset $\mathcal{M} \subseteq \mathcal{N}$ of buses, define a row vector $E_{\mathcal{M}} \in \{0,1\}^{1\times|\mathcal{N}|}$ such that its j-th component $E_{\mathcal{M},j} = 1$ if bus $j \in \mathcal{M}$, and $E_{\mathcal{M},j} = 0$ otherwise. Then the inequality constraint

$$\underline{p}_{\mathcal{M}} \leq \quad E_{\mathcal{M}} C P \quad \leq \overline{p}_{\mathcal{M}}, \tag{3.50}$$

where C is the incidence matrix of graph $(\mathcal{N}, \mathcal{E})$, limits the net power flow out of $\mathcal{M}$ within $[\underline{p}_{\mathcal{M}}, \overline{p}_{\mathcal{M}}]$. If the branch power flow P_{ij} can be expressed as $P_{ij} = E_{\mathcal{M}} C P$ for some $\mathcal{M}$, then (3.50) actually imposes thermal limit constraint $\underline{p}_{\mathcal{M}} \leq P_{ij} \leq \overline{p}_{\mathcal{M}}$. This is the case if and only if line (i, j) itself forms a cutset of graph $(\mathcal{N}, \mathcal{E})$. □

We make the following assumptions regarding OLC (3.49).

Assumption 3.5. OLC (3.49) is feasible. The cost functions c_j^p for $j \in \mathcal{G}$ and c_j^d for $j \in \mathcal{N}$ are strictly convex and twice continuously differentiable on $\left[\underline{p}_j,\ \overline{p}_j\right]$ and $\left[\underline{d}_j,\ \overline{d}_j\right]$, respectively.

Assumption 3.6. There exists an optimal $(p^*_{\mathcal{G}}, d^*, P^*)$ of OLC (3.49) and $\theta^* \in \mathbb{R}^{|\mathcal{N}|}$ where $\left|\theta_i^* - \theta_j^*\right| < \frac{\pi}{2}$ for all $(i, j) \in \mathcal{E}$, such that[8]

$$\begin{aligned} r_j + p_j^* &= d_j^* + P_j^{\text{out},*} - P_j^{\text{in},*} && \text{for all } j \in \mathcal{G}, && (3.51a)\\ r_j &= d_j^* + P_j^{\text{out},*} - P_j^{\text{in},*} && \text{for all } j \in \mathcal{L}, && (3.51b)\\ P_{ij}^* &= B_{ij} \sin\left(\theta_i^* - \theta_j^*\right) && \text{for all } (i,j) \in \mathcal{E}. && (3.51c) \end{aligned}$$

As a result of these assumptions, we have the following lemma.

Lemma 3.8. Suppose Assumptions 3.5 and 3.6 hold. Then there is a *unique* $(\theta^*, P^*, p^*_{\mathcal{G}}, d^*)$ that satisfies all of the following:

- $(\theta^*, P^*, p^*_{\mathcal{G}}, d^*)$ is a solution of (3.51);
- $\left|\theta_i^* - \theta_j^*\right| < \frac{\pi}{2}$ for all $(i, j) \in \mathcal{E}$; and

[8] (3.51a)–(3.51b) repeat constraints (3.49a)–(3.49b).

- $(p^*_{\mathcal{G}}, d^*, P^*)$ is optimal for OLC (3.49).

We skip the proof of Lemma 3.8 since it uses a similar technique to the proof of Lemma 3.7

Distributed secondary frequency control algorithm

Traditionally the goals of secondary frequency control formalized in (3.49) are achieved with automatic generation control (AGC), a centralized (within each control area) generator control scheme [14], [16], [17]. For scalability to a large number of participants, especially controllable loads, we design the following distributed control algorithm written in the vector form:

$$
\begin{aligned}
p_{\mathcal{G}} &= p_{\mathcal{G}}(\lambda_{\mathcal{G}} + \omega_{\mathcal{G}}), \qquad d = d(\lambda + \omega), && \text{(3.52a)}\\
\dot{\lambda} &= K^{\lambda}\left(M\dot{\omega} + D\omega + CP - CB\sin(C^T\phi)\right), && \text{(3.52b)}\\
\dot{\pi} &= K^{\pi}\left(ECB\sin(C^T\phi) - \hat{P}_{\mathcal{K}}\right), && \text{(3.52c)}\\
\dot{\phi} &= \lambda - E^T\pi, && \text{(3.52d)}
\end{aligned}
$$

where $p_{\mathcal{G}}(\lambda_{\mathcal{G}} + \omega_{\mathcal{G}})$ and $d(\lambda + \omega)$ are vector valued functions $(p_j(\lambda_j + \omega_j),\ j \in \mathcal{G})$ and $(d_j(\lambda_j + \omega_j),\ j \in \mathcal{N})$ with $p_j(\cdot)$ and $d_j(\cdot)$ defined in (3.35). Diagonal matrices $K^{\lambda} \in \mathbb{R}^{|\mathcal{N}|\times|\mathcal{N}|}$ and $K^{\pi} \in \mathbb{R}^{|\mathcal{K}|\times|\mathcal{K}|}$ are positive constant control gains, diagonal matrices $M = \mathrm{diag}(M_{\mathcal{G}}, 0_{\mathcal{L}})$, $D = \mathrm{diag}(D_i,\ i \in \mathcal{N})$, and $B = \mathrm{diag}(B_{ij}\ (i,j) \in \mathcal{E})$ are system parameters, and C is the incidence matrix of graph $(\mathcal{N}, \mathcal{E})$.

The control algorithm (3.52) computes auxiliary variables $\lambda, \phi \in \mathbb{R}^{|\mathcal{N}|}$ and $\pi \in \mathbb{R}^{|\mathcal{K}|}$ in real time. It is a distributed algorithm in that it operates via local measurements and computations, as well as communication between neighbors. In (3.52b), each bus $j \in \mathcal{N}$ computes λ_j by local measurements of ω_j and the total power flow out of j, and by receiving ϕ_i from all of its neighbors i. In (3.52c), each area $k \in \mathcal{K}$ computes π_k by monitoring the differences of ϕ across lines connecting area k with other areas. The signal π_k is then broadcast to all the buses in area k. In (3.52d), each bus $j \in \mathcal{N}$ computes ϕ_j from its local λ_j and the signal π_k it receives.

Next we study the equilibrium and stability of the closed-loop system (3.33)(3.52).

Equilibrium analysis

We have the following theorem regarding the equilibrium point of the closed-loop dynamical system (3.33)(3.52). For convenience, let $y := (\lambda, \pi, \phi)$.

Theorem 3.6. Suppose Assumptions 3.5 and 3.6 hold. Then the closed-loop system (3.33)(3.52) has a unique equilibrium $(\theta^*, \omega^*, P^*, P^{m,*}_{\mathcal{G}} = a^*_{\mathcal{G}} = p^*_{\mathcal{G}}, d^*)$ that satisfies all of the following:

- $\omega^* = 0$;
- $\left|\theta^*_i - \theta^*_j\right| < \frac{\pi}{2}$ for all $(i, j) \in \mathcal{E}$; and
- $(p^*_{\mathcal{G}}, d^*, P^*)$ is optimal for OLC (3.49).

Proof. (Existence.) OLC (3.49) has differentiable objective and constraint functions and satisfies Slater's condition [93, Ch. 5.2.3]. Therefore a point $(p^*_{\mathcal{G}}, d^*, P^*)$ is optimal for OLC (3.49) if and only if there is a (λ^*, π^*) which, together with $(p^*_{\mathcal{G}}, d^*, P^*)$, satisfies the (equivalently modified version of) KKT conditions:[9]

$$
\begin{aligned}
0 &= r + p^* - d^* - CP^*, && \text{(3.53a)}\\
0 &= ECP^* - \hat{P}_{\mathcal{K}}, && \text{(3.53b)}\\
p^*_{\mathcal{G}} &= p_{\mathcal{G}}(\lambda^*_{\mathcal{G}}), \qquad d^* = d(\lambda^*), && \text{(3.53c)}\\
0 &= C^T E^T \pi^* - C^T \lambda^*, && \text{(3.53d)}
\end{aligned}
$$

where (3.53a)–(3.53b) are primal feasibility, and (3.53c)–(3.53d) combine stationarity, dual feasibility, and complementary slackness. By Lemma 3.8, there is a unique $(\theta^*, P^*, p^*_{\mathcal{G}}, d^*)$ which satisfies $\left|\theta^*_i - \theta^*_j\right| < \frac{\pi}{2}$ for all $(i, j) \in \mathcal{E}$, equation (3.51), and (3.53) with some (λ^*, π^*). These $(\theta^*, P^*, p^*_{\mathcal{G}}, d^*)$ and (λ^*, π^*), together with $\omega^* = 0$, $P^{m,*}_{\mathcal{G}} = a^*_{\mathcal{G}} = p^*_{\mathcal{G}}$, and $\phi^* = \theta^*$, form an equilibrium $(x^*, y^*, p^*_{\mathcal{G}}, d^*)$ of (3.33)(3.52) by Definition 3.2.[10]

(Uniqueness.) At any equilibrium $(x^*, y^*, p^*_{\mathcal{G}}, d^*)$, equation (3.53) must be satisfied as part of the definition for an equilibrium. Therefore $(p^*_{\mathcal{G}}, d^*, P^*)$ is optimal for OLC (3.49). Moreover, since $\left|\theta^*_i - \theta^*_j\right| < \frac{\pi}{2}$ for all $(i, j) \in \mathcal{E}$ and (3.51) is satisfied at this equilibrium, by Lemma 3.8, θ^* is also unique. Uniqueness of ω^*, $P^{m,*}_{\mathcal{G}}$, and $a^*_{\mathcal{G}}$ is straightforward. □

The uniqueness in Theorem 3.6 is only for physical quantities in equilibrium, such as generation $P^{m,*}_{\mathcal{G}}$, load d^*, power flows P^*, frequencies ω^*, and phase angles θ^*.

[9] For convenience, let $P^m_{\mathcal{L}} = p_{\mathcal{L}} \equiv 0$ through out this section.

[10] It is easy to check that $\dot{\lambda} = 0$ and $\dot{\pi} = 0$ at this point. However, by (3.52d)(3.53d) we have $\dot{\phi} = \lambda^* - E^T \pi^* \in \text{span}(1)$, which means ϕ^* at y^* is not a constant but instead rotates at a synchronized speed. We still call such $(x^*, y^*, p^*_{\mathcal{G}}, d^*)$ an equilibrium point.

It does not guarantee the uniqueness of auxiliary variables $y^* = (\lambda^*, \pi^*, \phi^*)$ in equilibrium. Let Z^* be the set of all equilibrium points of (3.33)(3.52). In the stability analysis below, we will consider the following subset of Z^*:

$$Z^*_\phi := \left\{ (x^*, y^*, p^*_\mathcal{G}, d^*) \in Z^* \mid \left| \phi^*_i - \phi^*_j \right| < \frac{\pi}{2},\ \forall (i,j) \in \mathcal{E} \right\}. \tag{3.54}$$

Due to the uniqueness of P^*, the fact that $CP^* = CB\sin(C^T\phi^*)$ (from (3.52b)), and the uniqueness of the power flow solution in the principal region [111], there must be a unique $\phi^* = \theta^*$ for all the points in Z^*_ϕ.

Stability analysis

Now we study stability of the closed-loop system (3.33)(3.52) at the set Z^*_ϕ of equilibrium points.

We make the following assumptions for our main result Theorem 3.7.

Assumption 3.7. For all $j \in \mathcal{N}$, load control action d^*_j in equilibrium stays strictly within its capacity limit, i.e., $\underline{d}_j < d^*_j < \overline{d}_j$.

Assumption 3.8. The following is satisfied in a neighborhood of $(x^*, p^*_\mathcal{G}, d^*)$:
For all $j \in \mathcal{G}$, there are constants $\underline{\beta}_j > L_j > 0$, such that the load control cost functions satisfy $\left(c^d_j\right)''(d_j) \le \frac{1}{\underline{\beta}_j}$ and the generator control cost functions satisfy $\left(c^p_j\right)''(p_j) \ge \frac{1}{L_j}$.

Theorem 3.7. Suppose Assumptions 3.5–3.8 hold. Then any trajectory $(x(t), y(t), p_\mathcal{G}(t), d(t), t \ge 0)$ of the closed-loop system (3.33)(3.52), as $t \to \infty$, converges to an equilibrium $(x^*, y^*, p^*_\mathcal{G}, d^*) \in Z^*_\phi$, given that $(x(0), y(0), p_\mathcal{G}(0), d(0))$ lies in a neighborhood[11] of Z^*_ϕ.

Proof. Fix any equilibrium $(x^*, y^*, p^*_\mathcal{G}, d^*)$ in Z^*_ϕ. Let

$$(\tilde{x}, \tilde{y}, \tilde{p}_\mathcal{G}, \tilde{d}) := (x, y, p_\mathcal{G}, d) - (x^*, y^*, p^*_\mathcal{G}, d^*).$$

Let $\theta_{ij} := \theta_i - \theta_j$ and $\phi_{ij} := \phi_i - \phi_j$ for all $(i,j) \in \mathcal{E}$. Consider the following Lyapunov function candidate:

$$U \;=\; U_0 + \sum_{j \in \mathcal{G}} U_j, \tag{3.55}$$

[11] See Remark 3.9 regarding estimation of this neighborhood.

where

$$\begin{aligned} U_0 &= \frac{1}{2}\tilde{\omega}_{\mathcal{G}}^T M_{\mathcal{G}} \tilde{\omega}_{\mathcal{G}} + \sum_{(i,j)\in\mathcal{E}} B_{ij} \int_{\theta_{ij}^*}^{\theta_{ij}} (\sin u - \sin\theta_{ij}^*) du \\ &\quad + \sum_{(i,j)\in\mathcal{E}} B_{ij} \int_{\phi_{ij}^*}^{\phi_{ij}} (\sin u - \sin\phi_{ij}^*) du \\ &\quad + \frac{1}{2}\tilde{\lambda}^T (K^\lambda)^{-1} \tilde{\lambda} + \frac{1}{2}\tilde{\pi}^T (K^\pi)^{-1} \tilde{\pi} \end{aligned} \tag{3.56}$$

and

$$U_j = \frac{1}{2}\left[\tilde{a}_i, \tilde{P}_j^m\right] Q_j \left[\tilde{a}_i, \tilde{P}_j^m\right]^T \qquad \text{for all } j \in \mathcal{G} \tag{3.57}$$

for some positive definite matrices $Q_j \in \mathbb{R}^{2\times 2}$.

In a neighborhood of the equilibrium $(x^*, y^*, p_{\mathcal{G}}^*, d^*)$, the Lyapunov function candidate U (3.55) is nonnegative, and zero only at $(x^*, y^*, p_{\mathcal{G}}^*, d^*)$. Moreover, the time derivative of U_0 along any trajectory of the system (3.33)(3.52) is

$$\begin{aligned} \dot{U}_0 &= \tilde{\omega}_{\mathcal{G}}^T \left\{ r_{\mathcal{G}} + P_{\mathcal{G}}^m - D_{\mathcal{G}}\omega_{\mathcal{G}} - d_{\mathcal{G}} - C_{\mathcal{G}} B \sin(C^T\theta) \right\} \\ &\quad + \tilde{\omega}^T \left\{ CB\sin(C^T\theta) - CB\sin(C^T\theta^*) \right\} \\ &\quad + (\tilde{\lambda} - E^T\tilde{\pi})^T \left\{ CB\sin(C^T\phi) - CB\sin(C^T\phi^*) \right\} \\ &\quad + \tilde{\lambda}^T \left\{ r + P^m - d - CB\sin(C^T\phi) \right\} \\ &\quad + \tilde{\pi}^T \left\{ ECB\sin(C^T\phi) - \hat{P}_{\mathcal{K}} \right\} \qquad (3.58) \\ &= \tilde{\omega}^T \left\{ r + P^m - D\omega - d - CB\sin(C^T\theta^*) \right\} \\ &\quad + \tilde{\lambda}^T \left\{ r + P^m - d - CB\sin(C^T\phi^*) \right\} \\ &\quad + \tilde{\pi}^T \left\{ ECB\sin(C^T\phi^*) - \hat{P}_{\mathcal{K}} \right\} \qquad (3.59) \\ &= -\tilde{\omega}^T D\tilde{\omega} - (\tilde{\omega} + \tilde{\lambda})^T \tilde{d} + (\tilde{\omega}_{\mathcal{G}} + \tilde{\lambda}_{\mathcal{G}})^T \tilde{P}_{\mathcal{G}}^m, \qquad (3.60) \end{aligned}$$

where we get (3.58) by system dynamics (3.33)(3.52) and the fact that $\lambda^* - E^T\pi^* \in$ span(1), get (3.59) by (3.33b), and get (3.60) by the definition of an equilibrium point. By Assumption 3.8 and $d_j(\cdot)$ in (3.35b) we have

$$\begin{aligned} -(\tilde{\omega} + \tilde{\lambda})^T \tilde{d} &= -\sum_{j\in\mathcal{N}} (\tilde{\omega}_j + \tilde{\lambda}_j)(d_j(\omega_j + \lambda_j) - d_j(\omega_j^* + \lambda_j^*)) \\ &\le -\sum_{j\in\mathcal{N}} \underline{\beta}_j \left(\tilde{\omega}_j + \tilde{\lambda}_j\right)^2 \end{aligned}$$

in a neighborhood of (ω^*, λ^*). Moreover, we construct U_i (3.57) using the approach in the proof of Theorem 3.5, and get

$$\begin{aligned}
\dot{U} &= \dot{U}_0 + \sum_{j\in\mathcal{G}} \dot{U}_j \\
&\leq -\tilde{\omega}^T D\tilde{\omega} - \sum_{j\in\mathcal{L}} \underline{\beta}_j \left(\tilde{\omega}_j + \tilde{\lambda}_j\right)^2 \\
&\quad + \sum_{j\in\mathcal{G}} \left\{ -(\underline{\beta}_j - \beta_j)\left(\tilde{\omega}_j + \tilde{\lambda}_j\right)^2 + \left(\tilde{\omega}_j + \tilde{\lambda}_j\right)\tilde{P}_j^m - \alpha_i \left(\tilde{P}_j^m\right)^2 \right\} \\
&\quad - \sum_{j\in\mathcal{G}} \gamma_j \left(\tilde{a}_j + \eta_j \tilde{P}_j^m\right)^2,
\end{aligned}$$

where constant α, β, γ, and η make $\dot{U}$ non-positive, and zero if and only if $\tilde{\omega} = \tilde{\lambda} = 0$ and $\tilde{P}_{\mathcal{G}}^m = \tilde{a}_{\mathcal{G}} = 0$. Hence U is a Lyapunov function. The rest of the proof uses the same approach as the proofs of Lemma 3.5 and Theorem 3.1. □

Theorem 3.7 states the stability result for closed-loop equilibrium points in Z_ϕ^* which satisfy $\theta^* = \phi^*$ both in the principal region. In practice, the initial values of θ and ϕ can be configured such that their trajectories are close enough to or lie in the principal region, if the disturbance is sufficiently small. Moreover, the conditions in Theorem 3.7 are satisfied in practice in the following manner: (i) the controllable loads have large enough control capacities such that they do not hit their bounds in equilibrium; (ii) around the equilibrium, the gains for fast-acting load control are large enough; (iii) around the equilibrium, the gains for generator control (which is slower than load control due to governor and turbine dynamics) are small enough. We remark that the condition in Theorem 3.7 is sufficient but may not be necessary for stability. It is our future work to find less conservative stability conditions.

3.6 Decentralized frequency integral control

Till now, all of our distributed frequency control schemes have been developed using the optimal load control (OLC) framework. Indeed, there is more than one way to design a distributed control scheme that stabilizes frequency and restores frequency to its nominal value. In this section, we show such an example design, a decentralized frequency integral control. This control ensures *global* convergence of the closed-loop system to a set of equilibrium points, whereas the schemes in Sections 3.4 and 3.5 only guarantee local asymptotic stability, under the nonlinear power flow model.

We consider the following power network model

$$\begin{aligned} M_j\dot{\omega}_j &= r_j + p_j - D_j\omega_j - P_j^{\text{out}} + P_j^{\text{in}} && \text{for all } j \in \mathcal{G}, && (3.61a)\\ 0 &= r_j + p_j - D_j\omega_j - P_j^{\text{out}} + P_j^{\text{in}} && \text{for all } j \in \mathcal{L}, && (3.61b)\\ P_{ij} &= B_{ij}\sin\left(\theta_i - \theta_j\right) && \text{for all } (i,j) \in \mathcal{E}, && (3.61c)\\ \dot{\theta}_j &= \omega_j && \text{for all } j \in \mathcal{N}, && (3.61d) \end{aligned}$$

which is a simplified version of (3.33). First, we ignore the generator governor and turbine dynamics (3.33e) and (3.33f). Second, we do not distinguish between generator and load controls, but instead consider a single control p_j in power injection at every bus $j \in \mathcal{N}$.

Our goal in this section is to design a distributed control scheme which, given step changes r_j in generation or load on an arbitrary subset of buses at time 0, can drive the system (3.61) to a new equilibrium point where frequency everywhere is restored to its nominal value. In this section, we do not require the new equilibrium to be an optimal point of any OLC problem. To this end, we propose the following *decentralized integral (DI)* control:

$$\begin{aligned} p_j &= -K_j s_j && \text{for all } j \in \mathcal{N}, && (3.62a)\\ \dot{s}_j &= \omega_j && \text{for all } j \in \mathcal{N}, && (3.62b) \end{aligned}$$

where $K_j > 0$ for all $j \in \mathcal{N}$ are arbitrarily selected constant control gains. The control scheme (3.62) is completely decentralized in that every participating unit only takes integral of the frequency deviation measured on its local bus, and does not require any explicit communication with other buses or a control center. Without loss of generality, we take $s_j(0) = 0$ for all $j \in \mathcal{N}$, and then have

$$p_j(t) = -K_j \int_0^t \omega_j(\tau)d\tau = -K_j\left(\theta_j(t) - \theta_j(0)\right) \qquad \text{for all } j \in \mathcal{N}. \tag{3.63}$$

Let $K := \text{diag}(K_j,\ j \in \mathcal{N})$, $\theta_0 := (\theta_j(0),\ j \in \mathcal{N})$, and

$$F(\theta) := r - K(\theta - \theta_0) - CB\sin(C^T\theta). \tag{3.64}$$

Then the set of equilibrium points of the closed-loop system (3.61)–(3.62) is[12]

$$\Theta^* := \left\{(\theta,\omega) \in \mathbb{R}^{2|\mathcal{N}|} \mid \omega = 0, F(\theta) = 0\right\}. \tag{3.65}$$

We have the following theorem regarding existence and stability of Θ^*.

[12]For simplicity, we omit variables p and s from the definition of equilibrium points.

Theorem 3.8. The closed-loop system (3.61)–(3.62) has a nonempty set Θ^* of equilibrium points. Moreover, starting from any feasible initial point $(\theta(0), \omega(0)) \in \mathbb{R}^{2|\mathcal{N}|}$, every trajectory $(\theta(t), \omega(t), t \geq 0)$ generated by (3.61)–(3.62) approaches Θ^* as $t \to \infty$.

Proof. By (3.61b)(3.63)(3.64) we have

$$\omega_{\mathcal{L}} \equiv D_{\mathcal{L}}^{-1} F_{\mathcal{L}}(\theta),$$

i.e., $\omega_{\mathcal{L}}$ is a continuous function of θ. Therefore we only need to show that

$$\Theta_{\mathcal{G}}^* := \left\{(\theta, \omega_{\mathcal{G}}) \in \mathbb{R}^{|\mathcal{N}|+|\mathcal{G}|} \mid \omega_{\mathcal{G}} = 0, F(\theta) = 0\right\}$$

is nonempty and any trajectory $(\theta(t), \omega_{\mathcal{G}}(t))$ of (3.61)–(3.62) globally converges to $\Theta_{\mathcal{G}}^*$ as $t \to \infty$. Consider the Lyapunov function[13]

$$U(\theta, \omega_{\mathcal{G}}) = \frac{1}{2}\omega_{\mathcal{G}}^T M_{\mathcal{G}} \omega_{\mathcal{G}} + V(\theta) + \frac{1}{2}(\theta - \theta_0)^T K (\theta - \theta_0) \tag{3.66}$$

where

$$V(\theta) := \sum_{(i,j)\in\mathcal{E}} B_{ij}\left(1 - \cos(\theta_i - \theta_j)\right) - \sum_{j\in\mathcal{N}} r_j \theta_j. \tag{3.67}$$

The time derivative of U (3.66) along any trajectory of (3.61)–(3.62) is

$$\begin{aligned}
\dot{U}(\theta, \omega_{\mathcal{G}}) &= \omega_{\mathcal{G}}^T M_{\mathcal{G}} \dot{\omega}_{\mathcal{G}} + \sum_{(i,j)\in\mathcal{E}} B_{ij} \sin(\theta_i - \theta_j)(\omega_i - \omega_j) \\
&\quad - \sum_{j\in\mathcal{N}} r_j \omega_j + \omega^T K(\theta - \theta_0) \\
&= -\omega_{\mathcal{G}}^T D_{\mathcal{G}} \omega_{\mathcal{G}} + \omega_{\mathcal{G}}^T F_{\mathcal{G}}(\theta) - \omega^T F(\theta) \qquad (3.68) \\
&= -\omega_{\mathcal{G}}^T D_{\mathcal{G}} \omega_{\mathcal{G}} - \omega_{\mathcal{L}}^T(\theta) D_{\mathcal{L}} \omega_{\mathcal{L}}(\theta) \leq 0, \qquad (3.69)
\end{aligned}$$

where the equality in (3.68) is from (3.61a) and (3.64), and the equality in (3.69) is from (3.61b). Take arbitrary $(\theta(0), \omega_{\mathcal{G}}(0)) \in \mathbb{R}^{|\mathcal{N}|+|\mathcal{G}|}$. Then the set

$$\Omega := \{(\theta, \omega_{\mathcal{G}}) \mid U(\theta, \omega_{\mathcal{G}}) \leq U(\theta(0), \omega_{\mathcal{G}}(0))\}$$

is compact. Indeed Ω is closed due to continuity of U (3.66), and is bounded since U (3.66) is radially unbounded due to the dominating quadratic terms in $\omega_{\mathcal{G}}$ and θ.

[13] Alternatively, one could construct a strictly decreasing Lyapunov function (outside equilibria) by applying Chetaev's trick [118] and adding the cross-term $\varepsilon(\nabla_{\mathcal{G}} V(\theta) - \nabla_{\mathcal{G}} V(\theta^*))^T M_{\mathcal{G}} \omega_{\mathcal{G}}$ to $U(\theta, \omega_{\mathcal{G}})$ in (3.66), for $\epsilon > 0$ sufficiently small.

Also Ω is invariant since $\dot{U} \leq 0$. Define

$$\begin{aligned} E &:= \left\{(\theta, \omega_{\mathcal{G}}) \in \mathbb{R}^{|\mathcal{N}|+|\mathcal{G}|} \mid \dot{U}(\theta, \omega_{\mathcal{G}}) = 0\right\} \\ &= \left\{(\theta, \omega_{\mathcal{G}}) \in \mathbb{R}^{|\mathcal{N}|+|\mathcal{G}|} \mid \omega_{\mathcal{G}} = 0, \omega_{\mathcal{L}}(\theta) = 0\right\}, \end{aligned} \tag{3.70}$$

where the equality in (3.70) is from (3.69). Define $E_\Omega := E \cap \Omega$, and let L_Ω^+ be the largest invariant subset of E_Ω. By [117, Theorem 3.3], the system (3.61)–(3.62) has a unique trajectory $(\theta(t), \omega_{\mathcal{G}}(t), t \geq 0)$, starting from $(\theta(0), \omega_{\mathcal{G}}(0))$, and by LaSalle's theorem [117, Theorem 4.4], as $t \to \infty$, $(\theta(t), \omega_{\mathcal{G}}(t))$ converges to a *nonempty*, compact, invariant limit set which is a subset of L_Ω^+. Hence it is sufficient to show $L_\Omega^+ \subseteq \Theta_{\mathcal{G}}^*$. Consider any point $(\theta', \omega'_{\mathcal{G}}) \in L_\Omega^+$. Due to the invariance of L_Ω^+, the trajectory $(\theta(\tau), \omega_{\mathcal{G}}(\tau))$ starting from $(\theta', \omega'_{\mathcal{G}})$ must stay in L_Ω^+ and hence must stay in E_Ω. Therefore, by (3.70) we have $\omega_{\mathcal{G}}(\tau) \equiv 0$ and hence $\dot{\omega}_{\mathcal{G}}(\tau) \equiv 0$, and $\omega_{\mathcal{L}}(\theta(\tau)) \equiv 0$. It follows that $F(\theta(\tau)) \equiv 0$, and in particular $(\theta', \omega'_{\mathcal{G}}) \in \Theta_{\mathcal{G}}^*$ (at $\tau = 0$). Hence $L_\Omega^+ \subseteq \Theta_{\mathcal{G}}^*$ as we wanted to show. □

In Theorem 3.8, Θ^* is nonempty essentially because $F(\theta) = 0$ always has a solution, even though the open-loop system (3.61) with some fixed p may not have an equilibrium due to insolvability of power flow. When Θ^* is composed of a finite number of isolated equilibrium points, which occurs with measure one on the set of system parameters [119], Theorem 3.8 implies that the system (3.61)–(3.62) globally converges to an equilibrium point. Unfortunately, it is in general not possible to control the final equilibrium to which the system will converge. In the corollary below, we show that Θ^* contains a unique equilibrium which is globally asymptotically stable when a condition on the integral gains K and line parameters B is satisfied. For convenience, let $N(j) := \{i \in \mathcal{N} \mid (i, j) \in \mathcal{E} \text{ or } (j, i) \in \mathcal{E}\}$ be the set of neighboring buses of j, and $B_{ji} := B_{ij}$ for all $(i, j) \in \mathcal{E}$.

Corollary 3.1. If $K_i > 2\sum_{j \in N(i)} B_{ij}$ for all $i \in \mathcal{N}$, then the closed-loop system (3.61)–(3.62) has a unique and globally asymptotically stable equilibrium.

Proof. The Jacobian matrix of function F (3.64) is

$$\frac{\partial F}{\partial \theta}(\theta) = -K - CB \cdot \mathrm{diag}(\cos(C^T\theta))C^T, \tag{3.71}$$

where $\cos(\cdot)$ is a vector-valued function with component-wise $\cos(\cdot)$. We drop the argument θ of $\frac{\partial F}{\partial \theta}$, and denote the (i, j)-th entry of $\frac{\partial F}{\partial \theta}$ by $\left(\frac{\partial F}{\partial \theta}\right)_{ij}$. By Gershgorin

circle theorem [120], for any eigenvalue λ of $\frac{\partial F}{\partial \theta}$, there exists $i \in \mathcal{N}$ such that

$$\left|\lambda - \left(\frac{\partial F}{\partial \theta}\right)_{ii}\right| \leq \sum_{j\in\mathcal{N}, j\neq i} \left|\left(\frac{\partial F}{\partial \theta}\right)_{ij}\right|. \tag{3.72}$$

By assumption we also have

$$K_i > 2\sum_{j\in N(i)} B_{ij} \geq \sum_{j\in N(i)} B_{ij}(|\cos\theta_{ij}| - \cos\theta_{ij}) \qquad \text{for all } i \in \mathcal{N}$$

where $\theta_{ij} := \theta_i - \theta_j$, which, by (3.71), implies

$$\left(\frac{\partial F}{\partial \theta}\right)_{ii} + \sum_{j\in\mathcal{N}, j\neq i} \left|\left(\frac{\partial F}{\partial \theta}\right)_{ij}\right| < 0 \qquad \forall i \in \mathcal{N}. \tag{3.73}$$

By (3.72)–(3.73), we have $\frac{\partial F}{\partial \theta}(\theta) \prec 0$ for all $\theta \in \mathbb{R}^{|\mathcal{N}|}$. Now suppose there are $\theta^*, \theta' \in \mathbb{R}^{|\mathcal{N}|}$ such that $\theta^* \neq \theta'$ and $F(\theta') = F(\theta^*) = 0$. Then we have, by the fundamental theorem of calculus [121], that

$$\begin{aligned} 0 &= F(\theta') - F(\theta^*) \\ &= \left[\int_0^1 \frac{\partial F}{\partial \theta}(\theta^* + h\Delta\theta)dh\right]\Delta\theta, \end{aligned} \tag{3.74}$$

where $\Delta\theta := \theta' - \theta^* \neq 0$. Note that the integral term in (3.74), denoted by int_F, is negative definite since $\frac{\partial F}{\partial \theta}(\theta^* + h\Delta\theta) \prec 0$ for all $h \in [0, 1]$. Hence we have $\Delta\theta^T \cdot \text{int}_F \cdot \Delta\theta < 0$. However we have from (3.74) that $\Delta\theta^T \cdot \text{int}_F \cdot \Delta\theta = 0$ which leads to a contradiction. Therefore, by Theorem 3.8 and the definition of Θ^* in (3.65), the system (3.61)–(3.62) has a unique equilibrium $(\theta^*, \omega^* = 0)$ to which all of its trajectories converge globally. Indeed, the unique global minimum of U (3.66) is attained at $(\theta^*, \omega^*_{\mathcal{G}})$, due to the facts that $\dot{U} \leq 0$, that $(\theta(t), \omega_{\mathcal{G}}(t)) \to (\theta^*, \omega^*_{\mathcal{G}})$ as $t \to \infty$, and that no solution can stay identically in the set E (3.70) except $(\theta(t), \omega_{\mathcal{G}}(t)) \equiv (\theta^*, \omega^*_{\mathcal{G}})$. Therefore [117, Theorem 4.1] implies global asymptotic stability of $(\theta^*, \omega^*_{\mathcal{G}})$ and hence that of (θ^*, ω^*). □

An important implication of Theorem 3.8 and Corollary 3.1 is that the *completely* decentralized integral (DI) control (3.62) achieves *global* asymptotic stability for a *nonlinear* power flow model, without requiring any knowledge of system parameters in the controller design. However, DI (3.62) may result in an equilibrium which is neither optimal nor feasible in the sense of OLC, and may lead to impractically large or fast-varying control actions especially under the parametric condition in Corollary 3.1, i.e., large control gains K_i. This issue is addressed in the next section, by adding distributed averaging filters to the decentralized integrators.

3.7 Distributed averaging-based proportional integral control

In this section, we still use the power network model (3.61). By modifying the completely decentralized integral control (3.62), we develop a distributed control scheme, which relies on local frequency sensing and communication between neighbors, to restore the frequency to its nominal value with minimum disutility. After step changes r_j in generation or load on an arbitrary subset of buses at time 0, we desire the closed-loop system to converge to a new equilibrium point which solves the following optimization problem.

OLC (network, secondary frequency control):

$$\min_{p} \qquad \sum_{j\in\mathcal{N}} \frac{1}{2}\alpha_j p_j^2 \tag{3.75a}$$

$$\text{subject to} \qquad \sum_{j\in\mathcal{N}} \left(r_j + p_j\right) = 0, \tag{3.75b}$$

which is a simplified version of (3.49) by considering a quadratic objective function (3.75a) where constants $\alpha_j > 0$ for $j \in \mathcal{N}$, consolidating controls $(p_{\mathcal{G}}, d)$ into p, and ignoring capacity limits $[\underline{p}_j, \overline{p}_j]$, branch power flows P_{ij}, and the inter-area flow constraint (3.49d). Obviously OLC (3.75) is feasible and has a unique optimal p^* which satisfies

$$\alpha_i p_i^* = \alpha_j p_j^* \qquad \text{for all } i, j \in \mathcal{N} \tag{3.76}$$

due to the KKT (stationarity) condition. We make the following assumption that a power flow solution (θ^*, P^*) exists in the principal region at the optimal of OLC (3.75).

Assumption 3.9. For the unique optimal p^* of OLC (3.75), there exist $P^* \in \mathbb{R}^{|\mathcal{E}|}$ and $\theta^* \in \mathbb{R}^{|\mathcal{N}|}$ where $\left|\theta_i^* - \theta_j^*\right| < \frac{\pi}{2}$ for all $(i, j) \in \mathcal{E}$, such that

$$r_j + p_j^* = P_j^{\text{out},*} - P_j^{\text{in},*} \qquad \text{for all } j \in \mathcal{N}, \tag{3.77a}$$

$$P_{ij}^* = B_{ij} \sin\left(\theta_i^* - \theta_j^*\right) \qquad \text{for all } (i, j) \in \mathcal{E}. \tag{3.77b}$$

As is proved in Lemma 3.7, there is a unique point (θ^*, P^*, p^*) satisfying Assumption 3.9. Indeed, this (θ^*, P^*, p^*) is also an equilibrium of (3.61). To drive (3.61) to this equilibrium, we design the following *distributed averaging-based proportional integral (DAPI)* control:

$$p_j = -K_j(s_j + q_j) \qquad \text{for all } j \in \mathcal{N}, \tag{3.78a}$$

$$\dot{s}_j = \omega_j \qquad \text{for all } j \in \mathcal{N}, \tag{3.78b}$$

$$\dot{q}_j = \alpha_j \sum_{k\in\mathcal{N}} Y_{jk}(\alpha_j p_j - \alpha_k p_k) \qquad \text{for all } j \in \mathcal{N}, \tag{3.78c}$$

where K_j for $j \in \mathcal{N}$ are constant control gains, and the weights $Y_{jk} \geq 0$ for $j, k \in \mathcal{N}$ induce an *undirected* and connected communication graph, i.e., $Y_{jj} = 0$ for $j \in \mathcal{N}$, $Y_{jk} = Y_{kj} > 0$ when the local controllers at buses j and k communicate, and $Y_{jk} = Y_{kj} = 0$ otherwise. Compared to the decentralized integral control (3.62), distributed averaging filters (3.78c) on q are added to form the DAPI control. We remark that the DAPI control (3.78) includes the control scheme proposed in [47], [48], which makes the additional parametric assumption $D = \mathrm{diag}(\alpha)^{-1}$ and merges the variables $s_j + q_j$.

In the principal region where $\left|\theta_i^* - \theta_j^*\right| < \frac{\pi}{2}$ for all $(i, j) \in \mathcal{E}$, the closed-loop system (3.61)(3.78) has a unique equilibrium $(\theta^*, \omega^* = 0, P^*, p^*)$.[14] We have the following theorem regarding stability of the closed-loop system (3.61)(3.78).

Theorem 3.9. Suppose Assumption 3.9 holds. Then any trajectory $(\theta(t), \omega(t), P(t), p(t), t \geq 0)$ of the closed-loop system (3.61)(3.78), as $t \to \infty$, converges to the unique $(\theta^*, \omega^* = 0, P^*, p^*)$ satisfying Assumption 3.9, given that $(\theta(0), \omega(0), P(0), p(0))$ lies in a neighborhood of $(\theta^*, \omega^*, P^*, p^*)$.

Proof. Consider the following incremental Lyapunov function candidate inspired by [43]:

$$\begin{aligned} U(\theta, \omega_{\mathcal{G}}, p) &= \frac{1}{2}\omega_{\mathcal{G}}^T M_{\mathcal{G}} \omega_{\mathcal{G}} + V(\theta) - V(\theta^*) \\ &\quad -\nabla V(\theta^*)(\theta - \theta^*) + \frac{1}{2}(p - p^*)^T K^{-1}(p - p^*), \end{aligned} \tag{3.79}$$

where $V(\theta)$ is defined in (3.67). Note that, within a neighborhood of θ^*,

$$V(\theta) - V(\theta^*) - \nabla V(\theta^*)(\theta - \theta^*)$$

is nonnegative, and zero only at θ^*,[15] due to the convexity of $V(\theta)$ in the principal region of θ. Therefore U (3.79) is locally nonnegative, and zero only at the

[14] Though $s^* + q^*$ is also unique by (3.78a), each of s^* and q^* is not unique.

[15] We ignore the rigid rotation of θ_j for all $j \in \mathcal{N}$ by the same amount.

equilibrium. The derivative of U (3.79) along any trajectory of (3.61)(3.78) is

$$\begin{aligned}
& \dot{U}(\theta, \omega_{\mathcal{G}}, p) \\
= \; & \omega_{\mathcal{G}}^T M_{\mathcal{G}} \dot{\omega}_{\mathcal{G}} + \left(\nabla_{\mathcal{L}} V - \nabla_{\mathcal{L}} V^*\right)^T \dot{\theta}_{\mathcal{L}} \\
& + \left(\nabla_{\mathcal{G}} V - \nabla_{\mathcal{G}} V^*\right)^T \dot{\theta}_{\mathcal{G}} + (p - p^*)^T K^{-1} \dot{p} \\
= \; & -\omega_{\mathcal{G}}^T D_{\mathcal{G}} \omega_{\mathcal{G}} - \omega_{\mathcal{G}}^T \left(\nabla_{\mathcal{G}} V - \nabla_{\mathcal{G}} V^*\right) + \omega_{\mathcal{G}}^T (p_{\mathcal{G}} - p_{\mathcal{G}}^*) \\
& - \left(\nabla_{\mathcal{L}} V - \nabla_{\mathcal{L}} V^*\right)^T D_{\mathcal{L}}^{-1} \left(\nabla_{\mathcal{L}} V - \nabla_{\mathcal{L}} V^*\right) + \left(\nabla_{\mathcal{L}} V - \nabla_{\mathcal{L}} V^*\right)^T D_{\mathcal{L}}^{-1} (p_{\mathcal{L}} - p_{\mathcal{L}}^*) \\
& + \left(\nabla_{\mathcal{G}} V - \nabla_{\mathcal{G}} V^*\right)^T \omega_{\mathcal{G}} - (p_{\mathcal{G}} - p_{\mathcal{G}}^*)^T \omega_{\mathcal{G}} \\
& + (p_{\mathcal{L}} - p_{\mathcal{L}}^*)^T D_{\mathcal{L}}^{-1} \left(\nabla_{\mathcal{L}} V - \nabla_{\mathcal{L}} V^*\right) \\
& - (p_{\mathcal{L}} - p_{\mathcal{L}}^*)^T D_{\mathcal{L}}^{-1} (p_{\mathcal{L}} - p_{\mathcal{L}}^*) - (p - p^*)^T \alpha L_Y \alpha (p - p^*) \\
= \; & -\omega_{\mathcal{G}}^T D_{\mathcal{G}} \omega_{\mathcal{G}} - (p - p^*)^T \alpha L_Y \alpha (p - p^*) \\
& - \left(\nabla_{\mathcal{L}} V - \nabla_{\mathcal{L}} V^* - (p_{\mathcal{L}} - p_{\mathcal{L}}^*)\right)^T D_{\mathcal{L}}^{-1} \left(\nabla_{\mathcal{L}} V - \nabla_{\mathcal{L}} V^* - (p_{\mathcal{L}} - p_{\mathcal{L}}^*)\right) \\
= \; & -\omega^T D \omega - (p - p^*)^T \alpha L_Y \alpha (p - p^*) \\
\leq \; & 0, \qquad (3.80)
\end{aligned}$$

where ∇V and ∇V^* denote $\nabla V(\theta)$ and $\nabla V(\theta^*)$ respectively, and L_Y is the Laplacian matrix [107] of the communication graph with weights Y_{ij}. Therefore U is non-increasing along any trajectory of (3.61)(3.78), and zero only when $\omega = 0$ and $\alpha p \in \text{span}(1)$. The rest of the proof is straightforward. □

Compared to the distributed secondary frequency control (3.52), the communication graph in the DAPI control (3.78) does not need to be the same as the power network, which allows for more flexibility in implementation. Simulations in Section 3.8 show that DAPI (3.78) works well even when not all the buses are controlled.

3.8 Simulations

Through simulations with more realistic models than those used in our design and analysis, we test performance of the control schemes developed in this chapter.

Load-side primary frequency control

We first illustrate performance of the load-side primary frequency control in Section 3.2, through simulations of the IEEE 68-bus New England/New York interconnection test system [105]. The single line diagram of the 68-bus system is given in Figure 3.3. We run the simulation on Power System Toolbox [58]. Unlike our analytic model, the simulation model is much more detailed and realistic, including a two-axis subtransient reactance generator model, IEEE type DC1 exciter model,

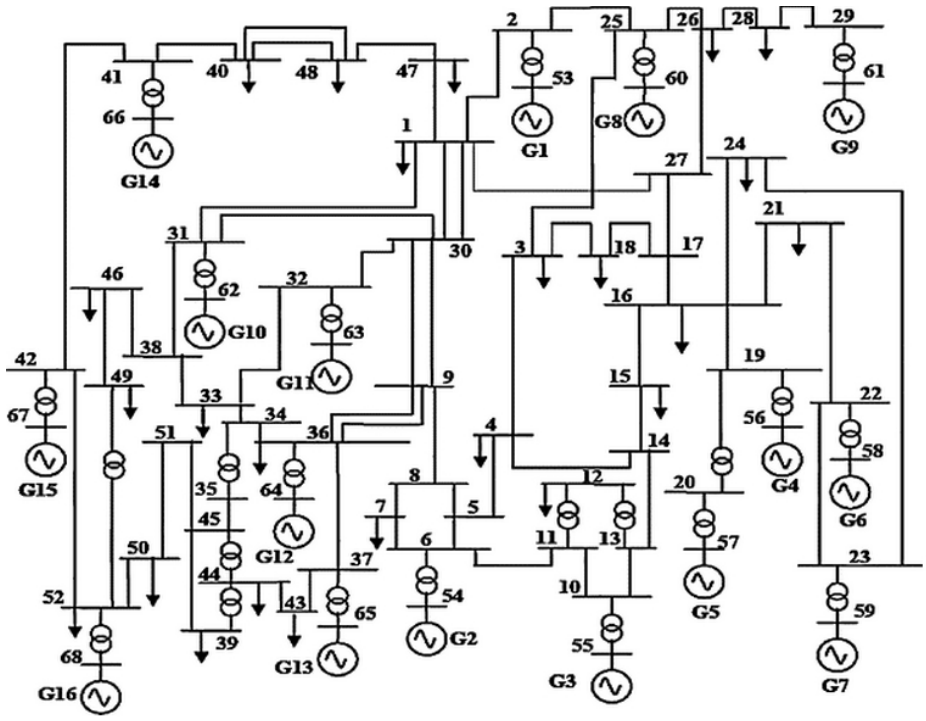

Figure 3.3: Single line diagram of the IEEE 68-bus test system [105].

classical power system stabilizer model, AC (nonlinear) power flows, and non-zero line resistances. The detail of the simulation model, including parameter values, can be found in the data files of the toolbox. It is shown in [103] that our analytic model is a good approximation of the simulation model.

In the test system there are 35 load buses serving different types of loads, including constant active current loads, constant impedance loads, and induction motor loads, with a total real power of 18.23 GW. In addition, we add three loads to buses 1, 7 and 27, each making a step increase of real power by 1 pu (based on 100 MVA), as the P^m in previous analysis in Sections 3.1–3.3. We also select 30 load buses to perform OLC. In the simulation we use the same bounds $\left[\underline{d}, \overline{d}\right]$ with $\underline{d} = -\overline{d}$ for each of the 30 controllable loads, and call the value of $30 \times \overline{d}$ the *total size of controllable loads*. We present simulation results below with different sizes of controllable loads. The disutility function of controllable load d_j is $c_j(d_j) = d_j^2/(2\alpha)$, with identical $\alpha = 100$ pu for all the loads. The loads are controlled every 250 ms, which is a relatively conservative estimate of the rate of load control in an existing testbed [25].

We look at the impact of OLC on both the steady state and the transient response of the system, in terms of both frequency and voltage. We present the results with a widely used generation-side stabilizing mechanism, known as a power system

stabilizer (PSS), either enabled or disabled. Fig. 3.4a and 3.4b respectively show the frequency and voltage at bus 66, under four cases: (i) no PSS, no OLC; (ii) with PSS, no OLC; (iii) no PSS, with OLC; and (iv) with PSS and OLC. In both cases (ii) and (iv), the total size of controllable loads is 1.5 pu.

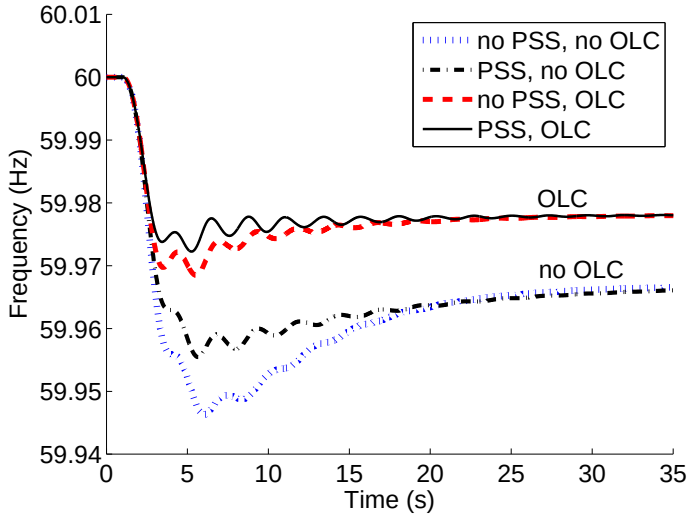

(a)

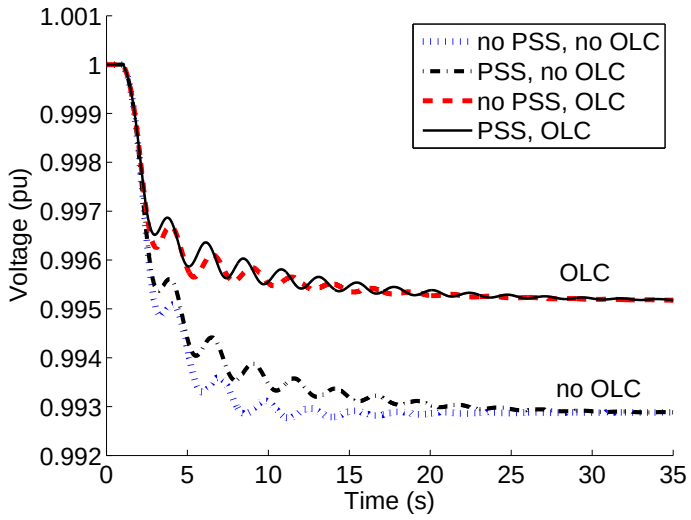

(b)

Figure 3.4: The (a) frequency and (b) voltage at bus 66, under four cases: (i) no PSS, no OLC; (ii) with PSS, no OLC; (iii) no PSS, with OLC; (iv) with PSS and OLC, where the OLC is for primary frequency control.

We observe in Fig. 3.4a that whether PSS is used or not, adding OLC always improves the transient response of frequency, in the sense that both the overshoot and the settling time (the time after which the difference between the actual frequency

and its new steady-state value never goes beyond 5% of the difference between its old and new steady-state values) are decreased. Using OLC also results in a smaller steady-state frequency error. Cases (ii) and (iii) suggest that using OLC solely without PSS produces a much better performance than using PSS solely without OLC. The impact of OLC on voltage, with and without PSS, is qualitatively demonstrated in Fig. 3.4b. Similar to its impact on frequency, OLC improves significantly both the transient and steady-state of voltage with or without PSS. For instance the steady-state voltage is within 4.5% of the nominal value with OLC and 7% without OLC.

To better quantify the performance improvement due to OLC we plot in Fig. 3.5 the new steady-state frequency, the lowest frequency (which indicates overshoot) and the settling time of frequency at bus 66, against the total size of controllable loads. PSS is always enabled. We observe that using OLC always leads to a

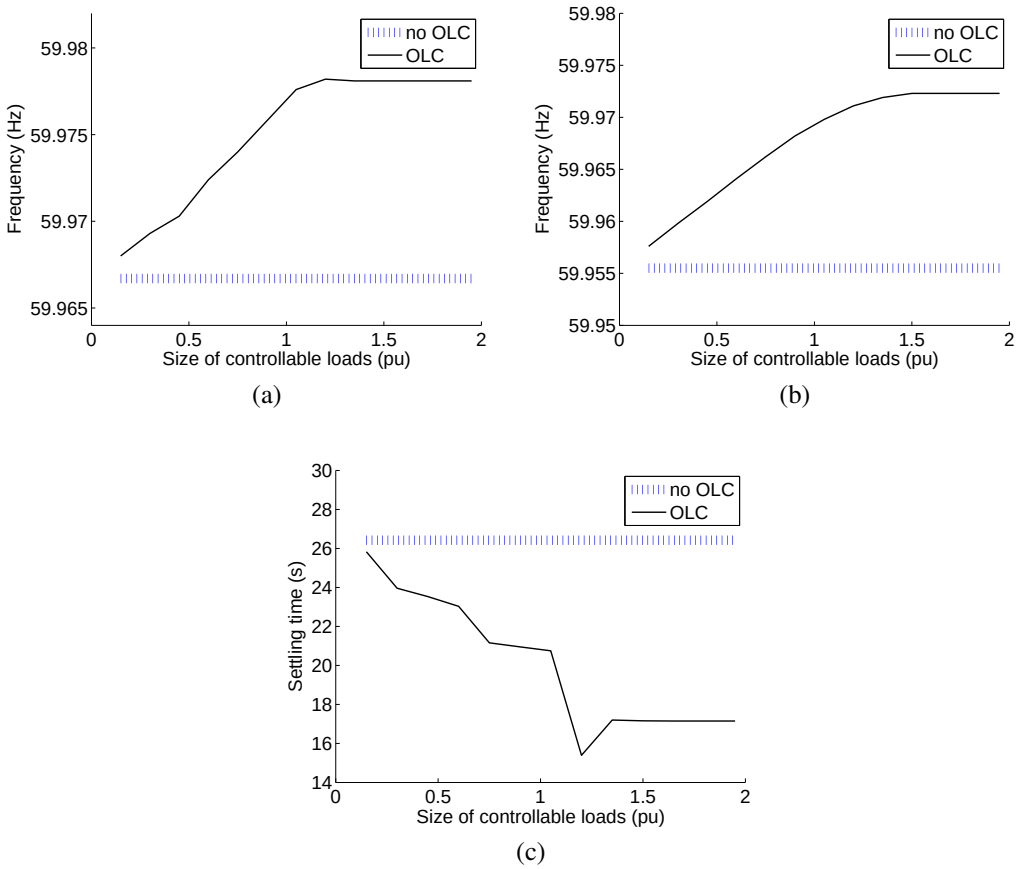

Figure 3.5: The (a) new steady-state frequency, (b) lowest frequency, and (c) settling time of frequency at bus 66, against the total size of controllable loads.

higher new steady-state frequency (a smaller steady-state error), a higher lowest frequency (a smaller overshoot), and a shorter settling time, regardless of the total size of controllable loads. As the total size of controllable loads increases, the steady-state error and overshoot decrease almost linearly until a saturation around 1.5 pu. There is a similar trend for the settling time, though the linear dependence is approximate. In summary OLC improves both the steady-state and transient performance of frequency, and in general deploying more controllable loads leads to a bigger improvement.

To verify the theoretical result that OLC minimizes the aggregate cost of load control, Fig. 3.6 shows the cost of OLC over time, obtained by evaluating the quantity defined in (3.7a) using the trajectory of controllable and frequency-sensitive loads from the simulation. We see that the cost indeed converges to the minimum cost for the given change in P^m.

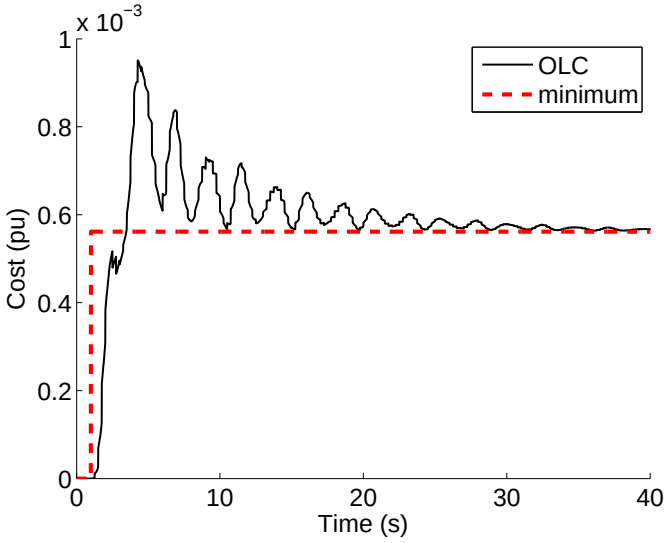

Figure 3.6: The cost trajectory of OLC compared to its minimum.

Generator and load-side primary control

We now illustrate performance of the generator and load-side primary frequency control in Section 3.4, through simulations of the IEEE 39-bus New England test system shown in Fig. 3.7. This system has 10 generators and 39 buses, and a total load of about 60 per unit (pu) where 1 pu represents 100 MVA. Details about this system including parameter values can be found in the Power System Toolbox [58].

The primary frequency control of generator or load j is designed with the cost function $c_j^p(p_j) = \frac{R_j}{2}\left(p_j - p_j^{\text{set}}\right)^2$, where p_j^{set} is the power injection at the setpoint,

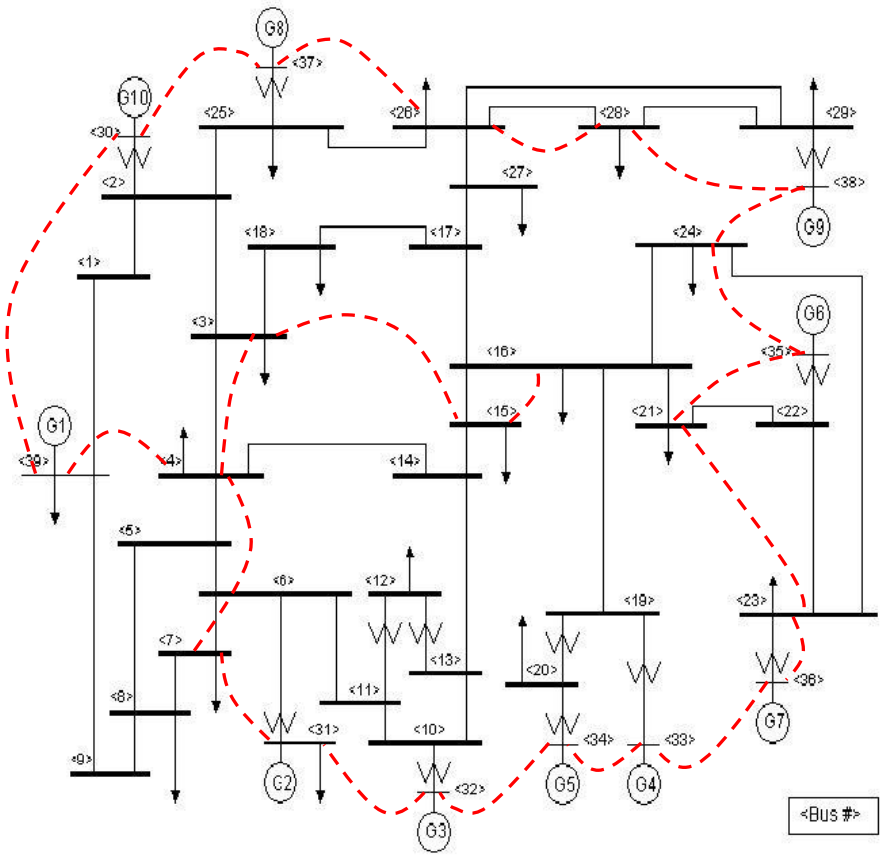

Figure 3.7: Single line diagram of the IEEE 39-bus test system [58]. Dashed lines are communication links used in the simulations of DAPI control.

an initial equilibrium point solved from static power flow problem. By choosing this cost function, we try to minimize the deviations of power injections from the setpoint, and have the control $p_j = \left[p_j^{\text{set}} - \frac{1}{R_j}\omega_j\right]_{\underline{p}_j}^{\overline{p}_j}$ from (3.35).[16]. We consider the following two cases in which the generators and loads have different control capabilities and hence different $[\underline{p}_j, \overline{p}_j]$:

1. All the 10 generators have $[\underline{p}_j, \overline{p}_j] = [p_j^{\text{set}}(1-c), p_j^{\text{set}}(1+c)]$, and all the loads are uncontrollable;

2. Generators 2, 4, 6, 8, 10 (which happen to provide half of the total generation) have the same bounds as in case (1). Generators 1, 3, 5, 7, 9 are uncontrollable, and all the loads have $[\underline{p}_j, \overline{p}_j] = [p_j^{\text{set}}(1+c/2), p_j^{\text{set}}(1-c/2)]$, if we suppose $p_j^{\text{set}} \leq 0$ for loads $j \in \mathcal{L}$.

[16]Only the generator control p_j is written since the load control d_j takes the same form.

Hence cases (1) and (2) have the same total control capacity across the network. Case (1) only has generator control while in case (2) the set of generators and the set of loads each have half of the total control capacity. We select $c = 10\%$, which implies the total control capacity is about 6 pu. For all $j \in \mathcal{N}$, the feedback gain $1/R_j$ is selected as $25p_j^{\text{set}}$, which is a typical value meaning a frequency change of 0.04 pu (2.4 Hz) causes the change of power injection from zero all the way to the setpoint. Note that this control is the same as frequency droop control, which implies that indeed frequency droop control implicitly solves an OLC problem with quadratic cost functions we use here. However, our controller design is more flexible by allowing a larger set of cost functions.

In the simulation, the system is initially at the setpoint with 60 Hz frequency. At time $t = 0.5$ second, buses 4, 15, 16 each make 1 pu step change in their real power consumptions, causing the frequency to drop. Fig. 3.8 shows the frequencies of all the 10 generators under the two cases above, (1) with red and (2) with black. We see in both cases that frequencies of different generators have relatively small differences during transient, and are synchronized towards the new steady-state frequency. Compared with generator-only control, the combined generator-and-load control improves both the transient and steady-state frequency, even though the total control capacities in both cases are the same.

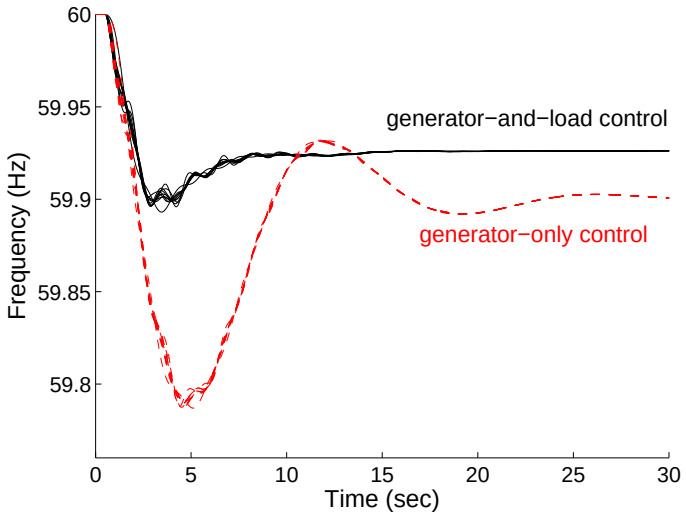

Figure 3.8: Frequencies of all the 10 generators under two cases of primary control: (1) only generators are controlled (dashed) and (2) both generators and loads are controlled (solid). The total control capacities are the same for both cases.

Generator and load-side secondary control

We now illustrate performance of the generator and load-side secondary frequency control in Section 3.5, through simulations of a four-machine network in Fig. 3.9, on Power System Toolbox. Network parameters are slightly modified from [58].

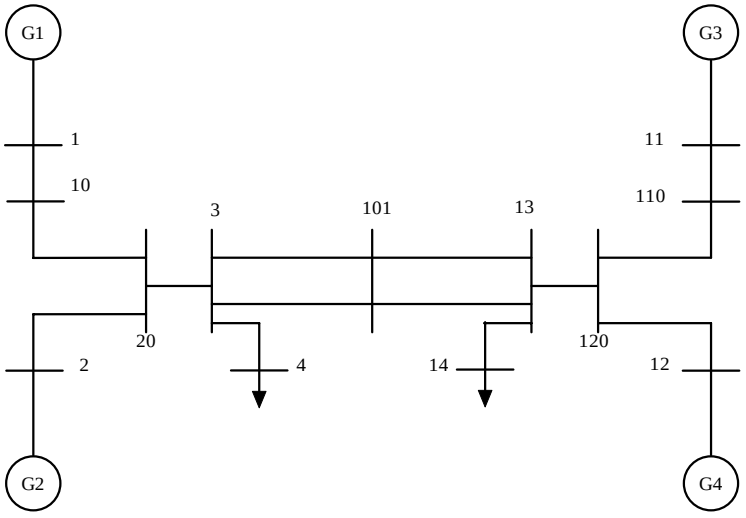

Figure 3.9: A four-machine network. This figure is from [58].

We use generation cost functions $c_j^p(p_j) = a_j(p_j)^2$, and user utility functions $c_j^d(d_j) = a_j(d_j - \overline{d}_j)^2 - a_j(\underline{d}_j - \overline{d}_j)^2$, for constant $a_j > 0$. Then the control functions are $p_j(x) = -x/(2a_j)$ for $x \in [-2a_j\overline{p}_j, -2a_j\underline{p}_j]$ for generators, and $d_j(x) = x/(2a_j) + \overline{d}_j$ for $x \in [2a_j(\underline{d}_j - \overline{d}_j), 0]$ for controllable loads. We set $[\underline{p}_j, \overline{p}_j]$ and $[\underline{d}_j, \overline{d}_j]$ such that the generators and controllable loads do not hit their capacity limits. Let the load on bus 14 make a step increase at $t = 2$ s. In different cases below, we implement different control strategies. Generators and loads are controlled once per second in all the cases.

We first compare the proposed OLC scheme with traditional automatic generation control (AGC) [14], [16], [17]. For simplicity, we regard the network as a single area and ignore the inter-area flow constraints, in which case AGC becomes a centralized control. For both OLC and AGC, all the bus frequencies are restored to 60 Hz. Fig. 3.10 shows the frequency of bus 12 under AGC and OLC. The control gains of AGC and OLC are tuned such that the frequency shows the best transient within each case. We see that OLC improves transient frequency compared to AGC.

We then look at the impact of load participation in OLC. Fig. 3.11 shows the frequency of bus 12 under two cases: (1) all the four generators are controlled, and

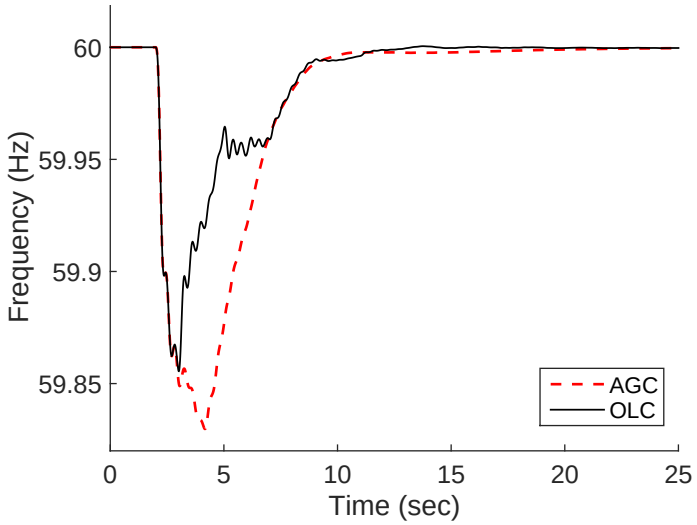

Figure 3.10: Frequency of bus 12 under AGC and OLC. Control gains are tuned for best transient frequency within each case. All the four generators and two loads are controlled in both cases.

(2) generators G1 and G3 and two loads on buses 4 and 14 are controlled. In both cases, constant a_j are tuned such that the aggregate control gain across the network is the same. We see that load participation in OLC improves transient frequency.

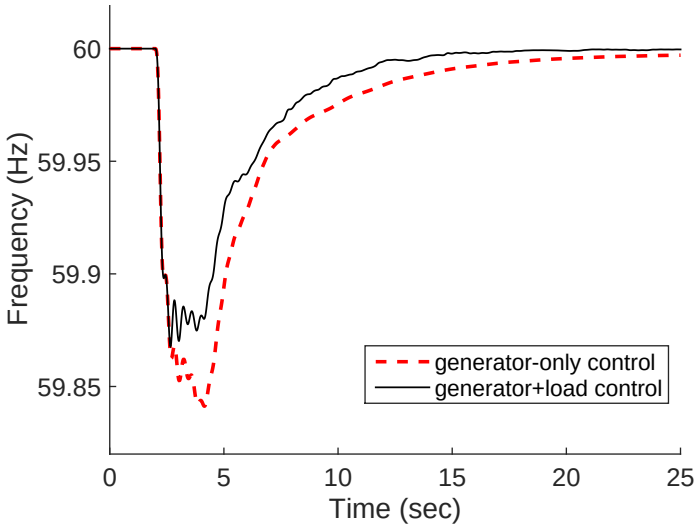

Figure 3.11: Frequency of bus 12 under cases (1) only generators are controlled and (2) both generators and loads are controlled. Both cases use OLC, and have the same aggregate control gain.

Frequency integral and DAPI controls

We evaluate performance of the frequency integral and DAPI controls in Sections 3.6 and 3.7, through simulations of the IEEE 39-bus system shown previously in Fig. 3.7. The generator inertia moments M_j and line susceptances B_{ij} are obtained from [58]. We choose uniform droop coefficients $D_j = 1$ pu for all the buses. Although the theoretical analysis requires controllers at every bus of the network, here we only control the generators and loads on buses 3, 4, 7, 15, 16, 21, 23, 24, 26, 28. We also relax our controller (3.78) to the form

$$\begin{aligned} p_j &= -K_j s_j - R_j q_j && \text{for all } j \in \mathcal{N}, \\ \dot{s}_j &= \omega_j && \text{for all } j \in \mathcal{N}, \\ \dot{q}_j &= Q_j \sum_{k \in \mathcal{N}} Y_{jk}(\alpha_j p_j - \alpha_k p_k) && \text{for all } j \in \mathcal{N}, \end{aligned}$$

using gains $K_j = 60$ pu, $R_j = 1$ pu for all the controlled buses j. For the DAPI control, a communication graph connecting generators and controllable loads is shown in Fig. 3.7, with $Y_{ij} = 1$ for all connected pairs (i, j). We select controller gains $Q_j = 50/\text{degree}(j)$ where $\text{degree}(j)$ denotes the degree of bus j in the communication graph. The coefficients α_j of OLC are generated uniformly randomly from $[0, 1]$.

In the simulation, the system is initially at a setpoint where supply and demand are balanced and the frequency is 60 Hz (nominal). At time $t = 1$ second, buses 4, 12, 20 each make a 33 MW step change in real power consumption, causing bus frequencies to drop. Fig. 3.12 shows the frequencies of five generators, under cases with different control schemes: droop control, the completely decentralized integral control, and DAPI. It can be seen that while droop control synchronizes bus frequencies to lower than 60 Hz, both the decentralized integral control and DAPI recover bus frequencies to 60 Hz, with similar transients.

Fig. 3.13 shows the trajectories of marginal costs $a_j p_j$, under the completely decentralized integral control and the DAPI control. While at the equilibrium of the decentralized integral control the marginal costs are different across the generators and controllable loads, they are the same under DAPI, which implies that the OLC is solved by DAPI. Moreover, for most of the displayed generators and controllable loads, DAPI reduces both transient and steady-state control actions compared to the decentralized integral control.

In Fig. 3.14 we compare the objective values of OLC, i.e., the control costs, along trajectories of control actions of the completely decentralized integral control and

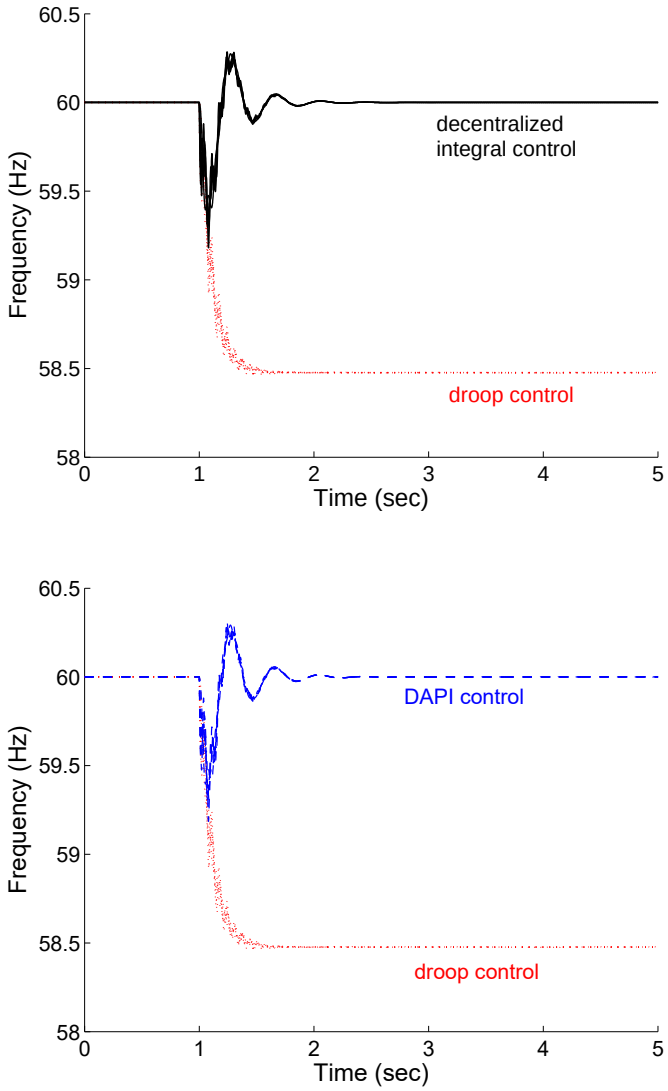

Figure 3.12: Frequencies of generators 2, 4, 6, 8, 10, under droop control, the completely decentralized integral control, and DAPI control.

DAPI, and compare them with the minimum objective value of OLC for a given step change in load. We see that DAPI, compared to the decentralized integral control, has a smaller control cost both during the transient and at the new equilibrium, and indeed converges to the optimal of OLC.

3.9 Conclusion

We have presented a systematic method to design ubiquitous continuous fast-acting distributed load control for primary frequency regulation in power networks, by formulating an optimal load control (OLC) problem where the objective is to minimize

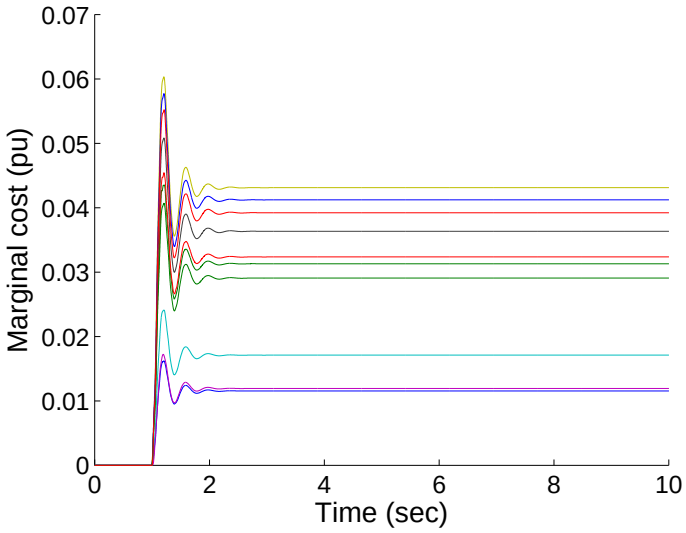

(a)

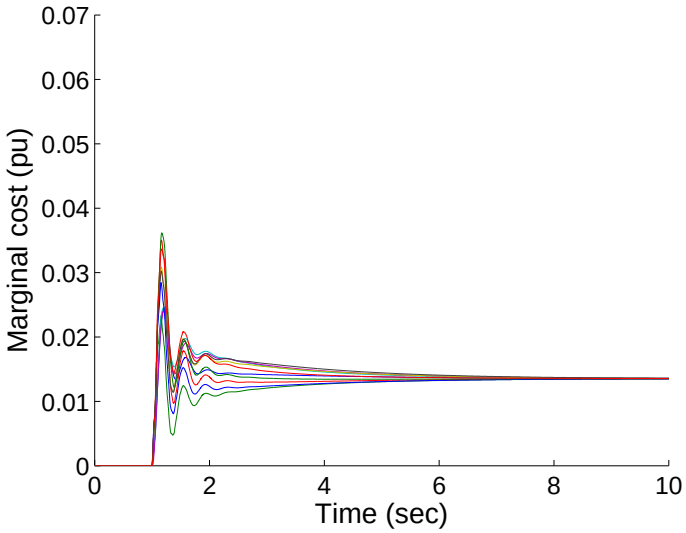

(b)

Figure 3.13: Marginal costs $a_j p_j$ for generators 2, 4, 6, 8, 10 and controllable loads on buses 4, 15, 21, 24, 28, under the completely decentralized integral control in (a) and the DAPI control in (b).

the aggregate control cost subject to power balance across the network. We have shown that the swing dynamics and the linearized branch power flows, coupled with a frequency-based load control, serve as a distributed primal-dual algorithm to solve the dual problem of OLC.

We then extend our framework to include generator dynamics and control, nonlinear power flows, and secondary frequency control. We also developed a completely

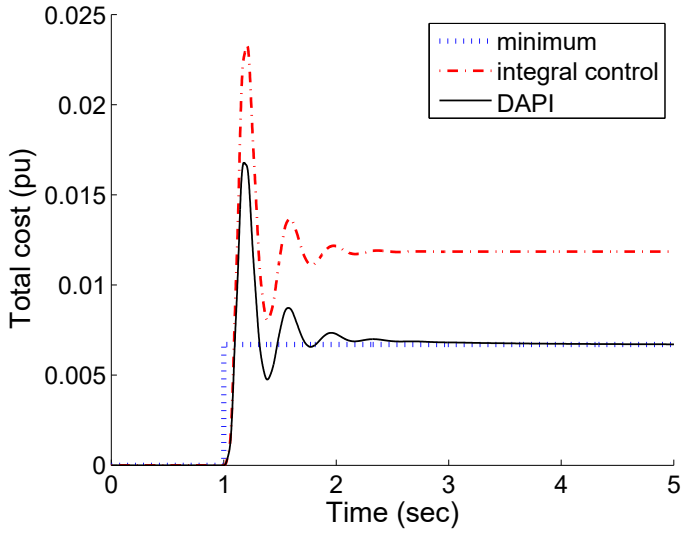

Figure 3.14: Trajectories of the OLC objective value under the completely decentralized integral control and DAPI control. The blue dotted line is the minimum OLC objective value.

decentralized frequency integral control to restore frequency to its nominal value, and a distributed averaging-based proportional integral (DAPI) control to solve OLC. Simulations with more realistic models have shown effectiveness of various control schemes we developed. In particular, both transient and steady-state frequencies are improved by our schemes.

APPENDICES

3.A Frequently used notations

$\theta := (\theta_j,\ j \in \mathcal{N})$	bus voltage phase angles with respect to the rotating frame at the nominal frequency.
$\omega := (\omega_j,\ j \in \mathcal{N})$	*deviations* of bus frequencies from their nominal value
$P^m := (P^m_j,\ j \in \mathcal{N})$	mechanical power injections to the generators, or uncontrollable load if $j \in \mathcal{L}$.
$p := (p_j,\ j \in \mathcal{G})$	generator control.
$a := (a_j,\ j \in \mathcal{G})$	generator/turbine valve positions.
$d := (d_j,\ j \in \mathcal{N})$	load control.
$D_j\omega_j,\ j \in \mathcal{N}$	aggregate power of generator friction and frequency-dependent loads like induction motors
$M_j > 0, j \in \mathcal{G}$	inertia constant of generators.
$C \in \mathbb{R}^{\lvert\mathcal{N}\rvert\times\lvert\mathcal{E}\rvert}$	incidence matrix: $C_{j,e} = 1$ if line $e = (j,k)$ is from bus j to some bus k, $C_{j,e} = -1$ if line $e = (i,j)$ is from some bus i to bus j, and $C_{j,e} = 0$ otherwise.
$B := \mathrm{diag}(B_{ij},\ (i,j) \in \mathcal{E})$	line parameters that depend on line susceptances and voltage magnitudes (assumed fixed).

Table 3.A.1: Frequently used notations in Chapter 3.

3.B Frequency behavior of the test system

A key assumption underlying the analytic model (3.6) is that different buses may have their own frequencies during transient, instead of resynchronizing almost instantaneously to a common system frequency which then converges to an equilibrium. Simulation of the 68-bus test system confirms this phenomenon. Fig. 3.B.1 shows all the 68 bus frequencies from the simulation with the same step change P^m as that in Section 3.8 but without OLC. To give a clearer view of the 68 bus frequencies, they are divided into the following 4 groups.

1. Group 1 has buses 41, 42, 66, 67, 52, and 68;
2. Group 2 has buses 2, 3, 4, 5, 6, 7, 8, 10, 11, 12, 13, 14, 15, 16, 17, 18, 19, 20, 21, 22, 23, 24, 25, 26, 27, 28, 29, 53, 54, 55, 56, 57, 58, 59, 60, and 61;
3. Group 3 has buses 1, 9, 30, 31, 32, 33, 34, 35, 36, 37, 38, 39, 40, 43, 44, 45, 46, 47, 48, 49, 51, 62, 63, 64, and 65;

4. Group 4 has bus 50 only.

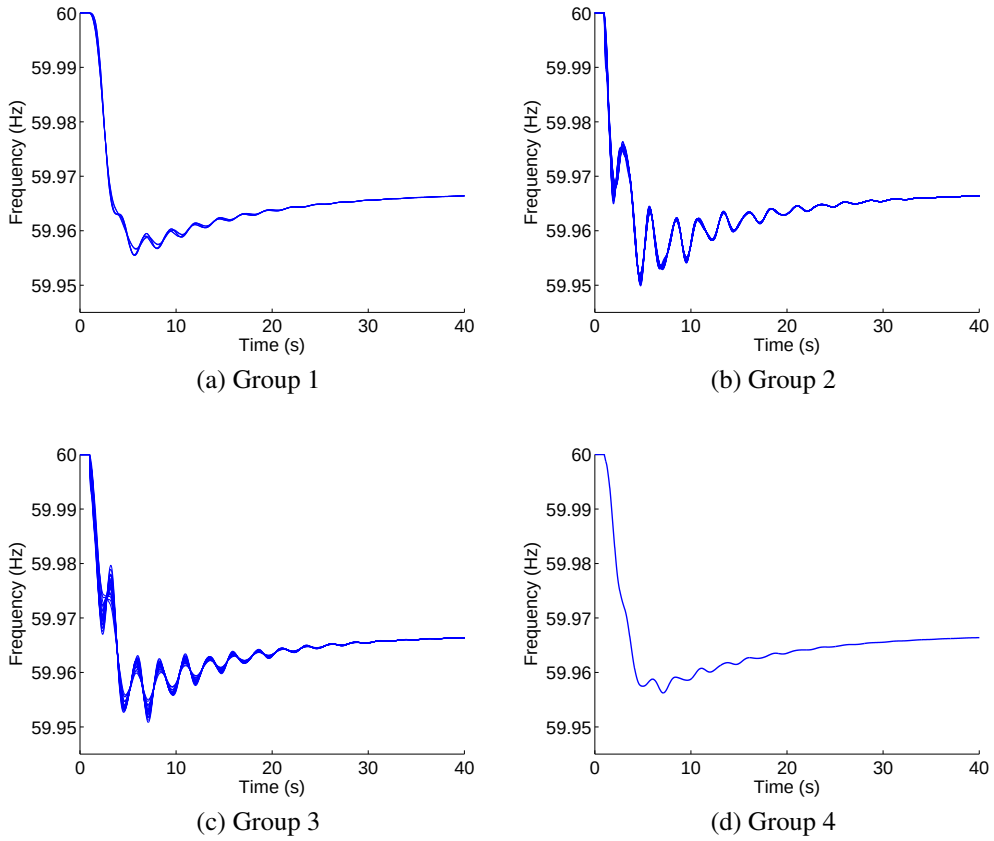

(a) Group 1 (b) Group 2

(c) Group 3 (d) Group 4

Figure 3.B.1: Frequencies at all the 68 buses shown in four groups, without OLC.

We see that, during transient, the frequencies at buses within the same group are almost identical, but the frequencies at buses from different groups are quite different. Moreover the time it takes for these different frequencies to converge to a common system frequency is on the same order as the time for these frequencies to reach their (common) equilibrium value.

3.C Proof of Lemma 3.1

From (3.9), either $c_j'(d_j(\nu)) = \nu$ or $d_j'(\nu) = 0$. Hence, in (3.8) we have

$$\frac{d}{d\nu}\Big(c_j(d_j(\nu)) - \nu d_j(\nu)\Big) \;=\; c_j'(d_j(\nu))d_j'(\nu) - d_j(\nu) - \nu d_j'(\nu) = -d_j(\nu)$$

and thus

$$\frac{\partial \Phi}{\partial \nu_j}(\nu) \;=\; \Phi_j'(\nu_j) \;=\; -d_j(\nu_j) - D_j\nu_j + P_j^m.$$

Hence the Hessian of Φ is diagonal. Moreover, since $d_j(\nu_j)$ given by (3.9) is nondecreasing in ν_j, we have

$$\frac{\partial^2 \Phi}{\partial \nu_j^2}(\nu) \;=\; \Phi_j''(\nu_j) \;=\; -d_j'(\nu_j) - D_j \;<\; 0.$$

Hence Φ is strictly concave over $\mathbb{R}^{|\mathcal{N}|}$.

3.D Proof of Lemma 3.2

Let g denote the objective function of OLC with the domain $\mathcal{D} := \left[\underline{d}_1, \overline{d}_1\right] \times \cdots \times \left[\underline{d}_{|\mathcal{N}|}, \overline{d}_{|\mathcal{N}|}\right] \times \mathbb{R}^{|\mathcal{N}|}$. Since c_j is continuous on $[\underline{d}_j, \overline{d}_j]$, $\sum_j c_j(d_j)$ is lower bounded, i.e., $\sum_j c_j(d_j) > \underline{C}$ for some $\underline{C} > -\infty$. Let $(d', \hat{d}')$ be a feasible point of OLC (which exists by Assumption 3.1). Define the set

$$\mathcal{D}' \;:=\; \left\{ (d, \hat{d}) \in \mathcal{D} \,\middle|\, \hat{d}_j^2 \le 2D_j(g(d', \hat{d}') - \underline{C}) \text{ for all } j \in \mathcal{N} \right\}.$$

Note that for any $(d, \hat{d}) \in \mathcal{D} \backslash \mathcal{D}'$, there is some $i \in \mathcal{N}$ such that $\hat{d}_i^2 > 2D_i(g(d', \hat{d}') - \underline{C})$, thus

$$g(d, \hat{d}) > \underline{C} + \frac{\hat{d}_i^2}{2D_i} > g(d', \hat{d}').$$

Hence any optimal point of OLC must lie in $\mathcal{D}'$. By Assumption 3.1 the objective function g of OLC is continuous and strictly convex over the compact convex set $\mathcal{D}'$, and thus has a minimum $g^* > -\infty$ attained at a unique point $(d^*, \hat{d}^*) \in \mathcal{D}'$.

Note that OLC has a feasible point $(d, \hat{d}) \in \text{relint } \mathcal{D}$, where relint denotes the relative interior [93]. Indeed, let $(d', \hat{d}') \in \mathcal{D}$ be a feasible point of OLC, then we can obtain $(d, \hat{d})$ by letting $d_j = \left(\underline{d}_j + \overline{d}_j\right)/2$, $\hat{d}_j = \hat{d}_j' - d_j + d_j'$. Moreover the only constraint of OLC is affine. Hence there is zero duality gap between OLC and its dual, and a dual optimal ν^* is attained since $g^* > -\infty$ [93, Section 5.2.3]. By Appendix 3.C, $\sum_{j\in\mathcal{N}} \Phi_j''(\nu) = -\sum_{j\in\mathcal{N}} \left(d_j'(\nu) + D_j\right) < 0$, i.e., the objective function of the dual of OLC is strictly concave over $\mathbb{R}$, which implies the uniqueness of ν^*. Moreover, by the definition of dual problem, the optimal point $(d^*, \hat{d}^*)$ of OLC satisfies $d_j^* = d_j(\nu^*)$ given by (3.9) and $\hat{d}_j^* = D_j\nu^*$ for all $j \in \mathcal{N}$.

3.E Proof of Lemma 3.3

From the proof of Lemma 3.1, the Hessian $\frac{\partial^2 \tilde{L}}{\partial \omega_{\mathcal{G}}^2}(\omega_{\mathcal{G}}, P) = \frac{\partial^2 \Phi_{\mathcal{G}}}{\partial \omega_{\mathcal{G}}^2}(\omega_{\mathcal{G}})$ is diagonal and negative definite for all $\omega_{\mathcal{G}} \in \mathbb{R}^{|\mathcal{G}|}$. Therefore $\tilde{L}$ is strictly concave in $\omega_{\mathcal{G}}$. Moreover from (3.22) and the fact that $\frac{\partial L_{\mathcal{L}}}{\partial \omega_{\mathcal{L}}}\left(\omega_{\mathcal{L}}(P), P\right) = 0$, we have

$$\frac{\partial \tilde{L}}{\partial P}(\omega_{\mathcal{G}}, P) \;=\; -\omega_{\mathcal{G}}^T C_{\mathcal{G}} - \omega_{\mathcal{L}}^T(P) C_{\mathcal{L}}. \tag{3.82}$$

Therefore we have (using (3.21))

$$\frac{\partial^2 \tilde{L}}{\partial P^2}(\omega_{\mathcal{G}}, P) = -C_{\mathcal{L}}^T \frac{\partial \omega_{\mathcal{L}}}{\partial P}(P) = -C_{\mathcal{L}}^T \left(\frac{\partial^2 \Phi_{\mathcal{L}}}{\partial \omega_{\mathcal{L}}^2} (\omega_{\mathcal{L}}(P)) \right)^{-1} C_{\mathcal{L}}.$$

From the proof of Lemma 3.1, $\frac{\partial^2 \Phi_{\mathcal{L}}}{\partial \omega_{\mathcal{L}}^2}$ is diagonal and negative definite. Hence $\frac{\partial^2 \tilde{L}}{\partial P^2}(\omega_{\mathcal{G}}, P)$ is positive semidefinite and $\tilde{L}$ is convex in P ($\tilde{L}$ may not be strictly convex in P because $C_{\mathcal{L}}$ is not necessarily of full rank).

3.F Proof of Lemma 3.4

The equivalence of (3.29) and (3.30) follows directly from the definition of $\omega_{\mathcal{L}}(P)$. To prove that (3.30) is necessary and sufficient for $\dot{U}(\omega, P) = 0$, we first claim that the discussion preceding the lemma implies that $(\omega, P) = (\omega_{\mathcal{G}}, \omega_{\mathcal{L}}, P)$ satisfies $\dot{U}(\omega, P) = 0$ if and only if

$$\omega_{\mathcal{G}} = \omega^* 1_{\mathcal{G}} \quad \text{and} \quad \frac{\partial \tilde{L}}{\partial P}(\omega_{\mathcal{G}}, P)\,(P - P^*) = 0. \tag{3.83}$$

Indeed if (3.83) holds then the expression in (3.24) evaluates to zero. Conversely, if $\dot{U}(\omega, P) = 0$, then the inequality in (3.25) must hold with equality, which is possible only if $\omega_{\mathcal{G}} = \omega^* 1_{\mathcal{G}}$ since $\tilde{L}$ is *strictly* concave in $\omega_{\mathcal{G}}$. Then we must have $\frac{\partial \tilde{L}}{\partial P}(\omega_{\mathcal{G}}, P)\,(P - P^*) = 0$ since the expression in (3.24) needs to be zero. Hence we only need to establish the equivalence of (3.83) and (3.30). Indeed, with $\omega_{\mathcal{G}} = \omega^* 1_{\mathcal{G}}$, the other part of (3.83) becomes

$$\begin{aligned}
&\frac{\partial \tilde{L}}{\partial P}(\omega^* 1_{\mathcal{G}}, P)\,(P - P^*) \\
&= -\left[\omega^* 1_{\mathcal{G}}^T \;\; \omega_{\mathcal{L}}^T(P)\right] C(P - P^*) && (3.84)\\
&= -\left[0 \;\; \omega_{\mathcal{L}}^T(P) - \omega^* 1_{\mathcal{L}}^T\right] C(P - P^*) && (3.85)\\
&= -\left(\omega_{\mathcal{L}}(P) - \omega^* 1_{\mathcal{L}}\right)^T \left[\frac{\partial \Phi_{\mathcal{L}}}{\partial \omega_{\mathcal{L}}} (\omega_{\mathcal{L}}(P)) - \frac{\partial \Phi_{\mathcal{L}}}{\partial \omega_{\mathcal{L}}}(\omega^* 1_{\mathcal{L}})\right]^T, && (3.86)
\end{aligned}$$

where (3.84) follows from (3.82), and (3.85) follows from $1_{\mathcal{N}}^T C = 0$, and (3.86) follows from (3.15b) and (3.17). Note that $\Phi_{\mathcal{L}}$ is separable over ω_j for $j \in \mathcal{L}$ and, from (3.8), $\Phi_j'(\omega_j) = -d_j(\omega_j) - D_j \omega_j + P_j^m$. Writing $D_{\mathcal{L}} := \mathrm{diag}(D_j, j \in \mathcal{L})$ we have

$$\begin{aligned}
\frac{\partial \tilde{L}}{\partial P}(\omega^* 1_{\mathcal{G}}, P)\,(P - P^*) = \left(\omega_{\mathcal{L}}(P) - \omega^* 1_{\mathcal{L}}\right)^T D_{\mathcal{L}} \left(\omega_{\mathcal{L}}(P) - \omega^* 1_{\mathcal{L}}\right) \\
+ \sum_{j \in \mathcal{L}} \left(\omega_j(P) - \omega^*\right) \left(d_j\left(\omega_j(P)\right) - d_j(\omega^*)\right). \qquad (3.87)
\end{aligned}$$

Since $d_j(\omega_j)$ given by (3.9) is nondecreasing in ω_j, each term in the summation above is nonnegative for all P. Hence (3.87) evaluates to zero if and only if $\omega_{\mathcal{L}}(P) = \omega^* 1_{\mathcal{L}}$, establishing the equivalence between (3.83) and (3.30).

3.G Proof of Lemma 3.5

The proof of LaSalle's invariance principle in [117, Theorem 3.4] shows that $(\omega(t), P(t))$ approaches its positive limit set Z^+ which is nonempty, compact, invariant, and a subset of E, as $t \to \infty$. It is sufficient to show that $Z^+ \subseteq Z^*$, i.e., considering any point $(\omega, P) = (\omega_{\mathcal{G}}, \omega_{\mathcal{L}}, P) \in Z^+$, to show that $(\omega, P) \in Z^*$. By (3.19), (3.31) and the fact that $(\omega, P) \in E$, we only need to show that

$$C_{\mathcal{G}} P = \left[\frac{\partial \Phi_{\mathcal{G}}}{\partial \omega_{\mathcal{G}}} (\omega_{\mathcal{G}}) \right]^T . \tag{3.88}$$

Since Z^+ is invariant with respect to (3.15), a trajectory $(\omega(t), P(t))$ that starts in Z^+ must stay in Z^+, and hence stay in E. By (3.31), $\omega_{\mathcal{G}}(t) = \omega^* 1_{\mathcal{G}}$ for all $t \geq 0$, and therefore $\dot{\omega_{\mathcal{G}}}(t) = 0$ for all $t \geq 0$. Hence, by (3.15a), any trajectory $(\omega(t), P(t))$ in Z^+ should satisfy

$$C_{\mathcal{G}} P(t) = \left[\frac{\partial \Phi_{\mathcal{G}}}{\partial \omega_{\mathcal{G}}} (\omega_{\mathcal{G}}(t)) \right]^T$$

for all $t \geq 0$, which implies that (3.88) holds for any $(\omega, P) \in Z^+$.

Chapter 4

TWO-TIMESCALE VOLTAGE CONTROL

Chapters 2 and 3 focus on frequency control, which is a major problem for wide-area power transmission systems. In this chapter, we will study the voltage control problem in power distribution systems that are closer to the users.

The voltage of a power distribution system must be maintained closely around its nominal value in real time, even in the presence of highly volatile power supply or demand. For this purpose, we jointly control two types of reactive power sources: a capacitor operating at a slow timescale, and a power electronic device, such as a smart inverter or a D-STATCOM, operating at a fast timescale. Their control actions are solved from optimal power flow problems at two timescales. Specifically, the slow-timescale problem is a chance-constrained optimization, which minimizes power loss and regulates the voltage at the current time instant while limiting the probability of future voltage violations due to stochastic changes in power supply or demand. This control framework forms the basis of an optimal sizing problem, which determines the installation capacities of the control devices by minimizing the sum of power loss cost and capital cost. We develop computationally efficient heuristics to solve the optimal sizing problem and implement real-time control. Numerical experiments with a high-performance computing (HPC) load show that the proposed sizing and control schemes significantly improve the reliability of voltage control with a moderate increase in cost.

This chapter is organized as follows. Section 4.1 describes the model of the distribution circuit and the HPC load. Section 4.2 formulates the control and sizing problems. Section 4.3 describes our heuristics to solve the sizing problem and implement real-time control. Section 4.4 presents the results of optimal sizing as well as simulations of the real-time control. Finally, Section 4.5 concludes this chapter.

4.1 Distribution circuit and load models

We consider a high-performance computing (HPC) load, whose trajectory is shown in Fig. 1.1, as the motivating example for this chapter. Modern HPC platforms are typically supplied by multiple distribution circuits to ensure a redundant power supply. Here we simplify this configuration by considering a single radial circuit

(see Fig. 4.1) with a single HPC load concentrated at its end. A single branch of

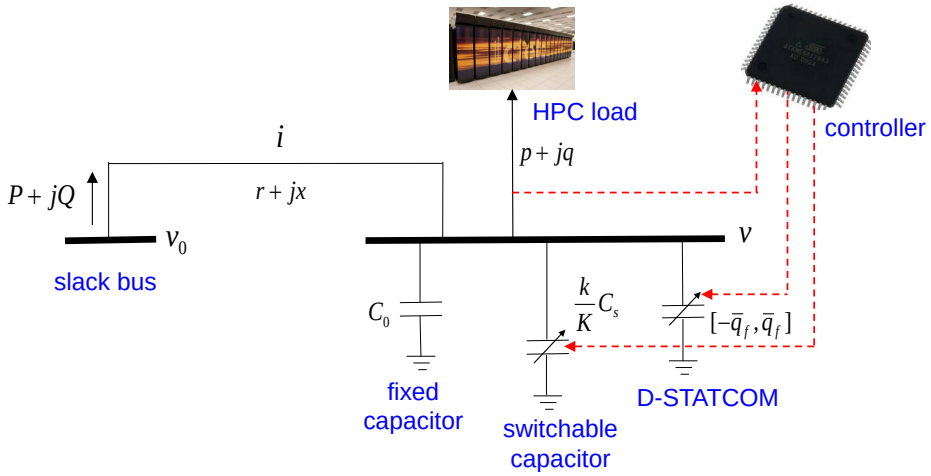

Figure 4.1: Schematic of the simplified circuit with resistance r and reactance x supplying an HPC load at a voltage magnitude of v from a slack bus at a voltage magnitude of v_0. Variables P and Q are real and reactive power injections from the slack bus, and p and q are real and reactive power consumed by the HPC load. The current magnitude in the circuit is i. Three reactive power sources and a controller are installed near the load. Black lines are actual circuit lines and red lines represent signal flows.

resistance r and reactance x connects the HPC load to a slack bus of fixed voltage magnitude and phase angle. Without loss of generality, the voltage phase angle at the slack bus is set to zero. We denote the voltage magnitude at the slack bus by v_0, the voltage magnitude at the HPC load by v, the current magnitude on the branch by i, the real and reactive powers sent from the slack bus by P and Q, and the real and reactive power consumptions of the HPC load by p and q. We assume

$$q = \phi p, \tag{4.1}$$

where ϕ is a positive constant. The constant load power factor represented by (4.1) is typical of the HPC power consumptions.

The following devices are installed at the end of the circuit for voltage control. First, a fixed capacitor with capacitance C_0 injects voltage-dependent reactive power $v^2 f_0 C_0$, where f_0 is the frequency of the circuit and is assumed to be constant. Second, a switchable capacitor can take a small number $K + 1$ of discrete values of capacitance $c_s \in \left\{\frac{k}{K}C_s | k = 0, ..., K\right\}$. In most distribution circuits, capacitors switch only a few times each day to adapt to the gradual changes of the aggregate load, due to their limited life cycles [77]. In the specific system we consider, however,

the capacitor switches more frequently than a few times a day to adapt to the highly intermittent HPC load, but still much less frequently than the changes in HPC load to avoid excessive wear and tear. Moreover, the capacitor cannot switch as fast as the changes in HPC load since the mechanical switching time of the capacitor will delay the implementation of control by many AC cycles even if a change in load is detected instantaneously. In this work, as explained below, we determine when to switch the capacitor in real time based on the actual load and take into account the switching time delay. Third, a D-STATCOM injects reactive power q_f ranging continuously within a preset range $\left[-\overline{q}_f,\ \overline{q}_f\right]$. A D-STATCOM is much more expensive than a capacitor with the same maximum reactive power injection, but can respond within an AC cycle to a change in load and does not suffer from wear and tear from frequent changes in q_f. We call $\left(C_0, C_s, \overline{q}_f\right)$ the *sizes* of reactive power sources and $\left(c_s, q_f\right)$ the control variables. A real-time feedback controller is installed at the load side of the circuit, which measures variables such as load power, voltage and current, takes them as input, and computes the values of control variables and sends them to various control devices.

Suppose the parameter values (r, x, f_0, v_0, ϕ) are given and fixed. Then, incorporating (4.1), the real power p of HPC load, the size C_0 of fixed capacitor, the control $\left(c_s, q_f\right)$ and the state variables (v, i, P, Q) satisfy

$$
\begin{aligned}
i^2 &= \frac{P^2 + Q^2}{v_0^2}, && \text{(4.2a)}\\
P &= p + i^2 r, && \text{(4.2b)}\\
Q &= \phi p - v^2 f_0 \left(C_0 + c_s\right) - q_f + i^2 x, && \text{(4.2c)}\\
v^2 &= v_0^2 - 2(rP + xQ) + i^2(r^2 + x^2). && \text{(4.2d)}
\end{aligned}
$$

The equations are known as the DistFlow equations [61]. Note that $i^2 r$ and $i^2 x$ in (4.2b) and (4.2c) are respectively the real and reactive power losses. With (p, C_0, c_s, q_f) specified, the four variables (v, i, P, Q) can be solved from the four equations (4.2). Indeed, there are two solutions (both with nonnegative values of v and i), one with v close to v_0, small i and hence small power loss, and the other with v close to zero, large i and hence large power loss. We only care about the first one and take it as the unique solution because we desire good voltage control and minimized power loss [122], [123]. Hence v, i, P, Q can be written as functions of (p, C_0, c_s, q_f), e.g., $v = v\left(p, C_0, c_s, q_f\right)$ and $i = i\left(p, C_0, c_s, q_f\right)$.[1]

[1] We abuse notations by using v and i to denote either the variables or the functions.

Equations (4.2) describe the behavior of the circuit at a particular instant. In practice, the real power p of HPC load constantly changes over time, and so may the control (c_s, q_f) and state variables (v, i, P, Q). Here, we focus on characterizing the changes in p over time. As an example, we consider the real power usage recorded at a large HPC platform at the Los Alamos National Laboratory.

Fig. 1.1 shows the time-series trace of p over four days, sampled every 5 seconds. The minimum and maximum values of the trace in the four days are $\underline{p} = 2150$ kW and $\overline{p} = 3650$ kW, and we assume $p \in \left[\underline{p},\ \overline{p}\right]$ always holds. Let $\tau \in \mathbb{N}_0 = \{0, 1, ...\}$ index the time at which the (real) power is sampled and $p(\tau)$ denote the power sampled at time τ. We see from Fig. 1.1 that $|p(\tau + 1) - p(\tau)|$ are relatively small (less than 200 kW) for most of the time while large changes from $p(\tau)$ to $p(\tau + 1)$ are infrequent and usually separated by minutes or even hours.

To capture this pattern, we divide the sequence $\{p(\tau),\ \tau \in \mathbb{N}_0\}$ into *stages*. A stage, indexed by $t \in \mathbb{N}_0$, is a subsequence $\{p(\tau_t), p(\tau_t + 1), ..., p(\tau_{t+1} - 1)\}$ where τ_t and τ_{t+1} are the times of two consecutive large changes in p. The average power of stage t is $p[t] := \frac{1}{T_t}\left(p(\tau_t) + p(\tau_t + 1) + ... + p(\tau_{t+1} - 1)\right)$ where $T_t := \tau_{t+1} - \tau_t$ is the duration of stage t. In Section 4.3 we propose a method to determine the durations and average powers of different stages for a given sequence $\{p(\tau),\ \tau \in \mathbb{N}_0\}$.

We assume the sequence of (average load powers of) stages $\{p[t],\ t \in \mathbb{N}_0\}$ forms a first-order homogeneous Markov chain characterized by transition probability $\pi(p^+ \mid p)$, where p is the average power of the current stage and p^+ is the average power of the next stage. The formal validation of this assumption is our future work, and here we give a partial justification. We determine the sequence of stages from the time-series in Fig. 1.1 using the method in Section 4.3, and measure the probability density of the next-stage power p^+ conditioned on the current-stage power p and the last-stage power p^-, across all the transitions of stage powers. Fig. 4.2 shows two examples in which, given p, the probability density of p^+ is approximately independent of p^-, which hints that the sequence of stages may have a first-order homogeneous Markovian property. We also assume the sequence of samples $\{p(\tau),\ \tau \in \mathbb{N}_0\}$ has a stationary distribution $\rho(\cdot)$. Note that ρ is different from the stationary distribution of the Markov chain of average stage powers.

4.2 Optimal voltage control and device sizing

Suppose the number $K + 1$ of switchable capacitor levels is fixed, and the sizes $(C_0, C_s, \overline{q}_f)$ of reactive power sources are given. We design a real-time voltage

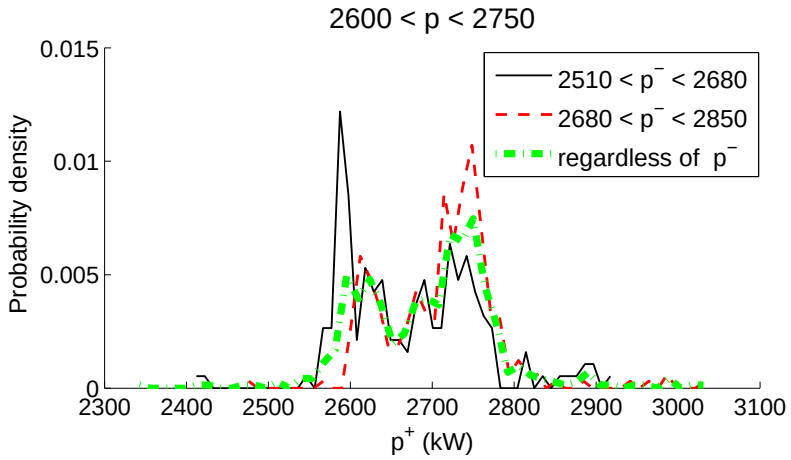

(a)

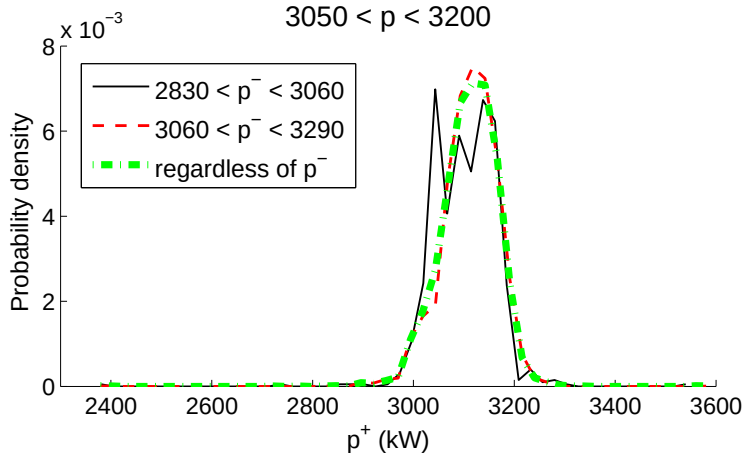

(b)

Figure 4.2: Examples of probability density of p^+ conditioned on p and p^-. Subfigures (a) and (b) are for different p, and the legends label different p^-.

control which, at every time τ, takes a new input $p(\tau)$ and computes optimal output $(c_s^*(\tau), q_f^*(\tau))$.

The control is performed at two timescales: at slow timescale the capacitor c_s is switched at most once per stage, and at fast timescale the D-STATCOM q_f may be adjusted at every time τ when a new sample $p(\tau)$ is measured. We assume there is a fixed time delay $d \in \mathbb{N}$ in capacitor switching, and $d < T_t$ for all t. This delay complicates the control time line, as demonstrated in Fig. 4.3. During the bulk of stage $t-1$, the control output of the switchable capacitor is a constant, $c_s^*[t-1]$. At the beginning time τ_t of the next stage t, a large change in p occurs. A new control output $c_s^*[t]$ of the switchable capacitor is computed using the average load power $p[t]$ of stage t (which is assumed to be known at τ_t if we consider the

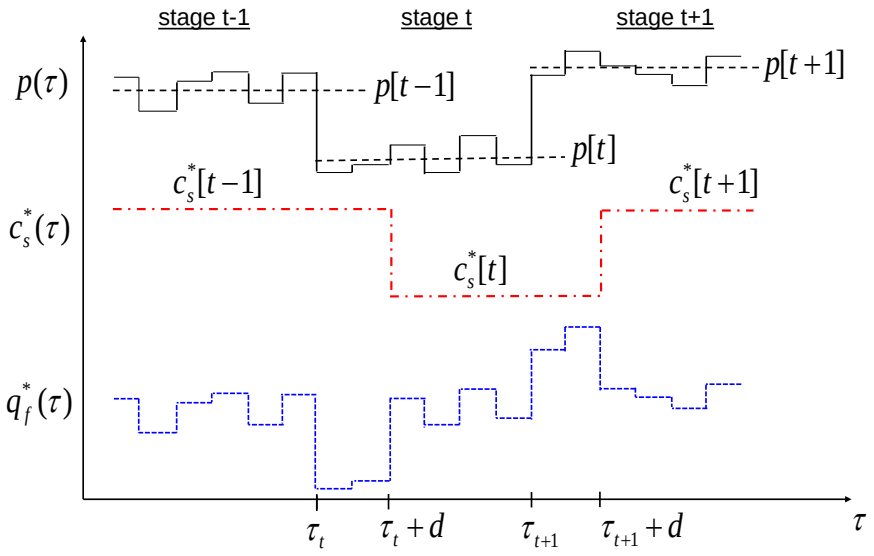

Figure 4.3: Time line of voltage control, which is broken into stages with significantly different average load power $p[t]$. The transition between stages $t-1$ and t occurs at time τ_t. Following this transition, a new optimal output $c_s^*[t]$ of the switchable capacitor is computed but not implemented until a time delay d after the transition. The D-STATCOM output $q_f^*(\tau)$ is computed and implemented at every time when $p(\tau)$ changes, which is especially important for voltage control during the interval from τ_t to $\tau_t + d$.

problem offline; see Section 4.3 for the online case). However, due to the delay in switchable capacitor operation, $c_s(\tau)$ cannot change from $c_s^*[t-1]$ to $c_s^*[t]$ until $\tau_t + d$. A similar delay will occur after the transition from stage t to $t+1$. For the D-STATCOM, however, a control output $q_f(\tau)$ is computed based on $p(\tau)$ and $c_s^*(\tau)$ and implemented instantaneously at every time τ.

In the time line depicted in Fig. 4.3, the control of c_s is coupled across every two consecutive stages. Specifically, the computation of $c_s^*[t]$ should incorporate a prediction about the behavior of $p[t+1]$ to limit the probability of unacceptable voltage deviations during the capacitor switching delay period τ_{t+1} to $\tau_{t+1} + d$, otherwise the uncertainty in $p[t+1]$ and the finite output range of q_f could easily lead to a situation where the voltage at the load exceeds acceptable bounds in this period. Given $p[t]$, the prediction of $p[t+1]$ is based on the transition probability $\pi(\cdot \mid p[t])$ introduced in Section 4.1.

For simplicity, we write $p[t]$, $p[t+1]$, $c_s[t]$ as p, p^+, c_s. Then (the offline version

of) the slow-timescale capacitor control problem, denoted $C_s(p, C_0, C_s, \overline{q}_f)$, is

$$\min_{c_s, q_f, q_f^+} \quad [i\left(p, C_0, c_s, q_f\right)]^2 r \tag{4.3a}$$

$$\text{subject to} \quad -\epsilon \le [v\left(p, C_0, c_s, q_f\right)]^2 - v_0^2 \le \epsilon, \tag{4.3b}$$

$$\Pr\left\{[v(p^+, C_0, c_s, q_f^+)]^2 - v_0^2 \ge \epsilon \mid p\right\} \le \delta, \tag{4.3c}$$

$$\Pr\left\{[v(p^+, C_0, c_s, q_f^+)]^2 - v_0^2 \le -\epsilon \mid p\right\} \le \delta, \tag{4.3d}$$

$$c_s \in \left\{\frac{k}{K} C_s | k = 0, ..., K\right\}, \tag{4.3e}$$

$$-\overline{q}_f \le q_f \le \overline{q}_f, \quad -\overline{q}_f \le q_f^+ \le \overline{q}_f, \tag{4.3f}$$

where i and v as functions of (p, C_0, c_s, q_f) or (p^+, C_0, c_s, q_f^+) are specified by the DistFlow equations (4.2). With respect to the average load power of the current stage, the objective (4.3a) minimizes real power loss, and the deterministic constraint (4.3b) regulates voltage. Chance constraints (4.3c)(4.3d) limit the probability of voltage violations during the capacitor switching delay period of the next stage, by incorporating transition probability from p to p^+. Instead of limiting the voltage magnitude, we choose to limit its square, which simplifies the analysis below. Constraint (4.3e) specifies a discrete feasible set of c_s. Note that the optimal solutions $(q_f^*, q_f^{+,*})$ of the problem $C_s(p, C_0, C_s, \overline{q}_f)$ (4.3) will not be applied to the D-STATCOM. The actual control actions of the D-STATCOM will be determined by a separate problem $C_f(p, C_0, c_s^*, \overline{q}_f)$ (4.4) below. The variables q_f, q_f^+ are included in $C_s(p, C_0, C_s, \overline{q}_f)$ (4.3) to guarantee the existence of feasible (satisfying (4.3f)) operation points of the D-STATCOM in the current stage and in the capacitor switching delay period of the next stage, when we optimize over c_s.

At time τ_t, problem $C_s(p[t], C_0, C_s, \overline{q}_f)$ is solved for $c_s^*[t]$. The actions of the switchable capacitor are $c_s^*(\tau) = c_s^*[t]$ for $\tau_t + d \le \tau < \tau_{t+1} + d$. Then at every time τ, with $c_s^*(\tau)$ known, a fast-timescale D-STATCOM control problem $C_f(p(\tau), C_0, c_s^*(\tau), \overline{q}_f)$ is solved for $q_f^*(\tau)$. For simplicity, write $p(\tau)$, $c_s^*(\tau)$, $q_f(\tau)$ as p, c_s^*, q_f. Then $C_f(p, C_0, c_s^*, \overline{q}_f)$ is

$$\min_{q_f} \quad [i\left(p, C_0, c_s^*, q_f\right)]^2 r \tag{4.4a}$$

$$\text{subject to} \quad -\epsilon \le \left[v\left(p, C_0, c_s^*, q_f\right)\right]^2 - v_0^2 \le \epsilon, \tag{4.4b}$$

$$-\overline{q}_f \le q_f \le \overline{q}_f, \tag{4.4c}$$

where q_f is chosen to minimize power loss while regulating the voltage at the current instant. While C_s in (4.3) is a chance-constrained OPF problem, C_f in (4.4) is a simpler OPF problem without chance constraints.

For both the capacitor and the D-STATCOM control problems above, the objective is to minimize power loss as long as voltage violations are avoided, which is common in practice and also makes sense for this specific system with a large HPC facility (potentially large associated power loss) and a simple circuit. Indeed, different control objectives might be chosen for different systems. For example, in a more complex distribution network with multiple loads, the objective might be finding a particular voltage profile across the network to minimize the total energy consumption, through mechanisms such as Conservative Voltage Reduction [69], [77], [124].

The optimal objective value of $C_s(p, C_0, C_s, \overline{q}_f)$, i.e., the minimum power loss with respect to the average load power p of a stage, is denoted by $L(p, C_0, C_s, \overline{q}_f)$. When planning the sizes of reactive power devices that will be installed in the circuit, we need to account for the cost of the expected minimum power loss and the capital cost of devices. Hence, an optimal sizing problem is formulated as

$$\min_{(C_0, C_s, \overline{q}_f) \in \mathcal{X}} \; k_p \int_{\underline{p}}^{\overline{p}} L(p, C_0, C_s, \overline{q}_f)\rho(p)dp + L_0(C_0) + L_s(C_s) + L_f(\overline{q}_f). \quad (4.5)$$

The integral term in (4.5) is the expectation of minimum power loss resulting from the capacitor control C_s. Note that though C_s takes average load powers of stages as input, the integral in (4.5) is taken over the stationary distribution $\rho(\cdot)$ of load powers sampled at a 5-second timescale, since the stationary distribution of average stage powers does not include information of durations of stages.

In (4.5), the coefficient k_p converts the expected power loss into a cost which has the same unit as the capital costs, L_0, L_s and L_f, of the fixed capacitor, the switchable capacitor and the D-STATCOM. Let $\mathbb{R}_0^+$ denote the set of non-negative real numbers. The domain $\mathcal{X}$ of the optimal sizing problem is the set of points $(C_0, C_s, \overline{q}_f) \in \left(\mathbb{R}_0^+\right)^3$ such that $C_s(p, C_0, C_s, \overline{q}_f)$ is feasible for all $p \in [\underline{p}, \overline{p}]$.

4.3 Heuristic solution and implementation

We formulated our control problem as two OPF problems on a one-branch, single-phase circuit, which are usually simple to solve. The optimal sizing problem, however, is more difficult to solve analytically, since neither its objective function (4.5) nor its domain $\mathcal{X}$ has a closed-form expression. Probabilistic metaheuristics, e.g., simulated annealing, genetic algorithm and particle swarm optimization, are considered good candidate numerical methods to search for a (usually approximate) globally optimal solution for the sizing problem. In the rest of this paper we use

simulated annealing (SA) [125], but the techniques we develop can be applied to other metaheuristics in a similar way.

A key process in SA is to evaluate the objective value and, in particular, the integral term in (4.5) for any given $(C_0, C_s, \overline{q}_f)$. In practice, we use the numerical approximation

$$\sum_{n=1}^{N} L(p_n, C_0, C_s, \overline{q}_f)\tilde{\rho}_n, \tag{4.6}$$

where $\underline{p} = p_0 < p_1 < \ldots < p_N = \overline{p}$ is a partition of the interval $\left[\underline{p}, \overline{p}\right]$, and $\tilde{\rho}_n = \int_{p_{n-1}}^{p_n} \rho(p)dp$ is the probability that the real power load lies in the subinterval $[p_{n-1}, p_n]$. If $C_s(p_n, C_0, C_s, \overline{q}_f)$ is infeasible for any $n \in \{1, \ldots, N\}$, then $(C_0, C_s, \overline{q}_f) \notin \mathcal{X}$ and is assigned an infinitely high objective value for the sizing problem. If $\left(C_0, C_s, \overline{q}_f\right) \in \mathcal{X}$, evaluation of the integral term in (4.5) requires solving C_s for N times, one for each bin in the approximation in (4.6). If N is large, the computation of the objective value becomes expensive. Moreover, the chance constraints (4.3c)(4.3d) do not have closed-form expressions, making it more complex to solve $C_s(p_n, C_0, C_s, \overline{q}_f)$.

To reduce the computational burden in our SA-based approach, we make simplifications for the underlying capacitor control problems and develop a heuristic to approximately solve them by exploiting the structure of the simplified problems. By doing this the evaluation of the integral term in (4.5) is simplified, and we develop a computationally efficient heuristic to solve the optimal sizing problem. We also design a heuristic to implement the voltage control proposed in Section 4.2 in an online manner in real time. Below we describe in detail our approach.

Heuristic for capacitor control

Indeed, from (4.2) one can solve for v and i explicitly in closed forms of (p, C_0, c_s, q_f), using the classic formula of roots of quadratic equations. However, these explicit solutions still take such complicated forms that solving for C_s is computationally expensive. Hence we perform the following approximations to obtain a simplified version of C_s, which has a clearer structure of how the solution depends on the input.

First, we simplify the expression of i^2. In a realistic distribution circuit, the real and reactive power losses $i^2 r$ and $i^2 x$ are much smaller than the sending-end real and

reactive powers P and Q, respectively. Hence by (4.2a)–(4.2c) we have

$$i^2 \approx \frac{p^2 + \left(v^2 f_0(C_0 + c_s) + q_f - \phi p\right)^2}{v_0^2}. \tag{4.7}$$

Second, we convert constraint (4.3b) into affine inequalities in (c_s, q_f, p, i^2). From (4.2b)–(4.2d) we have

$$v^2 = \frac{v_0^2 - 2(r + \phi x)p + 2xq_f - i^2(r^2 + x^2)}{1 - 2x f_0 (C_0 + c_s)}. \tag{4.8}$$

We only consider $1 - 2x f_0 (C_0 + c_s) > 0$ since it is a stability requirement that an increase in reactive power injection (or equivalently, in C_0, c_s or q_f) results in an increase in voltage magnitude [123]. Substituting (4.8) into (4.3b), we have

$$\begin{aligned} & q_{\text{vc},1}\left(c_s, q_f\right) := f_0\left(v_0^2 + \epsilon\right)(C_0 + c_s) + q_f \\ \leq\ & \left(\frac{r}{x} + \phi\right)p + \frac{\epsilon}{2x} + \frac{i^2\left(r^2 + x^2\right)}{2x} =: g_1(p, i^2), \qquad (4.9) \\ & q_{\text{vc},2}\left(c_s, q_f\right) := f_0\left(v_0^2 - \epsilon\right)(C_0 + c_s) + q_f \\ \geq\ & \left(\frac{r}{x} + \phi\right)p - \frac{\epsilon}{2x} + \frac{i^2\left(r^2 + x^2\right)}{2x} =: g_2(p, i^2), \qquad (4.10) \end{aligned}$$

where the left-hand-sides and right-hand-sides are affine functions of (c_s, q_f) and affine functions of (p, i^2).

Third, we convert chance constraints (4.3c)(4.3d) into simpler deterministic constraints. Similar to how we obtained (4.9)(4.10) from (4.3b), we have, from (4.3c)(4.3d), that

$$\begin{aligned} \Pr\left(q_{\text{vc},1}(c_s, q_f^+) \geq g_1(p^+, (i^+)^2) \mid p\right) &\leq \delta, \qquad (4.11) \\ \Pr\left(q_{\text{vc},2}(c_s, q_f^+) \leq g_2(p^+, (i^+)^2) \mid p\right) &\leq \delta, \qquad (4.12) \end{aligned}$$

where i^+ denotes $i(p^+, C_0, c_s, q_f^+)$. Given the current-stage average load power p, find two powers $\tilde{h}_1$ and $\tilde{h}_2$ as

$$\begin{aligned} \tilde{h}_1(p) &:= \sup\left\{h \in [\underline{p},\ \overline{p}] \middle| \int_{\underline{p}}^{h} \pi\left(p^+|p\right) dp^+ \leq \delta\right\}, \\ \tilde{h}_2(p) &:= \inf\left\{h \in \left[\underline{p},\ \overline{p}\right] \middle| \int_{h}^{\overline{p}} \pi\left(p^+|p\right) dp^+ \leq \delta\right\}. \end{aligned}$$

Then from (4.11)(4.12), the chance constraints are converted into deterministic constraints:

$$\begin{aligned} q_{\mathrm{vc},1}(c_s, q_f^+) &\leq \left(\frac{r}{x} + \phi\right)\tilde{h}_1(p) + \frac{\epsilon}{2x} + \frac{r^2 + x^2}{2x}(i^+)^2 \\ &=: h_1\left(p, (i^+)^2\right), \end{aligned} \tag{4.13}$$

$$\begin{aligned} q_{\mathrm{vc},2}(c_s, q_f^+) &\geq \left(\frac{r}{x} + \phi\right)\tilde{h}_2(p) - \frac{\epsilon}{2x} + \frac{r^2 + x^2}{2x}(i^+)^2 \\ &=: h_2\left(p, (i^+)^2\right). \end{aligned} \tag{4.14}$$

Fourth, we approximate the $\left(p, C_0, c_s, q_f\right)$-dependent argument i^2 in $g_1(p, i^2)$ and $g_2(p, i^2)$ in (4.9)(4.10) with a constant $\tilde{I}$.[2] Moreover we replace the (p^+, C_0, c_s, q_f^+)-dependent argument $(i^+)^2$ in $h_1(p, (i^+)^2)$ in (4.13) with its estimated lower bound $\underline{I}^+$, and replace $(i^+)^2$ in $h_2(p, (i^+)^2)$ in (4.14) with its estimated upper bound $\overline{I}^+$, where both $\underline{I}^+$ and $\overline{I}^+$ are constant. Section 4.3 explains the way we obtain $\tilde{I}$, while $\underline{I}^+$ and $\overline{I}^+$ are estimated as follows. Suppose (4.3b)(4.9)(4.10) are also satisfied when (p, q_f) is replaced by (p^+, q_f^+) (which indeed occurs with a high probability $1 - 2\delta$). Then (4.7), which also holds when (i, p, q_f) is replaced by (i^+, p^+, q_f^+), implies

$$\begin{aligned} (i^+)^2 &\geq \frac{1}{v_0^2}\left[\underline{p}^2 + \left(\frac{r}{x}\cdot\underline{p} - \frac{\epsilon}{2x} + \frac{\left(r^2 + x^2\right)}{2x}(i^+)^2\right)^2\right] \\ &\approx \frac{1}{v_0^2}\left[\underline{p}^2 + \left(\frac{r}{x}\cdot\underline{p} - \frac{\epsilon}{2x}\right)^2\right] =: \underline{I}^+, \\ (i^+)^2 &\leq \frac{1}{v_0^2}\left[\overline{p}^2 + \left(\frac{r}{x}\cdot\overline{p} + \frac{\epsilon}{2x} + \frac{\left(r^2 + x^2\right)}{2x}(i^+)^2\right)^2\right] \\ &\approx \frac{1}{v_0^2}\left[\overline{p}^2 + \left(\frac{r}{x}\cdot\overline{p} + \frac{\epsilon}{2x}\right)^2\right] =: \overline{I}^+, \end{aligned}$$

where the approximate equalities result from dropping the term associated with relatively small power loss. A significant component of these simplifications is that $g_1(p, \tilde{I})$, $g_2(p, \tilde{I})$, $h_1(p, \underline{I}^+)$, $h_2(p, \overline{I}^+)$ are known a priori when p is given. Hence, with those terms on the right-hand-sides, inequalities (4.9)(4.10)(4.13)(4.14) become simple affine constraints in (c_s, q_f, q_f^+).

The four approximation steps above render us a simple way to approximately solve C_s, which becomes to minimize (4.7) subject to (4.9)(4.10) (with i^2 replaced by a

[2] We abuse the notation by letting $\tilde{I}$ denote a vector in Section 4.3. Its meaning should be clear given the context.

constant $\tilde{l}$), and (4.13)(4.14) (with $(i^+)^2$ replaced by constants $\underline{l}^+$ and $\overline{l}^+$, respectively), and (4.3e)(4.3f). A further observation is that the objective (4.7) of the simplified problem is decreased by decreasing c_s and q_f. Indeed, in practice ϵ is selected to be much smaller than $2r\underline{p}$, which makes $v^2 f_0(C_0 + c_s) + q_f > \phi p$ by (4.3b)(4.10). Moreover, decreasing c_s and q_f results in decrease in v^2 by (4.8).

Hence we design the following heuristic $\mathcal{H}_s$ to approximately solve the capacitor control problem $C_s(p, C_0, C_s, \overline{q}_f)$ and get $\tilde{L}(p, C_0, C_s, \overline{q}_f; \tilde{l})$, an approximation of the actual optimal objective $L(p, C_0, C_s, \overline{q}_f)$. Moreover, a variable "feasibility_flag" is set to be 1, which means $C_s(p, C_0, C_s, \overline{q}_f)$ is feasible, if a c_s^* is found by the heuristic, and 0 otherwise.

Heuristic. $\mathcal{H}_s(p, C_0, C_s, \overline{q}_f; \tilde{l})$*: capacitor control*
feasibility_flag = 0;
for $k = 0, 1, ..., K$ **do**
if $q_{\text{vc},1}\left(\frac{k}{K}C_s, -\overline{q}_f\right) \le \min\left(g_1(p, \tilde{l}), h_1(p, \underline{l}^+)\right)$
and $q_{\text{vc},2}\left(\frac{k}{K}C_s, \overline{q}_f\right) \ge \max\left(g_2(p, \tilde{l}), h_2(p, \overline{l}^+)\right)$ **do**
  feasibility_flag = 1;
  $c_s^* = \frac{k}{K}C_s$;
  $q_f^* = \max\left(-\overline{q}_f, g_2(p, \tilde{l}) - f_0\left(v_0 - \epsilon\right)\left(C_0 + c_s^*\right)\right)$;
  $\tilde{L}(p, C_0, C_s, \overline{q}_f; \tilde{l}) = [i(p, C_0, c_s^*, q_f^*)]^2 r$;
  return;[3]
end if;
end for;
return;

Note that the result of $\mathcal{H}_s$ depends on the constant $\tilde{l}$, whose selection will be explained below. The heuristic $\mathcal{H}_s$ forms a basis for developing the heuristic to solve the optimal sizing problem.

Heuristic for optimal sizing

Suppose a partition $\underline{p} = p_0 < p_1 < ... < p_N = \overline{p}$ is given and fixed, and for every $n \in \{1, ..., N\}$ the probability $\tilde{\rho}_n$ of load power lying in the subinterval $[p_{n-1}, p_n]$ is known. When solving the optimal sizing problem with SA, the function $\tilde{E}(C_0, C_s, \overline{q}_f; \tilde{l})$ below is used to approximate the objective value (4.5) at a given point $(C_0, C_s, \overline{q}_f)$, where $\tilde{l}$ is a vector $(\tilde{l}_1, ..., \tilde{l}_N)$ of constants used to

[3] In the pseudo code of this chapter, "return" means terminating the current heuristic and returning the values of all variables computed.

approximate the minimum value of i^2 for each input p_n to the underlying problem C_s. Note that $\tilde{E}(C_0, C_s, \overline{q}_f; \tilde{l})$ is assigned an extremely high value as $+\infty$, i.e., $(C_0, C_s, \overline{q}_f)$ is marked as infeasible, if $\mathcal{H}_{\mathrm{s}}(p_n, C_0, C_s, \overline{q}_f; \tilde{l}_n)$ for any $n \in \{1, ..., N\}$ returns feasibility_flag$_n$ = 0.

Heuristic. $\tilde{E}(C_0, C_s, \overline{q}_f; \tilde{l})$*: approximate sizing objective*
for $n = 1, ..., N$ **do**
Run $\mathcal{H}_{\mathrm{s}}(p_n, C_0, C_s, \overline{q}_f; \tilde{l}_n)$;
if feasibility_flag$_n$ == 0 **do**
$\tilde{E}(C_0, C_s, \overline{q}_f; \tilde{l}) = +\infty$;
return;
end if;
end for;
$\tilde{E}(C_0, C_s, \overline{q}_f; \tilde{l}) = k_p \sum_{n=1}^{N} \tilde{L}(p_n, C_0, C_s, \overline{q}_f; \tilde{l}_n)\tilde{\rho}_n + L_0(C_0) + L_s(C_s) + L_f(\overline{q}_f)$;
return;

Based on the approximate objective function above, an iterative heuristic $\mathcal{H}_{\mathrm{osz}}$ is developed to approximately solve the optimal sizing problem. In the j-th iteration, $\mathcal{H}_{\mathrm{osz}}$ runs SA with objective function $\tilde{E}(\cdot; \tilde{l}^{*,j})$ to obtain an optimal $(C_0^{*,j}, C_s^{*,j}, \overline{q}_f^{*,j})$. Based on the outputs of underlying $\mathcal{H}_{\mathrm{s}}$ heuristics, $\tilde{l}^{*,j}$ is updated to $\tilde{l}^{*,j+1}$.

Heuristic. $\mathcal{H}_{osz}$*: optimal sizing*
$j = 0$; $\tilde{l}^{*,0} = 0$;
while termination condition == false **do**
Run SA with $\tilde{E}(\cdot; \tilde{l}^{*,j})$ and get $(C_0^{*,j}, C_s^{*,j}, \overline{q}_f^{*,j})$;
for $n = 1, ..., N$ **do**
$\tilde{l}_n^{*,j+1} = \frac{1}{r} \cdot \tilde{L}(p_n, C_0^{*,j}, C_s^{*,j}, \overline{q}_f^{*,j}; \tilde{l}_n^{*,j})$;
end for;
$j = j + 1$;
end while;
$(C_0^*, C_s^*, \overline{q}_f^*) = (C_0^{*,j}, C_s^{*,j}, \overline{q}_f^{*,j})$;
return;

An example of the termination condition is that some norms $\|\tilde{l}^{*,j+1} - \tilde{l}^{*,j}\|$, $\|C_0^{*,j+1} - C_0^{*,j}\|$, etc. are smaller than certain thresholds. In the numerical experiments in Section 4.4 this condition is always satisfied within a small number of iterations. The fact that only a small number of iterations are required and each iteration

works on SA with a simple objective function indicates that $\mathcal{H}_{\text{osz}}$ is computationally efficient in solving the optimal sizing problem.

Heuristic for real-time control

Now we suppose reactive power sources of optimal sizes $\left(C_0^*, C_s^*, \overline{q}_f^*\right)$ have been installed in the circuit and look at the implementation of real-time control. Recall that we formulated the capacitor control problem in Section 4.2 in an offline manner, i.e., by assuming that the average load power $p[t]$ of stage t is known at the beginning τ_t of stage t. This assumption, however, does not hold in practice since $p[t]$ also depends on inputs $p(\tau)$ for $\tau > \tau_t$. Therefore the heuristic for real-time control should be implemented online for sequential arrivals of input $\{p(\tau), \tau \in \mathbb{N}_0\}$.

To this end, we develop a heuristic $\mathcal{H}_{\text{rt}}$ which determines the start of a new stage online, estimates the average load powers of the new stage, solves C_s for capacitor control at every stage and solves C_f for D-STATCOM control at every time when the load power is sampled. Specifically, a threshold p_{th} is used to determine the starting time τ_t of a stage t. At τ_t the controller takes $p(\tau_t)$ as an estimate of $p[t]$ and solves $C_s(p(\tau_t), C_0^*, C_s^*, \overline{q}_f^*)$ for $c_s^*(\tau_t + d)$, due to the operation delay d of the switchable capacitor. The estimate of $p[t]$ is updated for $\tau = \tau_t + 1, ..., \tau_t + T_t - 1$. Whenever the updated estimate of $p[t]$ deviates from the previous input to C_s by more than a preset threshold p_{est}, problem C_s needs to be solved again with the updated estimate of $p[t]$ as a new input. The D-STATCOM control problem C_f is a simple OPF problem and can be solved using standard techniques, which are beyond the scope of this paper. Details of $\mathcal{H}_{\text{rt}}$ are given below. Suppose $\mathcal{H}_{\text{rt}}$ has been running for $\tau < 0$ so that the values of t, $p[t]$, $\tilde{p}[t]$, T_t and $c_s^*(\tau), ..., c_s^*(\tau + d - 1)$ are known at $\tau = 0$.

Heuristic. $\mathcal{H}_{rt}$: real-time voltage control
for $\tau = 0, 1, 2, ...$ **do**
if $|p(\tau) - p[t]| > p_{\text{th}}$ **do**
$t = t + 1$; $p[t] = p(\tau)$; $\tilde{p}[t] = p[t]$; $T_t = 1$;
Solve $C_s\left(\tilde{p}[t], C_0^*, C_s^*, \overline{q}_f^*\right)$ for $c_s^*(\tau + d)$;
else do
$p[t] = \frac{p[t] \times T_t + p(\tau)}{T_t + 1}$; $T_t = T_t + 1$;
if $|p[t] - \tilde{p}[t]| > p_{\text{est}}$ **do**
$\tilde{p}[t] = p[t]$;
Solve $C_s\left(\tilde{p}[t], C_0^*, C_s^*, \overline{q}_f^*\right)$ for $c_s^*(\tau + d)$;
else do
$c_s^*(\tau + d) = c_s^*(\tau + d - 1)$;

end if;
end if;
Solve $C_f(p(\tau), C_0^*, c_s^*(\tau), \overline{q}_f^*)$;
end for;

Note that the previous process of running $\mathcal{H}_{\text{osz}}$ for optimal sizing has provided us with a great deal of information to simplify computations in $\mathcal{H}_{\text{rt}}$. For example, for all $n \in \{1, ..., N\}$ we have $\tilde{l}_n^*$, $g_1(p_n, \tilde{l}_n^*)$, $g_2(p_n, \tilde{l}_n^*)$, $h_1(p_n, \underline{l}^+)$, $h_2(p_n, \overline{l}^+)$ and $c_{s,n}^*$. When solving $C_s\left(\tilde{p}[t], C_0^*, C_s^*, \overline{q}_f^*\right)$ in real-time control $\mathcal{H}_{\text{rt}}$, if it happens that $\tilde{p}[t] = p_n$ for some n, then we know its solution is $c_{s,n}^*$ without actually solving it. Otherwise it can be solved by running $\mathcal{H}_{\text{s}}(\tilde{p}[t], C_0^*, C_s^*, \overline{q}_f^*; \tilde{l}^*[t])$, in which $\tilde{l}^*[t]$, $g_1(\tilde{p}[t], \tilde{l}^*[t])$, etc. can be obtained through interpolation of $\tilde{l}_n^*$, $g_1(p_n, \tilde{l}_n^*)$, etc. for p_n neighboring $\tilde{p}[t]$. Such simplifications can accelerate the computations in real-time control. Indeed, in the numerical experiments in Section 4.4, the computation time of running $\mathcal{H}_{\text{rt}}$ is negligible compared to the time step between consecutive control actions.

As an additional remark to this section, the multiple heuristics proposed above are inspired by the insight we obtain from the structure of the simplified problem resulting from a series of approximations to the original capacitor control problem. Rigorous analysis of the impact of those approximations and the performance of the proposed heuristics, e.g., sub-optimality bounds of $\mathcal{H}_{\text{s}}$ and $\mathcal{H}_{\text{osz}}$ and convergence rate of $\mathcal{H}_{\text{osz}}$, is our future work.

4.4 Numerical results

We solve the optimal sizing problem with the proposed heuristic and run simulations to test the proposed real-time control. We also study the dependence of the optimal device sizes and the performance of the proposed control on the choice of parameter δ, the tolerable probability of voltage violations due to transitions of load power.

We take the model in Fig. 4.1 with the following parameter values. The per unit base power is 1 kW, $v_0 = f_0 = 1$ pu, $\phi = 0.2$, and $r = x = 1.1 \times 10^{-5}$ pu. The parameter ϵ for voltage control is 0.02 pu, which allows the voltage magnitude v to fluctuate between 0.99 pu and 1.01 pu.[4] Suppose the capital costs of reactive power sources are

$$L_0(C_0) = k_0 v_0^2 f_0 C_0, \quad L_s(C_s) = k_s v_0^2 f_0 C_s, \quad L_f(\overline{q}_f) = k_f \overline{q}_f.$$

[4]We make the acceptable voltage range very tight to exercise the proposed schemes. Larger loads (or distributed generation) will cause larger voltage swings that are closer to realistic limits.

The price of energy (that supplies the real power loss) is \$50/MWh. Both the prices of the fixed capacitor and the switchable capacitor, in terms of dollars spent on per unit reactive power injection under nominal voltage and frequency, are \$1000/Mvar. The price of D-STATCOM, in terms of dollars spent on per unit reactive power injection, is \$100,000/Mvar. Suppose all the reactive power devices can be used for 30 years. The prices above are then converted to values of k_p, k_0, k_s and k_f such that the objective (4.5) of the optimal sizing problem measures the cost in dollars every day. For the switchable capacitor $K = 1$, i.e., it can switch to either 0 or C_s.

From the four-day trace of load power in Fig. 1.1, we use samples in the first three days as the training set to measure the transition probabilities π between stages and the stationary distribution ρ of load power samples. We use different values of parameter δ in different cases of the experiments, where a case means the process of solving the optimal sizing problem using $\mathcal{H}_{\text{osz}}$ and then, with the resulting optimal sizes of the devices, implementing the real-time control $\mathcal{H}_{\text{rt}}$ on the load power trace in the last day from Fig. 1.1.

Fig. 4.4 shows the dependence of optimal device sizes on δ. Fig. 4.4a shows C_0^* and $C_0^* \pm \overline{q}_f^*$, i.e., the range of reactive power injection[5] when the switchable capacitor control $c_s = 0$, which usually happens under low load power. On the other hand, Fig. 4.4b shows $C_0^* + C_s^*$ and $C_0^* + C_s^* \pm \overline{q}_f^*$, i.e., the range of reactive power injection when $c_s = C_s^*$, which usually happens under high load power. We see in both subfigures that the range of reactive power injection gets broader as δ decreases, since with less tolerance of probabilistic voltage violations (smaller δ), the D-STATCOM is required to have larger control capacity $\overline{q}_f^*$ to regulate voltage more safely when c_s cannot switch immediately following a large transition of load power. Another observation is that the lower bound $C_0^* - \overline{q}_f^*$ of the total control is almost constant for $\delta \leq 0.9$. Indeed, for those δ, when $c_s = 0$, the chance constraint (4.3c) is not binding in any capacitor control problem underlying the sizing problem. For a similar reason $C_0^* + C_s^* + \overline{q}_f^*$ is almost constant for $\delta \geq 0.4$.

Note that we implement $\delta = 1$ by removing the chance constraints (4.3c)(4.3d) in all the capacitor control problems underlying the sizing problem. Hence in Fig. 4.4a there is a significant drop of the whole range of reactive power injection when δ is increased from 0.9 to 1. Indeed, after removing (4.3d) it is no longer necessary to maintain a high level of $C_0^* + q_f^*$ for voltage control during the capacitor switching

[5]The capacitance C_0 and its nominal reactive power injection $v_0^2 f_0 C_0$ have the same per unit value, since $f_0 = v_0 = 1$ pu.

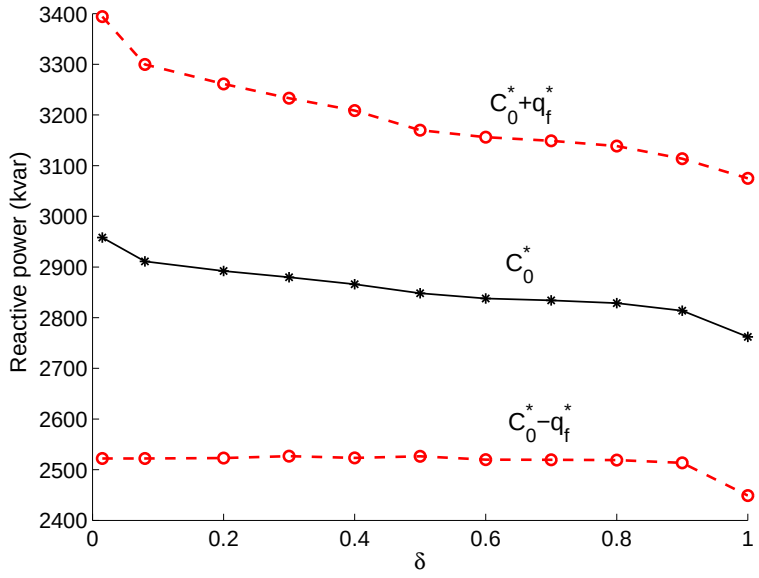

(a)

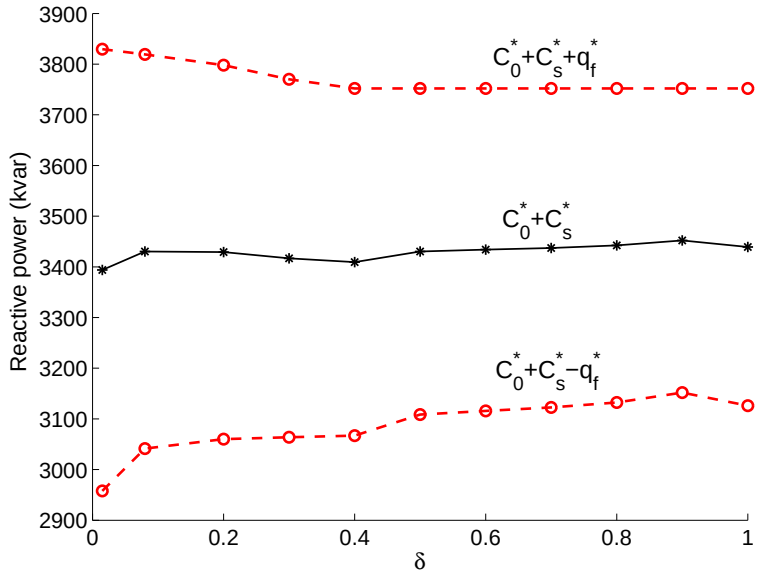

(b)

Figure 4.4: Sizes of control devices as functions of δ. The range of aggregate reactive power injection of the fixed capacitor and the D-STATCOM is plotted for (a) $c_s = 0$ and (b) $c_s = C_s^*$, respectively.

delay period immediately after any possible large load increase, and thus the range of reactive power injection can be moved down to decrease power loss as well as capital cost. This decrease in power loss and capital cost, however, is obtained by

suffering a higher risk of voltage violations, as shown in Figs. 4.5 and 4.6 below.

As sketched above we run the real-time control heuristic $\mathcal{H}_{\text{rt}}$ for many cases, each with a different δ and different device sizes depending on that δ. For two of the cases with $\delta = 0.1$ and $\delta = 1$, the real-time traces of voltage magnitude and real power loss are shown in Fig. 4.5. The traces of voltage and power loss are also plotted for a benchmark case with only a fixed capacitor (whose size equals $C_0^* + C_s^* + \overline{q}_f^*$ when $\delta = 0.1$) and no control. We see that, in the benchmark case with only a fixed capacitor, the larger time-independent reactive power injection from the fixed capacitor results in higher voltages and losses at nearly all times compared to the two cases with controls. The case $\delta = 0.1$ generally biases the voltage above the case $\delta = 1$ (no chance constraints). This bias protects the system against experiencing an undervoltage when the load suddenly increases, as revealed near the end of the day when the voltage in the case $\delta = 1$ dips below 0.99 pu. This extra voltage safety provided by the chance constraints incurs increased power loss during periods when the case $\delta = 0.1$ biases the voltage up with additional reactive power injections.

For each case with different δ, we record the proportion of 5-second samples in one day at which the voltage drops below 0.99 pu (indeed the voltage never swings above 1.01 pu so those recorded are all the samples with voltage violations). We also sum up the real-time power loss over one day, and add up the cost of that power loss and the average capital cost in one day. Fig. 4.6 shows the proportion of samples with voltage violations and the one-day total (capital plus power-loss-induced) cost for different δ. As δ is decreased, the voltage control becomes more reliable as demonstrated by the significantly decreasing proportion of samples with voltage violations in the upper subfigure. The increased reliability only brings a modest increase in cost, as shown in the lower subfigure. Not shown in Fig. 4.6 is a benchmark case with only a fixed capacitor and no control. In that case the fixed capacitor is set high enough so that the voltage never drops below 0.99 pu, but the cost is as high as \$215/day due to the high power loss. We also consider another benchmark case in which there is only a D-STATCOM and there are no fixed and switchable capacitors. In this case the deterministic-constrained OPF problem $C_f(p, C_0, c_s^*, \overline{q}_f)$ is solved every 5 seconds in real time with $C_0 = c_s^* = 0$ and $\overline{q}_f$ being the minimum value such that C_f is feasible for the peak load (and hence feasible all the time). The total cost is as high as \$207/day due to the high capital cost of the D-STATCOM. Therefore the cost for either benchmark case is much higher than the cost under the proposed control, which ranges within \$182–184/day

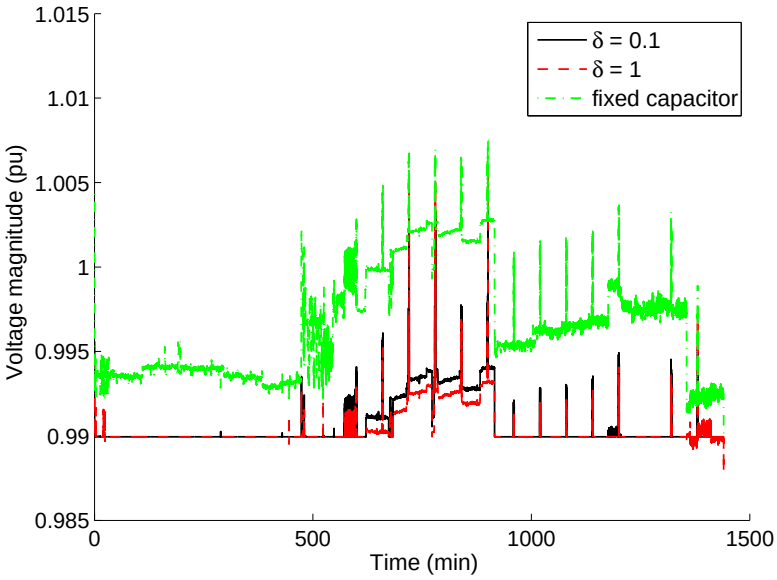

(a)

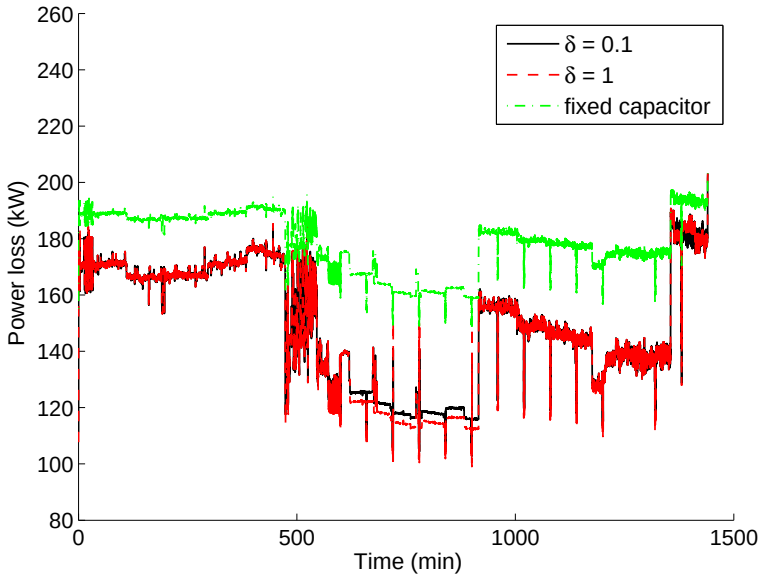

(b)

Figure 4.5: Real-time traces of (a) voltage magnitude and (b) power loss for different δ, and a benchmark case with only a fixed capacitor and no control.

as the value of δ changes.

As a main result of the experiments above, with the proposed heuristics to solve the optimal sizing problem and implement real-time control, the reliability of voltage control is significantly improved with moderate increase in cost, and hence a desired

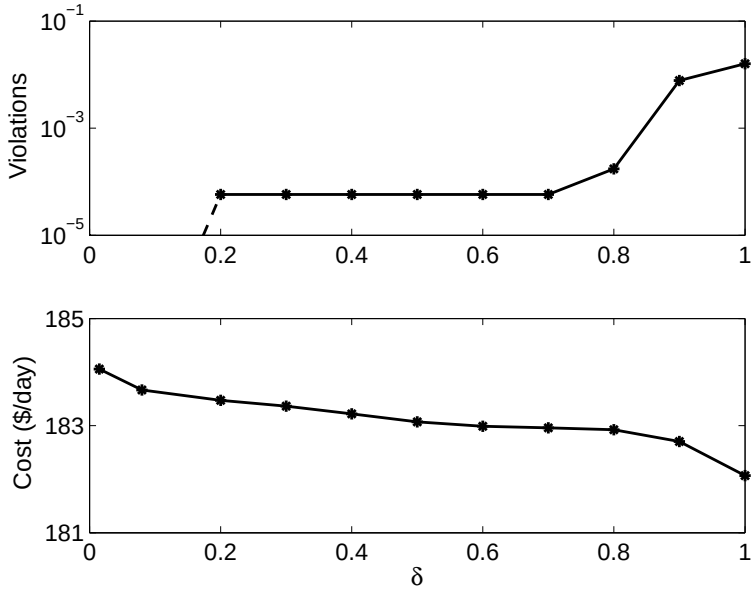

Figure 4.6: Upper: the proportion of samples with voltage violations, which drops to zero when $\delta < 0.2$. Lower: cost of the system in one day, including cost of power loss and capital cost.

tradeoff can be achieved between performance of voltage control and cost efficiency.

4.5 Conclusion

We have formulated a two-timescale optimization problem for joint control of a switchable capacitor and a D-STATCOM for voltage control in a distribution circuit with intermittent load. The slow-timescale capacitor control problem solves a chance-constrained OPF, which balances power loss with the probability of future voltage violations, by incorporating statistics of load changes over time. We have also integrated the result of the control problem into a sizing problem that determines the optimal sizes of reactive power sources. The optimal sizing problem allows a tradeoff between the expected cost due to power loss and the capital cost. We developed computationally efficient heuristics to solve the sizing problem and implement real-time control. In numerical experiments these heuristics were applied to measured data from an HPC load that routinely undergoes large and fast changes in power consumption. The results demonstrate the ability of the proposed schemes in improving the reliability of voltage control with a modest increase in cost.

BIBLIOGRAPHY

[1] "Annual energy outlook 2015 with projections to 2040," U.S. Energy Information Administration, Tech. Rep. DOE/EIA-0383(2015), 2015.

[2] H. K. Trabish. (2015). California finalizes 50%-by-2030 renewables mandate, [Online]. Available: http://www.utilitydive.com/news/california-finalizes-50-by-2030-renewables-mandate/407028/ (visited on 04/24/2016).

[3] J. Richardson. (2015). 100% renewable energy goal for Hawaii: Governor signs bill, [Online]. Available: http://cleantechnica.com/2015/06/11/100-renewable-energy-goal-hawaii-governor-signs-bill/ (visited on 04/24/2016).

[4] "2014 smart grid system report," U.S. Department of Energy, Tech. Rep., 2014.

[5] L. Alejandro, C. Blair, L. Bloodgood, M. Khan, M. Lawless, D. Meehan, P. Schneider, and K. Tsuji, "Global market for smart electricity meters: Government policies driving strong growth," Office of Industries, U.S. International Trade Commission, Tech. Rep. ID-037, 2014.

[6] IHS. (2015). Growth in smart connected home appliance market expected to accelerate from 2015 onward, IHS says, [Online]. Available: http://press.ihs.com/press-release/technology/growth-smart-connected-home-appliance-market-expected-accelerate-2015-onwar (visited on 04/24/2016).

[7] Wikipedia. (2016). Plug-in electric vehicles in the United States, [Online]. Available: https://en.wikipedia.org/wiki/Plug-in_electric_vehicles_in_the_United_States (visited on 04/24/2016).

[8] M. Munsell. (2015). US energy storage market to grow 250% in 2015, [Online]. Available: http://www.greentechmedia.com/articles/read/us-energy-storage-market-grew-400-in-2014 (visited on 04/24/2016).

[9] D. S. Callaway and I. A. Hiskens, "Achieving controllability of electric loads," *Proceedings of the IEEE*, vol. 99, no. 1, pp. 184–199, 2011.

[10] F. C. Schweppe, R. D. Tabors, J. L. Kirtley, H. R. Outhred, F. H. Pickel, and A. J. Cox, "Homeostatic utility control," *IEEE Transactions on Power Apparatus and Systems*, vol. PAS-99, no. 3, pp. 1151–1163, 1980.

[11] D. Trudnowski, M. Donnelly, and E. Lightner, "Power-system frequency and stability control using decentralized intelligent loads," in *Proceedings of IEEE PES Transmission and Distribution Conference and Exhibition*, Dallas, TX, USA, 2006, pp. 1453–1459.

[12] D. Hammerstrom, J. Brous, D. Chassin, *et al.*, "Pacific Northwest GridWise testbed demonstration projects, part II: Grid Friendly Appliance project," Pacific Northwest National Laboratory, Richland, WA, USA, Tech. Rep. PNNL-17079, 2007.

[13] U. K. Market Transformation Program, "Dynamic demand control of domestic appliances," Market Transformation Programme, Tech. Rep., 2008.

[14] P. Kundur, *Power System Stability and Control*. McGraw-Hill, 1994.

[15] A. J. Wood and B. F. Wollenberg, *Power Generation, Operation, and Control*, 2nd. John Wiley & Sons, Inc., 1996.

[16] A. R. Bergen and V. Vittal, *Power Systems Analysis*, 2nd. Prentice Hall, 2000.

[17] J. Machowski, J. W. Bialek, and J. R. Bumby, *Power System Dynamics: Stability and Control*, 2nd. John Wiley & Sons, Inc., 2008.

[18] A. Molina-Garcia, F. Bouffard, and D. S. Kirschen, "Decentralized demand-side contribution to primary frequency control," *IEEE Transactions on Power Systems*, vol. 26, no. 1, pp. 411–419, 2011.

[19] A. Kiani and A. Annaswamy, "A hierarchical transactive control architecture for renewables integration in smart grids," in *Proceedings of IEEE Conference on Decision and Control*, Maui, HI, USA, 2012, pp. 4985–4990.

[20] M. D. Ilic, "From hierarchical to open access electric power systems," *Proceedings of the IEEE*, vol. 95, no. 5, pp. 1060–1084, 2007.

[21] N. Lu and D. J. Hammerstrom, "Design considerations for frequency responsive grid friendly tm appliances," in *Proceedings of IEEE PES Transmission and Distribution Conference and Exhibition*, Dallas, TX, USA, 2006, pp. 647–652.

[22] J. A. Short, D. G. Infield, and L. L. Freris, "Stabilization of grid frequency through dynamic demand control," *IEEE Transactions on Power Systems*, vol. 22, no. 3, pp. 1284–1293, 2007.

[23] M. Donnelly, D. Harvey, R. Munson, and D. Trudnowski, "Frequency and stability control using decentralized intelligent loads: Benefits and pitfalls," in *Proceedings of IEEE Power and Energy Society General Meeting*, Minneapolis, MN, USA, 2010, pp. 1–6.

[24] A. Brooks, E. Lu, D. Reicher, C. Spirakis, and B. Weihl, "Demand dispatch," *IEEE Power and Energy Magazine*, vol. 8, no. 3, pp. 20–29, 2010.

[25] P. J. Douglass, R. Garcia-Valle, P. Nyeng, J. Ostergaard, and M. Togeby, "Smart demand for frequency regulation: Experimental results," *IEEE Transactions on Smart Grid*, vol. 4, no. 3, pp. 1713–1720, 2013.

[26] Y. J. Zhang, C. Zhao, W. Tang, and S. H. Low, "Profit-maximizing planning and control of battery energy storage systems for primary frequency control," *ArXiv preprint arXiv:1604.00952*, 2016.

[27] G. Heffner, C. Goldman, and M. Kintner-Meyer, "Loads providing ancillary services: Review of international experience," Lawrence Berkeley National Laboratory, CA, USA, Tech. Rep. LBNL-62701, 2007.

[28] B. J. Kirby, "Spinning reserve from responsive loads," Oak Ridge National Laboratory, TN, USA, Tech. Rep. ORNL/TM-2003/19, 2003.

[29] Q. Lu and Y.-Z. Sun, "Nonlinear stabilizing control of multimachine systems," *IEEE Transactions on Power Systems*, vol. 4, no. 1, pp. 236–241, 1989.

[30] Z. Qu, J. F. Dorsey, J. Bond, and J. D. McCalley, "Application of robust control to sustained oscillations in power systems," *IEEE Transactions on Circuits and Systems I: Fundamental Theory and Applications*, vol. 39, no. 6, pp. 470–476, 1992.

[31] H. Jiang, H. Cai, J. F. Dorsey, and Z. Qu, "Toward a globally robust decentralized control for large-scale power systems," *IEEE Transactions on Control Systems Technology*, vol. 5, no. 3, pp. 309–319, 1997.

[32] Y. Wang, D. J. Hill, and G. Guo, "Robust decentralized control for multimachine power systems," *IEEE Transactions on Circuits and Systems I: Fundamental Theory and Applications*, vol. 45, no. 3, pp. 271–279, 1998.

[33] Y. Guo, D. J. Hill, and Y. Wang, "Nonlinear decentralized control of large-scale power systems," *Automatica*, vol. 36, no. 9, pp. 1275–1289, 2000.

[34] D. D. Siljak, D. M. Stipanovic, and A. I. Zecevic, "Robust decentralized turbine/governor control using linear matrix inequalities," *IEEE Transactions on Power Systems*, vol. 17, no. 3, pp. 715–722, 2002.

[35] S. Y. Caliskan and P. Tabuada, "Compositional transient stability analysis of multimachine power networks," *IEEE Transactions on Control of Network Systems*, vol. 1, no. 1, pp. 4–14, 2014.

[36] A. R. Bergen and D. J. Hill, "A structure preserving model for power system stability analysis," *IEEE Transactions on Power Apparatus and Systems*, vol. PAS-100, no. 1, pp. 25–35, 1981.

[37] D. J. Hill and A. R. Bergen, "Stability analysis of multimachine power networks with linear frequency dependent loads," *IEEE Transactions on Circuits and Systems*, vol. 29, no. 12, pp. 840–848, 1982.

[38] N Tsolas, A. Arapostathis, and P. P. Varaiya, "A structure preserving energy function for power system transient stability analysis," *IEEE Transactions on Circuits and Systems*, vol. 32, no. 10, pp. 1041–1049, 1985.

[39] M. Andreasson, D. V. Dimarogonas, K. H. Johansson, and H. Sandberg, "Distributed vs. centralized power systems frequency control," in *Proceedings of European Control Conference*, Zürich, Switzerland, 2013, pp. 3524–3529.

[40] X. Zhang and A. Papachristodoulou, "A real-time control framework for smart power networks with star topology," in *Proceedings of American Control Conference*, Washington, D.C., USA, 2013, pp. 5062–5067.

[41] ——, "Distributed dynamic feedback control for smart power networks with tree topology," in *Proceedings of American Control Conference*, Portland, OR, USA, 2014, pp. 1156–1161.

[42] N. Li, L. Chen, C. Zhao, and S. H. Low, "Connecting automatic generation control and economic dispatch from an optimization view," in *Proceedings of American Control Conference*, Portland, OR, USA, 2014, pp. 735–740.

[43] M. Bürger, C. De Persis, and S. Trip, "An internal model approach to (optimal) frequency regulation in power grids," *ArXiv preprint arXiv:1403.7019v3*, 2015.

[44] S. You and L. Chen, "Reverse and forward engineering of frequency control in power networks," in *Proceedings of IEEE Conference on Decision and Control*, Los Angeles, CA, USA, 2014, pp. 191–198.

[45] E. Mallada and S. H. Low, "Distributed frequency-preserving optimal load control," in *Proceedings of IFAC World Congress*, Cape Town, South Africa, 2014, pp. 5411–5418.

[46] E. Mallada, C. Zhao, and S. H. Low, "Optimal load-side control for frequency regulation in smart grids," *ArXiv preprint arXiv:1410.2931v2*, 2015.

[47] J. W. Simpson-Porco, F. Dörfler, and F. Bullo, "Synchronization and power sharing for droop-controlled inverters in islanded microgrids," *Automatica*, vol. 49, no. 9, pp. 2603–2611, 2013.

[48] F. Dörfler, J. W. Simpson-Porco, and F. Bullo, "Breaking the hierarchy: Distributed control & economic optimality in microgrids," *IEEE Transactions on Control of Network Systems*, in press.

[49] C. Zhao, U. Topcu, and S. H. Low, "Frequency-based load control in power systems," in *Proceedings of American Control Conference*, Montréal, Canada, 2012, pp. 4423–4430.

[50] ——, "Fast load control with stochastic frequency measurement," in *Proceedings of IEEE Power and Energy Society General Meeting*, San Diego, CA, USA, 2012, pp. 1–8.

[51] C. Zhao, U. Topcu, and S. H. Low, "Optimal load control via frequency measurement and neighborhood area communication," *IEEE Transactions on Power Systems*, vol. 28, no. 4, pp. 3576–3587, 2013.

[52] M. D. Ilic and Q. Liu, "Toward sensing, communications and control architectures for frequency regulation in systems with highly variable resources," in *Control and Optimization Methods for Electric Smart Grids*, Springer, 2012, pp. 3–33.

[53] C. Zhao, U. Topcu, and S. Low, "Swing dynamics as primal-dual algorithm for optimal load control," in *Proceedings of IEEE SmartGridComm*, Tainan City, Taiwan, 2012, pp. 570–575.

[54] C. Zhao, U. Topcu, N. Li, and S. Low, "Design and stability of load-side primary frequency control in power systems," *IEEE Transactions on Automatic Control*, vol. 59, no. 5, pp. 1177–1189, 2014.

[55] C. Zhao and S. Low, "Optimal decentralized primary frequency control in power networks," in *Proceedings of IEEE Conference on Decision and Control*, Los Angeles, CA, USA, 2014, pp. 2467–2473.

[56] C. Zhao, E. Mallada, and S. H. Low, "Distributed generator and load-side secondary frequency control in power networks," in *Proceedings of Conference on Information Sciences and Systems*, Baltimore, MD, USA, 2015, pp. 1–6.

[57] C. Zhao, E. Mallada, S. H. Low, and J. Bialek, "A unified framework for frequency control and congestion management," in *Proceedings of Power Systems Computation Conference*, Genoa, Italy, 2016.

[58] J. Chow and G. Rogers, *Power System Toolbox*. Cherry Tree Scientific Software, 2000.

[59] C. Zhao, E. Mallada, and F. Dörfler, "Distributed frequency control for stability and economic dispatch in power networks," in *Proceedings of American Control Conference*, Chicago, IL, USA, 2015, pp. 2359–2364.

[60] K. Turitsyn, S. Backhaus, M. Chertkov, *et al.*, "Options for control of reactive power by distributed photovoltaic generators," *Proceedings of the IEEE*, vol. 99, no. 6, pp. 1063–1073, 2011.

[61] M. E. Baran and F. F. Wu, "Optimal sizing of capacitors placed on a radial distribution system," *IEEE Transactions on Power Delivery*, vol. 4, no. 1, pp. 735–743, 1989.

[62] ——, "Optimal capacitor placement on radial distribution systems," *IEEE Transactions on Power Delivery*, vol. 4, no. 1, pp. 725–734, 1989.

[63] A. Moreno-Muñoz, *Power Quality: Mitigation Technologies in a Distributed Environment*. Springer, 2007.

[64] Y. Liu, J. Bebic, B. Kroposki, J. De Bedout, and W. Ren, "Distribution system voltage performance analysis for high-penetration pv," in *Proceedings of IEEE Energy 2030 Conference*, Abu Dhabi, United Arab Emirates, 2008, pp. 1–8.

[65] J. Smith, W. Sunderman, R. Dugan, and B. Seal, "Smart inverter volt/var control functions for high penetration of pv on distribution systems," in *Proceedings of IEEE/PES Power Systems Conference and Exposition*, Phoenix, AZ, USA, 2011, pp. 1–6.

[66] K. Turitsyn, S. Backhaus, M. Chertkov, *et al.*, "Local control of reactive power by distributed photovoltaic generators," in *Proceedings of IEEE SmartGridComm*, Gaithersburg, MD, USA, 2010, pp. 79–84.

[67] P. Šulc, S. Backhaus, and M. Chertkov, "Optimal distributed control of reactive power via the alternating direction method of multipliers," *IEEE Transactions on Energy Conversion*, vol. 29, no. 4, pp. 968–977, 2014.

[68] S. Kundu, S. Backhaus, and I. A. Hiskens, "Distributed control of reactive power from photovoltaic inverters," in *Proceedings of IEEE International Symposium on Circuits and Systems*, Beijing, China, 2013, pp. 249–252.

[69] M. Farivar, R. Neal, C. Clarke, and S. Low, "Optimal inverter var control in distribution systems with high pv penetration," in *Proceedings of IEEE Power and Energy Society General Meeting*, San Diego, CA, USA, 2012, pp. 1–7.

[70] H.-G. Yeh, D. F. Gayme, and S. H. Low, "Adaptive VAR control for distribution circuits with photovoltaic generators," *IEEE Transactions on Power Systems*, vol. 27, no. 3, pp. 1656–1663, 2012.

[71] M. Farivar, X. Zhou, and L. Chen, "Local voltage control in distribution systems: An incremental control algorithm," in *Proceedings of IEEE SmartGridComm*, Miami, FL, USA, 2015, pp. 732–737.

[72] G. Joos, B. Ooi, D. McGillis, F. Galiana, and R. Marceau, "The potential of distributed generation to provide ancillary services," in *Proceedings of IEEE Power Engineering Society Summer Meeting*, vol. 3, Seattle, WA, USA, 2000, pp. 1762–1767.

[73] J. Grainger and S. Civanlar, "Volt/var control on distribution systems with lateral branches using shunt capacitors and voltage regulators Part I: The overall problem," *IEEE Transactions on Power Apparatus and Systems*, vol. PAS-104, no. 11, pp. 3278–3283, 1985.

[74] S. Civanlar and J. Grainger, "Volt/var control on distribution systems with lateral branches using shunt capacitors and voltage regulators Part II: The solution method," *IEEE Transactions on Power Apparatus and Systems*, vol. PAS-104, no. 11, pp. 3284–3290, 1985.

[75] ——, "Volt/var control on distribution systems with lateral branches using shunt capacitors and voltage regulators Part III: The numerical results," *IEEE Transactions on Power Apparatus and Systems*, vol. PAS-104, no. 11, pp. 3291–3297, 1985.

[76] R. Baldick and F. F. Wu, "Efficient integer optimization algorithms for optimal coordination of capacitors and regulators," *IEEE Transactions on Power Systems*, vol. 5, no. 3, pp. 805–812, 1990.

[77] M. Farivar, C. R. Clarke, S. H. Low, and K. M. Chandy, "Inverter var control for distribution systems with renewables," in *Proceedings of IEEE SmartGridComm*, Gaithersburg, MD, USA, 2010, pp. 457–462.

[78] T. Senjyu, Y. Miyazato, A. Yona, N. Urasaki, and T. Funabashi, "Optimal distribution voltage control and coordination with distributed generation," *IEEE Transactions on Power Delivery*, vol. 23, no. 2, pp. 1236–1242, 2008.

[79] J. J. Grainger and S. Lee, "Optimum size and location of shunt capacitors for reduction of losses on distribution feeders," *IEEE Transactions on Power Apparatus and Systems*, vol. PAS-100, no. 3, pp. 1105–1118, 1981.

[80] M. Salama, E. Mansour, A. Chikhani, and R. Hackam, "Control of reactive power in distribution systems with an end-load and varying load condition," *IEEE Transactions on Power Apparatus and Systems*, vol. PAS-104, no. 4, pp. 941–947, 1985.

[81] H. Dura, "Optimum number, location, and size of shunt capacitors in radial distribution feeders a dynamic programming approach," *IEEE Transactions on Power Apparatus and Systems*, vol. PAS-87, no. 9, pp. 1769–1774, 1968.

[82] T. Ananthapadmanabha, A. D. Kulkarni, A. S. G. Rao, K. R. Rao, and K. Parthasarathy, "Knowledge-based expert system for optimal reactive power control in distribution system," *International Journal of Electrical Power & Energy Systems*, vol. 18, no. 1, pp. 27–31, 1996.

[83] G. Boone and H.-D. Chiang, "Optimal capacitor placement in distribution systems by genetic algorithm," *International Journal of Electrical Power & Energy Systems*, vol. 15, no. 3, pp. 155–161, 1993.

[84] S. Sundhararajan and A. Pahwa, "Optimal selection of capacitors for radial distribution systems using a genetic algorithm," *IEEE Transactions on Power Systems*, vol. 9, no. 3, pp. 1499–1507, 1994.

[85] H. Ng, M. Salama, and A. Chikhani, "Classification of capacitor allocation techniques," *IEEE Transactions on Power Delivery*, vol. 15, no. 1, pp. 387–392, 2000.

[86] C. Zhao, M. Chertkov, and S. Backhaus, "Optimal sizing of voltage control devices for distribution circuit with intermittent load," in *Proceedings of Hawaii International Conference on System Sciences*, Kauai, HI, USA, 2015, pp. 2680–2689.

[87] A. Rubtsov, "Approach to stochastic modeling of power systems," *Scientific Proceedings of Riga Technical University, Series 4: Power and Electrical Engineering*, vol. 27, pp. 37–40, 2010.

[88] B. Ramanathan and V. Vittal, "A framework for evaluation of advanced direct load control with minimum disruption," *IEEE Transactions on Power Systems*, vol. 23, no. 4, pp. 1681–1688, 2008.

[89] Z. Ma, D. Callaway, and I. Hiskens, "Decentralized charging control for large populations of plug-in electric vehicles," in *Proceedings of IEEE Conference on Decision and Control*, Atlanta, GA, USA, 2010, pp. 206–212.

[90] N. Li, L. Chen, and S. H. Low, "Optimal demand response based on utility maximization in power networks," in *Proceedings of IEEE Power and Energy Society General Meeting*, Detroit, MI, USA, 2011, pp. 1–8.

[91] M. Fahrioglu and F. L. Alvarado, "Designing incentive compatible contracts for effective demand management," *IEEE Transactions on Power Systems*, vol. 15, no. 4, pp. 1255–1260, 2000.

[92] P. Samadi, A. Mohsenian-Rad, R. Schober, V. W. Wong, and J. Jatskevich, "Optimal real-time pricing algorithm based on utility maximization for smart grid," in *Proceedings of IEEE SmartGridComm*, Gaithersburg, MD, USA, 2010, pp. 415–420.

[93] S. P. Boyd and L. Vandenberghe, *Convex Optimization*. Cambridge University Press, 2004.

[94] P. K. Kitanidis, "Unbiased minimum-variance linear state estimation," *Automatica*, vol. 23, no. 6, pp. 775–778, 1987.

[95] S. S. Ram, A. Nedić, and V. V. Veeravalli, "Distributed stochastic subgradient projection algorithms for convex optimization," *Journal of optimization theory and applications*, vol. 147, no. 3, pp. 516–545, 2010.

[96] I. Trilliant. (2013). The multi-tier smart grid architecture, [Online]. Available: `http://www.trilliantinc.com/solutions/multi-tier-architecture/` (visited on 04/23/2013).

[97] W. Jewell, V. Namboodiri, V. Aravinthan, B. Karimi, M. Kezunovic, and Y. Dong, "Communication requirements and integration options for smart grid deployment," *Final Project Report, Power Systems Engineering Research Center*, no. 12-03, 2012.

[98] B. Karimi, V. Namboodiri, V. Aravinthan, and W. Jewell, "Feasibility, challenges, and performance of wireless multi-hop routing for feeder level communication in a smart grid," in *Proceedings of the International Conference on Energy-Efficient Computing and Networking*, New York, NY, USA, 2011, pp. 31–40.

[99] B. D. Anderson and J. B. Moore, *Optimal Filtering*. Courier Corporation, 2012.

[100] E. Weisstein. (2016). Mean-value theorem, [Online]. Available: `http://mathworld.wolfram.com/Mean-ValueTheorem.html`.

[101] S. H. Low and D. E. Lapsley, "Optimization flow control—i: Basic algorithm and convergence," *IEEE/ACM Transactions on Networking*, vol. 7, no. 6, pp. 861–874, 1999.

[102] D. P. Bertsekas and J. N. Tsitsiklis, *Parallel and Distributed Computation: Numerical Methods*. Prentice Hall, 1989.

[103] C. Zhao, U. Topcu, N. Li, and S. Low, "Power system dynamics as primal-dual algorithm for optimal load control," *ArXiv preprint arXiv:1305.0585v1*, 2013.

[104] M. D Ilic, L. Xie, U. A. Khan, and J. M. Moura, "Modeling of future cyber-physical energy systems for distributed sensing and control," *IEEE Transactions on Systems, Man and Cybernetics, Part A: Systems and Humans*, vol. 40, no. 4, pp. 825–838, 2010.

[105] G. Rogers, *Power System Oscillations*. Kluwer Academic, 2000.

[106] W. Rudin, *Principles of Mathematical Analysis*, 3rd. McGraw-Hill, 1976.

[107] V. Mieghem, *Graph Spectra for Complex Networks*. Cambridge University Press, 2011.

[108] K. J. Arrow, L. Hurwicz, H. Uzawa, and H. B. Chenery, *Studies in Linear and Non-linear Programming*. Stanford University Press, 1958.

[109] D. Feijer and F. Paganini, "Stability of primal-dual gradient dynamics and applications to network optimization," *Automatica*, vol. 46, no. 12, pp. 1974–1981, 2010.

[110] A. Rantzer, "Dynamic dual decomposition for distributed control," in *Proceedings of American Control Conference*, St. Louis, MO, USA, 2009, pp. 884–888.

[111] A. Araposthatis, S. Sastry, and P. Varaiya, "Analysis of power-flow equation," *International Journal of Electrical Power & Energy Systems*, vol. 3, no. 3, pp. 115–126, 1981.

[112] Wikipedia. (2016). Equivalent class, [Online]. Available: `https://en.wikipedia.org/wiki/Equivalence_class` (visited on 05/01/2016).

[113] U. Topcu, A. K. Packard, and R. M. Murray, "Compositional stability analysis based on dual decomposition," in *Proceedings of IEEE Conference on Decision and Control*, Shanghai, China, 2009, pp. 1175–1180.

[114] H.-D. Chiang, F. F. Wu, and P. P. Varaiya, "Foundations of direct methods for power system transient stability analysis," *IEEE Transactions on Circuits and Systems*, vol. 34, no. 2, pp. 160–173, 1987.

[115] A. Pai, *Energy Function Analysis for Power System Stability*. Springer, 2012.

[116] T. L. Vu and K. Turitsyn, "Lyapunov functions family approach to transient stability assessment," *IEEE Transactions on Power Systems*, vol. 31, no. 2, pp. 1269–1277, 2016.

[117] H. K. Khalil, *Nonlinear Systems*, 2nd. Prentice Hall, 2002.

[118] F. Bullo and A. D. Lewis, *Geometric Control of Mechanical Systems*. Springer, 2005.

[119] J. Baillieul and C. I. Byrnes, "Geometric critical point analysis of lossless power system models," *IEEE Transactions on Circuits and Systems*, vol. 29, no. 11, pp. 724–737, 1982.

[120] R. S. Varga, *Geršgorin and His Circles*. Springer, 2010.

[121] M. Spivak, *Calculus on Manifolds*. WA Benjamin, 1965.

[122] H.-D. Chiang and M. E. Baran, "On the existence and uniqueness of load flow solution for radial distribution power networks," *IEEE Transactions on Circuits and Systems*, vol. 37, no. 3, pp. 410–416, 1990.

[123] G. Andersson, "Modelling and analysis of electric power systems," *EEH-Power Systems Laboratory, ETH Zürich, Switzerland*, 2004.

[124] K. P. Schneider, J. Fuller, F. Tuffner, and R. Singh, "Evaluation of conservation voltage reduction (cvr) on a national level," Pacific Northwest National Laboratory, Richland, WA, USA, Tech. Rep. PNNL-19596, 2010.

[125] S. Kirkpatrick, "Optimization by simulated annealing: Quantitative studies," *Journal of Statistical Physics*, vol. 34, no. 5-6, pp. 975–986, 1984.